ISSN 2732–0189 (Online)
ISSN 1586–2070 (Print)

JOURNAL OF COMPUTATIONAL AND APPLIED MECHANICS

An Open Access International Journal

Published by the University of Miskolc

VOLUME 17, NUMBER 2 (2022)

MISKOLC UNIVERSITY PRESS

ISSN 2732–0189 (Online)
ISSN 1586–2070 (Print)

JOURNAL OF COMPUTATIONAL AND APPLIED MECHANICS

An Open Access International Journal

Published by the University of Miskolc

VOLUME 17 NUMBER 2 (2022)

MISKOLC UNIVERSITY PRESS

Journal of Computational and Applied Mechanics, Vol. 17, No. 2, (2022), pp. 85–104
DOI: 10.32973/jcam.2022.005

FUNDAMENTAL SOLUTIONS IN THE THEORY OF THERMOELASTIC DIFFUSIVE MATERIALS WITH MICROTEMPERATURES AND MICROCONCENTRATIONS

Tarun Kansal
Department of Mathematics, Markanda National College,
Shahabad-136135, India
tarun1_kansal@yahoo.co.in

[Received: September 22, 2022; Accepted: December 27, 2022]

Abstract. The main aim of this paper is to construct the fundamental solutions of a system of equations for isotropic thermoelastic diffusive materials with microtemperatures and microconcentrations in the case of steady oscillations in terms of elementary functions. In addition to this, the fundamental solutions of the system of equations of equilibrium theory of isotropic thermoelastic diffusivity materials with microtemperatures and microconcentrations are also established.

Mathematical Subject Classification: 74A15, 74A20, 74B05, 74E10, 74F05.
Keywords: Thermoelasticity, diffusivity, microtemperatures, microconcentrations

1. Introduction

Eringen and his co-workers [1–7] formulated the theories of micromorphic continua. In these theories, the particles of a continuous body are assumed to be composed of microelements which undergo homogeneous deformations called microdeformations. The system of differential equations and boundary conditions governing a continuum with microstructure are deduced from the principles of conservation of mass, conservation of microinertia, balance of linear momentum, balance of first moment of momentum, and the balance of energy. The theory of thermodynamics of elastic bodies with microstructure was extended by [8] with the assumption that the microelements have different temperatures. He modified the Clausius–Duhem inequality to include microtemperatures and added first-order moment of energy equations to the basic balance laws for determining the microtemperatures of a continuum. Iesan and Quintanilla [9] constructed a linear theory for elastic materials with an inner structure whose particles, in addition to the classical displacement and temperature fields, possess microtemperatures. They established the continuous dependence of initial data and body loads and proved an existence theorem for initial boundary value problems using semigroup theory. The field equations of a theory of microstretch thermoelastic bodies with microtemperatures were established in [10], where Iesan proved a uniqueness theorem in the dynamic theory of anisotropic materials and then derived a linear theory of microstretch elastic solids with microtemperatures in which a microelement of a continuum is equipped with the mechanical degrees of freedom for rigid rotations and microdilatation in addition to the classical translation degrees of freedom [11]. He also established a uniqueness result in the dynamic theory of anisotropic bodies.

The mass transfer of a substance from a high concentration region to low-concentration regions is called diffusivity. Nowacki [12–15], Sherief and his co-workers [16], Aouadi [17] and Kansal [18] developed various thermoelastic diffusivity theories to describe coupled mechanical behavior among temperature, concentration, and strain fields in elastic solids. Aouadi et al. [19] developed the nonlinear theory of thermoelastic diffusivity materials with microtemperatures and microconcentrations. They also obtained the linear theory of thermoelastic diffusivity materials with microtemperatures and microconcentrations. They proved the well-posedness of a linear anisotropic problem with the help of the semigroup theory of linear operators and studied the asymptotic behaviour of the solutions. Bazarra et al. [20] introduced a numerical scheme in the linear theory of thermoelastic diffusivity materials with microtemperatures and microconcentrations based on the finite element method to approximate the spatial domain and the forwarded Euler scheme to discretize the time derivatives. They also deduced a priori error estimates for the approximative solutions, and obtained the linear convergence of the algorithm under suitable regularity assumptions. Chiril [21] derived the field equations and the consecutive equations of the linear theory of microstretch thermoelasticity for materials whose particles have microelements that are equipped with microtemperatures and microconcentrations.

There is a necessity to construct fundamental solutions for solving boundary value problems of elasticity and thermoelasticity by potential method [22]. The reason for constructing fundamental solutions is that an integral representation of the solution of a boundary value problem by fundamental solution is easily solved by numerical methods rather than a differential equation with specified boundary and initial conditions. Various authors [23, 24] and [25] constructed fundamental solutions in different theories of elasticity and thermoelasticity with microtemperatures.

In Section 2, the constitutive relations and field equations for isotropic thermoelastic diffusivity materials with microtemperatures and microconcentrations are written. The system of linearized equations for steady oscillations in the theory of thermoelastic diffusivity solids with microtemperatures and microconcentrations is obtained in Section 3. In Section 4, in terms of elementary functions, the fundamental solution of basic governing equations in the case of steady oscillations is constructed. Some basic properties of the fundamental matrix in the case of steady oscillations are discussed in Section 5. In Section 6, the fundamental solutions of basic governing equations in case of equilibrium are established.

2. Basic Equations

Let $\mathbf{x} = (x_1, x_2, x_3)$ be the point of the Euclidean three-dimensional space E^3, $|\mathbf{x}| = (x_1^2 + x_2^2 + x_3^2)^{\frac{1}{2}}$, $\mathbf{D_x} = (\frac{\partial}{\partial x_1}, \frac{\partial}{\partial x_2}, \frac{\partial}{\partial x_3})$ and t denotes the time variable. Following [8, 10] and [19], the basic equations for an isotropic homogeneous thermoelastic diffusivity solid with microtemperatures and microconcentrations in the absence of body forces, heat sources, and mass diffusive sources are as follows:

Constitutive relations

$$t_{ij} = \lambda\, e_{ll}\delta_{ij} + 2\mu e_{ij} - \beta_1\theta\delta_{ij} - \beta_2 C\delta_{ij}, \tag{2.1}$$

$$\rho S = \beta_1 e_{ll} + \frac{\rho C_E}{T_0}\theta + \varpi C, \tag{2.2}$$

$$P = -\beta_2 e_{ll} - \varpi\,\theta + \chi C, \tag{2.3}$$

$$\rho\varepsilon_i = -c_1 T_i - \kappa_1 C_i, \tag{2.4}$$

$$\rho\Omega_i = -m_1 C_i - \kappa_1 T_i, \tag{2.5}$$

$$q_{ij} = -k_4 T_{l,l}\delta_{ij} - k_5 T_{i,j} - k_6 T_{j,i}, \tag{2.6}$$

$$q_i = k\theta_{,i} + k_1 T_i, \tag{2.7}$$

$$\tilde{\varsigma}_i = (k - k_3)\theta_{,i} + (k_1 - k_2)T_i, \tag{2.8}$$

$$\eta_{ij} = -h_4 C_{l,l}\delta_{ij} - h_5 C_{i,j} - h_6 C_{j,i}, \tag{2.9}$$

$$\sigma_i = (h - h_3)P_{,i} + (h_1 - h_2)C_i, \tag{2.10}$$

$$\eta_i = hP_{,i} + h_1 C_i, \tag{2.11}$$

$$\rho T_0 \dot{S} = q_{i,i}, \tag{2.12}$$

$$\eta_{j,j} = \dot{C}, \tag{2.13}$$

Equations of motion

$$t_{ij,j} = \rho\ddot{u}_i, \tag{2.14}$$

Balance of first moment of energy

$$\rho\dot{\varepsilon}_i = q_{ji,i} + q_i - \tilde{\varsigma}_i, \tag{2.15}$$

Balance of first moment of mass diffusivity

$$\rho\dot{\Omega}_i = \eta_{ji,j} + \eta_i - \sigma_i, \tag{2.16}$$

where t_{ij} are the stress tensor components, $e_{ll} = u_{l,l}$ are the strain tensor components, and u_i are the displacement vector components. Lame's constants are λ and μ, $\beta_1 = (3\lambda + 2\mu)\alpha_t, \beta_2 = (3\lambda + 2\mu)\alpha_c$, α_t is the coefficient of linear thermal expansion and α_c is the coefficient of linear diffusivity expansion, δ_{ij} is Kronecker's delta. The temperature is represented by $\theta = T - T_0$. The absolute temperature is T. In the reference configuration, the absolute temperature is T_0. C represents the concentration of diffusive material, ρ represents density, S represents entropy, C_E represents specific heat at constant strain, and P represents chemical potential. The first moments of energy vector and mass diffusivity vector are ε_i and Ω_i, respectively. T_i and C_i are microtemperature and microconcentration components, respectively. The microheat flux average is $\tilde{\varsigma}_i$. q_{ij}, η_{ij} are the first moment of heat flux and mass diffusivity flux tensors, respectively; σ_i is the micromass diffusivity flux average; q_i are the heat flux vector components; and η_i are the mass diffusivity flux vector components. The material constants are $\varpi, \chi, c_1, m_1, \kappa_1, k, k_1, ..., k_6$ and $h, h_1, ..., h_6$.

The governing equations for homogeneous isotropic thermoelastic diffusivity solid with microtemperatures and microconcentrations are obtained using equation (2.1) in (2.14), equations (2.4), (2.6)-(2.8) in (2.15), equations (2.5), (2.9)-(2.11) in (2.16), equations (2.2) and (2.7) in (2.12) and equations (2.3) and (2.11) in (2.13), as follows

$$\begin{aligned}
&\mu\Delta\mathbf{u} + (\lambda+\mu)\,\mathrm{grad\,div}\,\mathbf{u} - \beta_1\,\mathrm{grad}\,\theta - \beta_2\,\mathrm{grad}\,C = \rho\ddot{\mathbf{u}},\\
&k_6\Delta\mathbf{v} + (k_4+k_5)\,\mathrm{grad\,div}\,\mathbf{v} - k_2\mathbf{v} - k_3\,\mathrm{grad}\,\theta = c_1\dot{\mathbf{v}} + \kappa_1\dot{\mathbf{w}},\\
&h_6\Delta\mathbf{w} + (h_4+h_5)\,\mathrm{grad\,div}\,\mathbf{w} - h_2\mathbf{w} - h_3\,\mathrm{grad}\,P = \kappa_1\dot{\mathbf{v}} + m_1\dot{\mathbf{w}},\\
&\beta_1 T_0\,\mathrm{div}\,\dot{\mathbf{u}} + \rho C_E\dot{\theta} + \varpi T_0\dot{C} = k\,\Delta\,\theta + k_1\,\mathrm{div}\,\mathbf{v},\\
&h\Delta[-\beta_2\,\mathrm{div}\,\mathbf{u} - \varpi\,\theta + \chi\,C] + h_1\,\mathrm{div}\,\mathbf{w} = \dot{C},
\end{aligned}\tag{2.17}$$

where Δ is the Laplacian operator, $\mathbf{v} = (T_1, T_2, T_3)$ and $\mathbf{w} = (C_1, C_2, C_3)$.

In the upcoming sections, the chemical potential has been used as a state variable rather than concentration. Therefore, the system of equations (2.17) with the help of equation (2.3) becomes

$$\begin{aligned}
&[\mu\Delta + (\lambda_0+\mu)\,\mathrm{grad\,div}]\mathbf{u} - \rho\,\ddot{\mathbf{u}} - \gamma_1\,\mathrm{grad}\,\theta - \gamma_2\,\mathrm{grad}\,P = \mathbf{0},\\
&[k_6\Delta + (k_4+k_5)\,\mathrm{grad\,div} - k_2]\mathbf{v} - c_1\,\dot{\mathbf{v}} - \kappa_1\dot{\mathbf{w}} - k_3\,\mathrm{grad}\,\theta = \mathbf{0},\\
&-\kappa_1\dot{\mathbf{v}} + [h_6\Delta + (h_4+h_5)\,\mathrm{grad\,div} - h_2]\mathbf{w} - m_1\,\dot{\mathbf{w}} - h_3\,\mathrm{grad}\,P = \mathbf{0},\\
&-\gamma_1 T_0\,\mathrm{div}\,\dot{\mathbf{u}} + k_1\,\mathrm{div}\,\mathbf{v} + k\,\Delta\,\theta - cT_0\,\dot{\theta} - \kappa T_0\dot{P} = 0,\\
&-\gamma_2\,\mathrm{div}\,\dot{\mathbf{u}} + h_1\,\mathrm{div}\,\mathbf{w} - \kappa\,\dot{\theta} + h\Delta\,P - m\,\dot{P} = 0.
\end{aligned}\tag{2.18}$$

The coefficients $m, \kappa, \gamma_1, \gamma_2, \lambda_0$, and c are given in Appendix A.

3. Steady Oscillations

The displacement vector, microtemperature, microconcentration, temperature change, and chemical potential functions are assumed as:

$$\Big[\mathbf{u}(\mathbf{x},t), \mathbf{v}(\mathbf{x},t), \mathbf{w}(\mathbf{x},t), \theta(\mathbf{x},t), P(\mathbf{x},t)\Big] = \mathrm{Re}\Big[(\mathbf{u}^*, \mathbf{v}^*, \mathbf{w}^*, \theta^*, P^*)e^{-\iota\omega t}\Big], \tag{3.1}$$

where ω is the frequency of oscillation.

Using equation (3.1) in the system of equations (2.18) and omitting the asterisk (*) for simplicity, the system of equations of steady oscillations is obtained as:

$$\begin{aligned}
&[\mu\Delta + (\lambda_0+\mu)\,\mathrm{grad\,div} + \rho\omega^2]\mathbf{u} - \gamma_1\,\mathrm{grad}\,\theta - \gamma_2\,\mathrm{grad}\,P = \mathbf{0},\\
&[k_6\Delta + (k_4+k_5)\,\mathrm{grad\,div} - k_2 + \iota\omega c_1]\mathbf{v} + \iota\omega\kappa_1\mathbf{w} - k_3\,\mathrm{grad}\,\theta = \mathbf{0},\\
&\iota\omega\kappa_1\mathbf{v} + [h_6\Delta + (h_4+h_5)\,\mathrm{grad\,div} - h_2 + \iota\omega m_1]\mathbf{w} - h_3\,\mathrm{grad}\,P = \mathbf{0},\\
&\iota\omega\gamma_1 T_0\,\mathrm{div}\,\mathbf{u} + k_1\,\mathrm{div}\,\mathbf{v} + [k\,\Delta + \iota\omega c T_0]\theta + \iota\omega\kappa T_0 P = 0,\\
&\iota\omega\gamma_2\,\mathrm{div}\,\mathbf{u} + h_1\,\mathrm{div}\,\mathbf{w} + \iota\omega\kappa\,\theta + [h\,\Delta + \iota\omega m]P = 0.
\end{aligned}\tag{3.2}$$

We introduce the second-order matrix differential operators with constant coefficients

$$\mathbf{F}(\mathbf{D_x}) = \Big(F_{gl}(\mathbf{D_x})\Big)_{11\times 11},$$

where

$$F_{pq}(\mathbf{D_x}) = [\mu\Delta + \rho\omega^2]\delta_{pq} + (\lambda_0+\mu)\frac{\partial^2}{\partial x_p \partial x_q}, F_{p;q+3}(\mathbf{D_x}) = F_{p+3;q}(\mathbf{D_x}) = 0,$$

$$F_{p;q+6}(\mathbf{D_x}) = F_{p+6;q}(\mathbf{D_x}) = 0, F_{p;10}(\mathbf{D_x}) = -\gamma_1\frac{\partial}{\partial x_p}, F_{p;11}(\mathbf{D_x}) = -\gamma_2\frac{\partial}{\partial x_p},$$

$$F_{p+3;q+3}(\mathbf{D_x}) = [k_6\Delta - k_2 + \iota\omega c_1]\delta_{pq} + (k_4+k_5)\frac{\partial^2}{\partial x_p \partial x_q},$$

$$F_{p+3;q+6}(\mathbf{D_x}) = F_{p+6;q+3}(\mathbf{D_x}) = \iota\omega\kappa_1\delta_{pq}, F_{p+3;10}(\mathbf{D_x}) = -k_3\frac{\partial}{\partial x_p},$$

$$F_{p+3;11}(\mathbf{D_x}) = F_{11;p+3}(\mathbf{D_x}) = 0, F_{p+6;q+6}(\mathbf{D_x}) =$$

$$= [h_6\Delta - h_2 + \iota\omega m_1]\delta_{pq} + (h_4+h_5)\frac{\partial^2}{\partial x_p \partial x_q},$$

$$F_{p+6;10}(\mathbf{D_x}) = F_{10;p+6}(\mathbf{D_x}) = 0, F_{p+6;11}(\mathbf{D_x}) = -h_3\frac{\partial}{\partial x_p}, F_{10;q}(\mathbf{D_x}) = \iota\omega\gamma_1 T_0\frac{\partial}{\partial x_q},$$

$$F_{10;q+3}(\mathbf{D_x}) = k_1\frac{\partial}{\partial x_q}, F_{10;10}(\mathbf{D_x}) = k\Delta + \iota\omega c T_0, F_{10;11}(\mathbf{D_x}) = \iota\omega\kappa T_0,$$

$$F_{11;q} = \iota\omega\gamma_2\frac{\partial}{\partial x_q}, F_{11;q+6}(\mathbf{D_x}) = h_1\frac{\partial}{\partial x_q}, F_{11;10}(\mathbf{D_x}) = \iota\omega\kappa,$$

$$F_{11;11}(\mathbf{D_x}) = h\Delta + \iota\omega m\,, \qquad p,q = 1,2,3.$$

and

$$\tilde{\mathbf{F}}(\mathbf{D_x}) = \Big(\tilde{F}_{gl}(\mathbf{D_x})\Big)_{11\times 11},$$

where

$$\tilde{F}_{pq}(\mathbf{D_x}) = \mu\Delta\delta_{pq} + (\lambda_0+\mu)\frac{\partial^2}{\partial x_p \partial x_q}, \tilde{F}_{p+3;q+3}(\mathbf{D_x}) = k_6\Delta\delta_{pq} + (k_4+k_5)\frac{\partial^2}{\partial x_p \partial x_q},$$

$$\tilde{F}_{p+6;q+6}(\mathbf{D_x}) = h_6\Delta\delta_{pq} + (h_4+h_5)\frac{\partial^2}{\partial x_p \partial x_q}, \tilde{F}_{10;10}(\mathbf{D_x}) = k\Delta, \tilde{F}_{11;11}(\mathbf{D_x}) = h\Delta,$$

$$\tilde{F}_{p;q+3}(\mathbf{D_x}) = \tilde{F}_{p;q+6}(\mathbf{D_x}) = \tilde{F}_{p+3;q}(\mathbf{D_x}) = \tilde{F}_{p+6;q}(\mathbf{D_x}) = 0,$$

$$\tilde{F}_{p+3;q+6}(\mathbf{D_x}) = \tilde{F}_{p+6;q+3}(\mathbf{D_x}) = \tilde{F}_{ie}(\mathbf{D_x}) = \tilde{F}_{ei}(\mathbf{D_x}) = 0,$$

$$\tilde{F}_{10;11}(\mathbf{D_x}) = \tilde{F}_{11;10}(\mathbf{D_x}) = 0\,, \quad p,q = 1,2,3; \quad e = 10,11; \quad i = 1,..,9.$$

The system of equations (3.2) can be represented as

$$\mathbf{F}(\mathbf{D_x})\mathbf{U}(\mathbf{x}) = \mathbf{0},$$

where $\mathbf{U} = (\mathbf{u}, \mathbf{v}, \mathbf{w}, \theta, P)$ is a vector function with eleven components on E^3. The matrix $\tilde{\mathbf{F}}(\mathbf{D_x})$ is called the principal part of operator $\mathbf{F}(\mathbf{D_x})$.

Definition 1: The operator $\mathbf{F}(\mathbf{D_x})$ is said to be elliptic if $|\tilde{\mathbf{F}}(\boldsymbol{k})| \neq 0$, $\boldsymbol{k} = (\mu_1, \mu_2, \mu_3)$.

Since $|\tilde{\mathbf{F}}(\boldsymbol{k})| = \mu^2\tilde{\lambda}kk_6k_7hh_6h_7|\boldsymbol{k}|^{22}$, $\tilde{\lambda} = \lambda_0 + 2\mu$, $k_7 = k_4+k_5+k_6$, $h_7 = h_4+h_5+h_6$.

Therefore, operator $\mathbf{F}(\mathbf{D_x})$ is an elliptic differential operator iff

$$\mu\tilde{\lambda}kk_6k_7hh_6h_7 \neq 0. \tag{3.3}$$

Definition 2: The fundamental solution of the system of equations (3.2) (the fundamental operator matrix $\mathbf{F}$) is the matrix $\mathbf{G}(\mathbf{x}) = \Big(G_{gl}(\mathbf{x})\Big)_{11\times 11}$ satisfying condition

$$\mathbf{F}(\mathbf{D_x})\mathbf{G}(\mathbf{x}) = \delta(\mathbf{x})\,\mathbf{I}(\mathbf{x}), \tag{3.4}$$

where $\delta(\mathbf{x})$ represents the Dirac delta, $\mathbf{I} = (\delta_{gl})_{11\times 11}$ is the unit matrix, and $\mathbf{x} \in \mathrm{E}^3$.

4. Construction of $\mathbf{G}(\mathbf{x})$ in Terms of Elementary Functions

Let us consider the system of non-homogeneous equations

$$[\mu\Delta + (\lambda_0+\mu)\,\mathrm{grad}\,\mathrm{div} + \rho\omega^2]\mathbf{u} + \iota\omega\gamma_1T_0\,\mathrm{grad}\,\theta + \iota\omega\gamma_2\,\mathrm{grad}\,P = \mathbf{H}, \tag{4.1}$$

$$[k_6\Delta + (k_4+k_5)\,\mathrm{grad}\,\mathrm{div} + k_8]\mathbf{v} + \iota\omega\kappa_1\mathbf{w} + k_1\,\mathrm{grad}\,\theta = \mathbf{V}, \tag{4.2}$$

$$\iota\omega\kappa_1\mathbf{v} + [h_6\Delta + (h_4+h_5)\,\mathrm{grad}\,\mathrm{div} + h_8]\mathbf{w} + h_1\,\mathrm{grad}\,P = \mathbf{W}, \tag{4.3}$$

$$-\gamma_1\,\mathrm{div}\,\mathbf{u} - k_3\,\mathrm{div}\,\mathbf{v} + [k\,\Delta + \iota\omega cT_0]\theta + \iota\omega\kappa P = Z, \tag{4.4}$$

$$-\gamma_2\,\mathrm{div}\,\mathbf{u} - h_3\,\mathrm{div}\,\mathbf{w} + \iota\omega\kappa T_0\,\theta + [h\,\Delta + \iota\omega m]P = X, \tag{4.5}$$

where $k_8 = -k_2 + \iota\omega c_1, h_8 = -h_2 + \iota\omega m_1$; $\mathbf{H}, \mathbf{V}, \mathbf{W}$ are vector functions with three components on E^3; Z and X are scalar functions on E^3.

Equations (4.1)-(4.5) can also be written as

$$\mathbf{F}^{tr}(\mathbf{D_x})\mathbf{U}(\mathbf{x}) = \mathbf{Q}(\mathbf{x}), \tag{4.6}$$

where $\mathbf{F}^{tr}$ is the transpose of matrix $\mathbf{F}$, $\mathbf{Q} = (\mathbf{H}, \mathbf{V}, \mathbf{W}, Z, X)$ and $\mathbf{x} \in \mathrm{E}^3$.

Using the divergence (div) operator on the equations (4.1) -(4.3), we get

$$[\tilde{\lambda}\Delta + \rho\omega^2]\,\mathrm{div}\,\mathbf{u} + \iota\omega\gamma_1T_0\Delta\,\theta + \iota\omega\gamma_2\Delta\,P = \mathrm{div}\,\mathbf{H}, \tag{4.7}$$

$$(k_7\Delta + k_8)\,\mathrm{div}\,\mathbf{v} + \iota\omega\kappa_1\,\mathrm{div}\,\mathbf{w} + k_1\Delta\theta = \mathrm{div}\,\mathbf{V}, \tag{4.8}$$

$$\iota\omega\kappa_1\,\mathrm{div}\,\mathbf{v} + (h_7\Delta + h_8)\,\mathrm{div}\,\mathbf{w} + h_1\Delta P = \mathrm{div}\,\mathbf{W}. \tag{4.9}$$

The equations (4.4), (4.5) and (4.7)-(4.9) can be expressed as

$$\mathbf{N}(\Delta)\mathbf{S} = \tilde{\mathbf{Q}}, \tag{4.10}$$

where $\mathbf{S}, \tilde{\mathbf{Q}}$, and $\mathbf{N}(\Delta)$ are given in Appendix A.

The equation (4.10) can be written in determinant form as

$$\Gamma_1(\Delta)\mathbf{S} = \mathbf{\Psi}, \tag{4.11}$$

where $\Gamma_1(\Delta)$, and $\mathbf{\Psi}$ are given in Appendix A.

On expanding $\Gamma_1(\Delta)$, we see that

$$\Gamma_1(\Delta) = \prod_{i=1}^{5}(\Delta + \lambda_i^2),$$

where $\lambda_i^2,\ i = 1, ..., 5$ are the roots of the equation $\Gamma_1(-\xi) = 0$(with respect to ξ).

Applying operator $\Gamma_1(\Delta)$ to the equation (4.1), we get

$$\Gamma_1(\Delta)(\Delta + \lambda_6^2)\mathbf{u} = \mathbf{\Psi}', \tag{4.12}$$

where λ_6^2, and $\mathbf{\Psi}'$ are given in Appendix A.

Multiplying equations (4.2) and (4.3) by $h_6\Delta + h_8$ and $\iota\omega\kappa_1$ respectively, we obtain

$$(h_6\Delta + h_8)[k_6\Delta + (k_4 + k_5)\,\mathrm{grad\,div} + k_8]\mathbf{v} + (h_6\Delta + h_8)\iota\omega\kappa_1\mathbf{w}$$
$$= (h_6\Delta + h_8)[\mathbf{V} - k_1\,\mathrm{grad}\,\theta], \tag{4.13}$$

and

$$(\iota\omega\kappa_1)^2\mathbf{v} + \iota\omega\kappa_1[h_6\Delta + (h_4 + h_5\,)\mathrm{grad\,div} + h_8]\mathbf{w} = \iota\omega\kappa_1[\mathbf{W} - h_1\,\mathrm{grad}\,P]. \tag{4.14}$$

Using equation (4.14) in equation (4.13), we obtain

$$[(h_6\Delta + h_8)(k_6\Delta + k_8) - (\iota\omega\kappa_1)^2]\mathbf{v} = \iota\omega\kappa_1(h_4 + h_5)\,\mathrm{grad\,div}\,\mathbf{w}$$
$$+(h_6\Delta + h_8)[\mathbf{V} - k_1\,\mathrm{grad}\,\theta - (k_4 + k_5)\,\mathrm{grad\,div}\,\mathbf{v}] - \iota\omega\kappa_1[\mathbf{W} - h_1\,\mathrm{grad}\,P]. \tag{4.15}$$

Applying operator $\Gamma_1(\Delta)$ to the equation (4.15) and using equation (4.11), we get

$$\Gamma_1(\Delta)\Gamma_2(\Delta)\mathbf{v} = \mathbf{\Psi}'', \tag{4.16}$$

where $\Gamma_2(\Delta)$, and $\mathbf{\Psi}''$ are given in Appendix A.

It can be seen that

$$\Gamma_2(\Delta) = (\Delta + \lambda_7^2)(\Delta + \lambda_8^2),$$

where λ_7^2, λ_8^2 are the roots of the equation $\Gamma_2(-\xi) = 0$(with respect to ξ).

Multiplying equations (4.2) and (4.3) by $\iota\omega\kappa_1$ and $k_6\Delta + k_8$ respectively, we obtain

$$(\iota\omega\kappa_1)[k_6\Delta + (k_4 + k_5)\,\mathrm{grad\,div} + k_8]\mathbf{v} + (\iota\omega\kappa_1)^2\mathbf{w} = (\iota\omega\kappa_1)[\mathbf{V} - k_1\,\mathrm{grad}\,\theta], \tag{4.17}$$

and

$$(\iota\omega\kappa_1)(k_6\Delta + k_8)\mathbf{v} + (k_6\Delta + k_8)[h_6\Delta + (h_4 + h_5\,)\mathrm{grad\,div} + h_8]\mathbf{w} =$$
$$= (k_6\Delta + k_8)[\mathbf{W} - h_1\,\mathrm{grad}\,P]. \tag{4.18}$$

Utilizing equation (4.17) in equation (4.18), we obtain

$$[(h_6\Delta + h_8)(k_6\Delta + k_8) - (\iota\omega\kappa_1)^2]\mathbf{w} = \iota\omega\kappa_1(k_4 + k_5)\,\mathrm{grad\,div}\,\mathbf{v}$$
$$+(k_6\Delta + k_8)[\mathbf{W} - h_1\,\mathrm{grad}\,P - (h_4 + h_5)\,\mathrm{grad\,div}\,\mathbf{w}] - \iota\omega\kappa_1[\mathbf{V} - k_1\,\mathrm{grad}\,\theta]. \tag{4.19}$$

Applying operator $\Gamma_1(\Delta)$ to the equation (4.19) and using equation (4.11), we get

$$\Gamma_1(\Delta)\Gamma_2(\Delta)\mathbf{w} = \mathbf{\Psi}''', \tag{4.20}$$

where $\mathbf{\Psi}'''$ is given in Appendix A.

From equations (4.11), (4.12), (4.16) and (4.20), we obtain

$$\mathbf{\Theta}(\Delta)\mathbf{U}(\mathbf{x}) = \hat{\mathbf{\Psi}}(\mathbf{x}), \tag{4.21}$$

where $\hat{\mathbf{\Psi}}$, and $\mathbf{\Theta}(\Delta)$ are given in Appendix B.

The expressions for $\mathbf{\Psi}', \mathbf{\Psi}'', \mathbf{\Psi}'''$ and Ψ_p, $(p = 4, 5)$ can be rewritten in the form

$$\mathbf{\Psi}' = \frac{1}{\mu}\Big[\Gamma_1(\Delta)\mathbf{J} + w_{11}(\Delta)\ \mathrm{grad\,div}\Big]\mathbf{H} + \sum_{i=2}^{5} w_{i1}(\Delta)\,\mathrm{grad}\, w_i, \tag{4.22a}$$

$$\begin{aligned}\mathbf{\Psi}'' &= \Big[\frac{1}{N^*}(h_6\Delta + h_8)\Gamma_1(\Delta)\mathbf{J} + w_{22}(\Delta)\,\mathrm{grad\,div}\Big]\mathbf{V} + w_{12}(\Delta)\,\mathrm{grad\,div}\,\mathbf{H} \\ &+ w_{42}(\Delta)\,\mathrm{grad}\,Z + w_{52}(\Delta)\,\mathrm{grad}\,X + \Big[-\frac{1}{N^*}\iota\omega\kappa_1\Gamma_1(\Delta)\mathbf{J} + w_{32}(\Delta)\,\mathrm{grad\,div}\Big]\mathbf{W},\end{aligned} \tag{4.22b}$$

$$\begin{aligned}\mathbf{\Psi}''' &= \Big[\frac{1}{N^*}(k_6\Delta + k_8)\Gamma_1(\Delta)\mathbf{J} + w_{33}(\Delta)\,\mathrm{grad\,div}\Big]\mathbf{W} + w_{13}(\Delta)\,\mathrm{grad\,div}\,\mathbf{H} \\ &+ w_{43}(\Delta)\,\mathrm{grad}\,Z + w_{53}(\Delta)\,\mathrm{grad}\,X + \Big[-\frac{1}{N^*}\iota\omega\kappa_1\Gamma_1(\Delta)\mathbf{J} + w_{23}(\Delta)\,\mathrm{grad\,div}\Big]\mathbf{V},\end{aligned} \tag{4.22c}$$

$$\Psi_p = w_{1p}(\Delta)\,\mathrm{div}\,\mathbf{H} + w_{2p}(\Delta)\,\mathrm{div}\,\mathbf{V} + w_{3p}(\Delta)\,\mathrm{div}\,\mathbf{W} + w_{4p}(\Delta)\,Z + w_{5p}(\Delta)\,X, \tag{4.22d}$$

where $\mathbf{J} = (\delta_{gh})_{3\times 3}$ is the unit matrix and the coefficients w_{pi}, $p, i = 1, ..., 5$ are given in Appendix B.

From equations (4.22), we have

$$\hat{\mathbf{\Psi}}(\mathbf{x}) = \mathbf{R}^{tr}(\mathbf{D_x})\mathbf{Q}(\mathbf{x}), \tag{4.23}$$

where the matrix $\mathbf{R}(\mathbf{D_x})$ is given in Appendix B.

From equations (4.6), (4.21) and (4.23), we obtain

$$\mathbf{\Theta}\mathbf{U} = \mathbf{R}^{tr}\mathbf{F}^{tr}\mathbf{U}.$$

The above relation implies

$$\mathbf{R}^{tr}\mathbf{F}^{tr} = \mathbf{\Theta}.$$

Therefore, we obtain

$$\mathbf{F}(\mathbf{D_x})\mathbf{R}(\mathbf{D_x}) = \mathbf{\Theta}(\Delta). \tag{4.24}$$

We assume that

$$\lambda_p^2 \neq \lambda_q^2 \neq 0 \ p, q = 1, \ldots.., 8 \ p \neq q.$$

Let

$$\mathbf{Y}(\mathbf{x}) = \Big(Y_{ij}(\mathbf{x}) \Big)_{11\times 11}, \ Y_{pp}(\mathbf{x}) = \sum_{g=1}^{6} r_{1g}\varsigma_g(\mathbf{x}),$$

$$Y_{p+3;p+3}(\mathbf{x}) = Y_{p+6;p+6}(\mathbf{x}) = \sum_{g=1, g\neq 6}^{8} r_{2g}\varsigma_g(\mathbf{x}),$$

$$Y_{ll}(\mathbf{x}) = \sum_{g=1}^{5} r_{3g}\varsigma_g(\mathbf{x}), Y_{qz}(\mathbf{x}) = 0 \ p = 1, 2, 3 \ l = 10, 11 \ q, z = 1, \ldots.., 11 \ q \neq z$$

where $\varsigma_g(\mathbf{x})$, $g = 1, \ldots.., 8$, r_{1p}, $p = 1, \ldots.., 6$, r_{2l}, $l = 1, \ldots.7, 8$, and r_{3q}, $q = 1, \ldots, 5$ are given in Appendix C.

Lemma 1: The matrix $\mathbf{Y}$ defined above is the fundamental matrix of operator $\mathbf{\Theta}(\Delta)$, i.e.

$$\mathbf{\Theta}(\Delta)\mathbf{Y}(\mathbf{x}) = \delta(\mathbf{x})\,\mathbf{I}(\mathbf{x}). \tag{4.25}$$

Proof: To prove the lemma, it is sufficient to prove that

$$\Gamma_1(\Delta)(\Delta + \lambda_6^2)Y_{11}(\mathbf{x}) = \delta(\mathbf{x}), \tag{4.26}$$

$$\Gamma_1(\Delta)\Gamma_2(\Delta)Y_{44}(\mathbf{x}) = \delta(\mathbf{x}), \tag{4.27}$$

$$\Gamma_1(\Delta)Y_{10;10}(\mathbf{x}) = \delta(\mathbf{x}). \tag{4.28}$$

Let us consider a sum

$$\sum_{i=1}^{6} r_{1i} = \frac{\sum_{j=1}^{6}(-1)^j z_j}{z_7},$$

where z_j, $j = 1, \ldots., 7$ are given in Appendix C.

On simplifying the right hand side of above relation, we obtain

$$\sum_{i=1}^{6} r_{1i} = 0. \tag{4.29}$$

Similarly, we find that

$$\sum_{i=2}^{6} r_{1i}(\lambda_1^2 - \lambda_i^2) = 0, \sum_{i=3}^{6} r_{1i}\left[\prod_{j=1}^{2}(\lambda_j^2 - \lambda_i^2)\right] = 0,$$

$$\sum_{i=4}^{6} r_{1i}\left[\prod_{j=1}^{3}(\lambda_j^2 - \lambda_i^2)\right] = 0, \sum_{i=5}^{6} r_{1i}\left[\prod_{j=1}^{4}(\lambda_j^2 - \lambda_i^2)\right] = 0,$$

$$\prod_{j=1}^{5} r_{16}(\lambda_j^2 - \lambda_6^2) = 1. \tag{4.30}$$

Also,

$$(\Delta+\lambda_p^2)\varsigma_g(\mathbf{x})=\delta(\mathbf{x})+(\lambda_p^2-\lambda_g^2)\varsigma_g(\mathbf{x}),\qquad p,g=1,...,8. \tag{4.31}$$

Now, consider

$$\Gamma_1(\Delta)(\Delta+\lambda_6^2)Y_{11}(\mathbf{x})=\prod_{i=1}^{6}(\Delta+\lambda_i^2)\sum_{g=1}^{6}r_{1g}\varsigma_g(\mathbf{x}).$$

Using equations (4.29)-(4.31) in the above relation, we obtain

$$\begin{aligned}
\Gamma_1(\Delta)(\Delta+\lambda_6^2)Y_{11}(\mathbf{x})&=\prod_{i=2}^{6}(\Delta+\lambda_i^2)\sum_{g=1}^{6}r_{1g}\Big[\delta(\mathbf{x})+(\lambda_1^2-\lambda_g^2)\varsigma_g(\mathbf{x})\Big]\\
&=\prod_{i=2}^{6}(\Delta+\lambda_i^2)\Big[\delta(\mathbf{x})\sum_{g=1}^{6}r_{1g}+\sum_{g=2}^{6}r_{1g}(\lambda_1^2-\lambda_g^2)\varsigma_g(\mathbf{x})\Big]\\
&=\prod_{i=2}^{6}(\Delta+\lambda_i^2)\Big[\sum_{g=2}^{6}r_{1g}(\lambda_1^2-\lambda_g^2)\varsigma_g(\mathbf{x})\Big]\\
&=\prod_{i=3}^{6}(\Delta+\lambda_i^2)\Big[\sum_{g=2}^{6}r_{1g}(\lambda_1^2-\lambda_g^2)\Big[\delta(\mathbf{x})+(\lambda_2^2-\lambda_g^2)\varsigma_g(\mathbf{x})\Big]\Big]\\
&=\prod_{i=3}^{6}(\Delta+\lambda_i^2)\Big[\sum_{g=3}^{6}r_{1g}\Big[\prod_{j=1}^{2}(\lambda_j^2-\lambda_g^2)\Big]\varsigma_g(\mathbf{x})\Big]\\
&=\prod_{i=4}^{6}(\Delta+\lambda_i^2)\Big[\sum_{g=3}^{6}r_{1g}\Big[\prod_{j=1}^{2}(\lambda_j^2-\lambda_g^2)\Big]\Big[\delta(\mathbf{x})+(\lambda_3^2-\lambda_g^2)\varsigma_g(\mathbf{x})\Big]\Big]\\
&=\prod_{i=4}^{6}(\Delta+\lambda_i^2)\Big[\sum_{g=4}^{6}r_{1g}\Big[\prod_{j=1}^{3}(\lambda_j^2-\lambda_g^2)\Big]\varsigma_g(\mathbf{x})\Big]\\
&=\prod_{i=5}^{6}(\Delta+\lambda_i^2)\Big[\sum_{g=4}^{6}r_{1g}\Big[\prod_{j=1}^{3}(\lambda_j^2-\lambda_g^2)\Big]\Big[\delta(\mathbf{x})+(\lambda_4^2-\lambda_g^2)\varsigma_g(\mathbf{x})\Big]\Big]\\
&=\prod_{i=5}^{6}(\Delta+\lambda_i^2)\Big[\sum_{g=5}^{6}r_{1g}\Big[\prod_{j=1}^{4}(\lambda_j^2-\lambda_g^2)\Big]\varsigma_g(\mathbf{x})\Big]\\
&=(\Delta+\lambda_6^2)\Big[\sum_{g=5}^{6}r_{1g}\Big[\prod_{j=1}^{4}(\lambda_j^2-\lambda_g^2)\Big]\Big[\delta(\mathbf{x})+(\lambda_5^2-\lambda_g^2)\varsigma_g(\mathbf{x})\Big]\Big]\\
&=(\Delta+\lambda_6^2)\varsigma_6(\mathbf{x})=\delta(\mathbf{x}).
\end{aligned}$$

Equations (4.27) and (4.28) can be proved in a similar way.

We introduce the matrix

$$\mathbf{G}(\mathbf{x})=\mathbf{R}(\mathbf{D}_\mathbf{x})\mathbf{Y}(\mathbf{x}). \tag{4.32}$$

From equations (4.24), (4.25) and (4.32), we obtain

$$\mathbf{F}(\mathbf{D_x})\mathbf{G}(\mathbf{x}) = \mathbf{F}(\mathbf{D_x})\mathbf{R}(\mathbf{D_x})\mathbf{Y}(\mathbf{x}) = \mathbf{\Theta}(\Delta)\mathbf{Y}(\mathbf{x}) = \delta(\mathbf{x})\,\mathbf{I}(\mathbf{x}).$$

Hence, $\mathbf{G}(\mathbf{x})$ is a solution to the equation (3.4).

Theorem 1: If condition (3.3) is satisfied, then the fundamental solution of the system of equations (3.2) is the matrix $\mathbf{G}(\mathbf{x})$ given by equation (4.32) and it is represented as follows:

$$G_{gl}(\mathbf{x}) = R_{gl}(\mathbf{D_x})Y_{11}(\mathbf{x}), G_{gq}(\mathbf{x}) = R_{gq}(\mathbf{D_x})Y_{44}(\mathbf{x}), G_{gj}(\mathbf{x}) = R_{gj}(\mathbf{D_x})Y_{10;10}(\mathbf{x}),$$
$$g = 1, ..., 11; \quad l = 1, 2, 3; \quad q = 4, ..., 9; \quad j = 10, 11.$$

5. Basic Properties of Matrix $\mathbf{G}(\mathbf{x})$

Theorem 2: Each column of the matrix $\mathbf{G}(\mathbf{x})$ is a solution of system of equations (3.2) at every point $\mathbf{x} \in \mathrm{E}^3$ except at the origin.

Theorem 3: If the condition (3.3) is satisfied, then the fundamental solution of the system $\tilde{\mathbf{F}}(\mathbf{D_x})\mathbf{U}(\mathbf{x}) = \mathbf{0}$ is the matrix

$$\mathbf{B}(\mathbf{x}) = \Big(B_{rz}(\mathbf{x})\Big)_{11\times 11},$$
$$B_{ij}(\mathbf{x}) = \left[\frac{1}{\tilde{\lambda}}\frac{\partial^2}{\partial x_i \partial x_j} - \frac{1}{\mu}\tilde{R}_{ij}\right]\varsigma_2^*(\mathbf{x}),$$
$$B_{i+3;j+3}(\mathbf{x}) = \left[\frac{1}{k_7}\frac{\partial^2}{\partial x_i \partial x_j} - \frac{1}{k_6}\tilde{R}_{ij}\right]\varsigma_2^*(\mathbf{x}),$$
$$B_{i+6;j+6}(\mathbf{x}) = \left[\frac{1}{h_7}\frac{\partial^2}{\partial x_i \partial x_j} - \frac{1}{h_6}\tilde{R}_{ij}\right]\varsigma_2^*(\mathbf{x}),$$
$$B_{10;10} = \frac{\varsigma_1^*(\mathbf{x})}{k}, B_{11;11} = \frac{\varsigma_1^*(\mathbf{x})}{h}, B_{iq} = B_{qi} = 0, B_{i+3;l} = B_{l;i+3} = 0,$$
$$B_{i+6;d} = B_{d;i+6} = 0, B_{10;11} = B_{11;10} = 0, \varsigma_1^* = -\frac{1}{4\pi|\mathbf{x}|}, \varsigma_2^* = -\frac{|\mathbf{x}|}{8\pi},$$
$$\tilde{R}_{ij} = \frac{\partial^2}{\partial x_i \partial x_j} - \Delta\delta_{ij}, \quad i, j = 1, 2, 3; \quad q = 4, ..., 11; \quad l = 7, ..., 11; \quad d = 10, 11.$$

6. Fundamental Solutions of System of Equations in Equilibrium Theory

If we put $\omega = 0$ in the system of equations (3.2), we obtain the system of equations in equilibrium theory of thermoelastic diffusivity with microtemperatures and microconcentrations as:

$$[\mu\Delta + (\lambda_0 + \mu)\,\mathrm{grad\,div}]\mathbf{u} - \gamma_1\,\mathrm{grad}\,\theta - \gamma_2\,\mathrm{grad}\,P = \mathbf{0},$$
$$[k_6\Delta + (k_4 + k_5)\,\mathrm{grad\,div} - k_2]\mathbf{v} - k_3\,\mathrm{grad}\,\theta = \mathbf{0},$$
$$[h_6\Delta + (h_4 + h_5)\,\mathrm{grad\,div} - h_2]\mathbf{w} - h_3\,\mathrm{grad}\,P = \mathbf{0},$$

$$k_1 \operatorname{div} \mathbf{v} + k\,\Delta\,\theta = 0,$$
$$h_1 \operatorname{div} \mathbf{w} + h\,\Delta\,P = 0. \tag{6.1}$$

The second-order matrix differential operator with constant coefficients is introduced as:

$$\mathbf{E}(\mathbf{D_x}) = \Big(E_{gl}(\mathbf{D_x})\Big)_{11\times 11},$$

where matrix $\mathbf{E}(\mathbf{D_x})$ can be obtained from $\mathbf{F}(\mathbf{D_x})$ by taking $\omega = 0$.

The system of equations (6.1) can be represented as

$$\mathbf{E}(\mathbf{D_x})\mathbf{U}(\mathbf{x}) = \mathbf{0}.$$

Definition 3: The operator $\mathbf{E}(\mathbf{D_x})$ is said to be elliptic differential operator iff equation (3.3) is satisfied.

Definition 4: The fundamental solution of the system of equations (6.1) (the fundamental matrix of operator $\mathbf{E}$) is the matrix $\mathbf{G}'(\mathbf{x}) = \Big(G'_{gl}(\mathbf{x})\Big)_{11\times 11}$ satisfying condition

$$\mathbf{E}(\mathbf{D_x})\mathbf{G}'(\mathbf{x}) = \delta(\mathbf{x})\,\mathbf{I}(\mathbf{x}). \tag{6.2}$$

We consider the system of non-homogeneous equations

$$[\mu\Delta + (\lambda_0 + \mu)\operatorname{grad}\operatorname{div}]\mathbf{u} = \mathbf{H}', \tag{6.3}$$
$$[k_6\Delta + (k_4 + k_5)\operatorname{grad}\operatorname{div} - k_2]\mathbf{v} + k_1 \operatorname{grad}\theta = \mathbf{V}', \tag{6.4}$$
$$[h_6\Delta + (h_4 + h_5)\operatorname{grad}\operatorname{div} - h_2]\mathbf{w} + h_1 \operatorname{grad} P = \mathbf{W}', \tag{6.5}$$
$$-\gamma_1 \operatorname{div}\mathbf{u} - k_3 \operatorname{div}\mathbf{v} + k\,\Delta\,\theta = Z', \tag{6.6}$$
$$-\gamma_2 \operatorname{div}\mathbf{u} - h_3 \operatorname{div}\mathbf{w} + h\,\Delta\,P = X', \tag{6.7}$$

where $\mathbf{H}', \mathbf{V}', \mathbf{W}'$ are vector functions with three components on E^3; Z' and X' are scalar functions on E^3.

The system of equations (6.3)-(6.7) can also be written in the form

$$\mathbf{E}^{tr}(\mathbf{D_x})\mathbf{U}(\mathbf{x}) = \mathbf{Q}'(\mathbf{x}), \tag{6.8}$$

where $\mathbf{E}^{tr}$ is the transpose of matrix $\mathbf{E}$ and $\mathbf{Q}'(\mathbf{x}) = (\mathbf{H}', \mathbf{V}', \mathbf{W}', Z', X')$.

Applying operator div to the equations (6.3)-(6.5), we obtain

$$\Delta \operatorname{div}\mathbf{u} = \frac{1}{\tilde{\lambda}} \operatorname{div}\mathbf{H}' = \Phi_1, \tag{6.9}$$
$$(k_7\Delta - k_2)\operatorname{div}\mathbf{v} + k_1\,\Delta\,\theta = \operatorname{div}\mathbf{V}', \tag{6.10}$$
$$(h_7\Delta - h_2)\operatorname{div}\mathbf{w} + h_1\,\Delta\,P = \operatorname{div}\mathbf{W}'. \tag{6.11}$$

Using equation (6.6) in the equation (6.10), we get

$$\Delta(\Delta - D^2)\operatorname{div}\mathbf{v} = \Phi_2, \tag{6.12}$$

where D^2, and Φ_2 are given in Appendix D.

Using equation (6.7) in equation (6.11), we get

$$\Delta(\Delta - L^2)\,\mathrm{div}\,\mathbf{w} = \Phi_3, \tag{6.13}$$

where L^2, and Φ_3 are given in Appendix D.

Applying operators $\Delta(\Delta - D^2)$ and $\Delta(\Delta - L^2)$ to the equations (6.6) and (6.7), respectively and using equations (6.12) and (6.13), we get

$$\Delta^2(\Delta - D^2)\,\theta = \Phi_4, \tag{6.14}$$

$$\Delta^2(\Delta - L^2)\,P = \Phi_5, \tag{6.15}$$

where Φ_4, and Φ_5 are given in Appendix D.

Applying the operators $\Delta, \Delta^2(\Delta - D^2), \Delta^2(\Delta - L^2)$ to the equations (6.3), (6.4) and (6.5) respectively and using equations (6.9) and (6.12)-(6.15), we obtain

$$\begin{gathered}\Delta^2\,\mathbf{u} = \mathbf{\Phi}',\\ \Delta^2(\Delta - D^2)\left(\Delta - \frac{k_2}{k_6}\right)\mathbf{v} = \mathbf{\Phi}'',\\ \Delta^2(\Delta - L^2)\left(\Delta - \frac{h_2}{h_6}\right)\mathbf{v} = \mathbf{\Phi}''',\end{gathered} \tag{6.16}$$

where $\mathbf{\Phi}'$, $\mathbf{\Phi}''$, and $\mathbf{\Phi}'''$ are given in Appendix D.

From equations (6.14)-(6.16), we get

$$\mathbf{\Lambda}(\Delta)\,\mathbf{U}(\mathbf{x}) = \hat{\mathbf{\Phi}}(\mathbf{x}), \tag{6.17}$$

where $\mathbf{\Lambda}(\Delta)$, and $\hat{\mathbf{\Phi}}(\mathbf{x})$ are given in Appendix D.

The expressions for $\mathbf{\Phi}'$, $\mathbf{\Phi}''$, $\mathbf{\Phi}'''$, and Φ_p, $p = 4, 5$ can be rewritten as

$$\hat{\mathbf{\Phi}}(\mathbf{x}) = \mathbf{T}^{tr}(\mathbf{D_x})\mathbf{Q}'(\mathbf{x}), \tag{6.18}$$

where matrix $\mathbf{T}(\mathbf{D_x})$ is given in Appendix E.

From equations (6.8), (6.17) and (6.18), we get

$$\mathbf{E}(\mathbf{D_x})\mathbf{T}(\mathbf{D_x}) = \mathbf{\Lambda}(\Delta). \tag{6.19}$$

Let

$$\begin{gathered}\mathbf{Y}'(\mathbf{x}) = \Big(Y'_{ij}(\mathbf{x})\Big)_{11\times 11},\\ Y'_{pp}(\mathbf{x}) = \varsigma_2^*(\mathbf{x}),\ Y'_{p+3;p+3}(\mathbf{x}) = r'_{11}\varsigma_2^*(\mathbf{x}) + r'_{12}\varsigma_1^*(\mathbf{x}) + r'_{13}\varsigma_3^*(\mathbf{x}) + r'_{15}\varsigma_5^*(\mathbf{x}),\\ Y'_{p+6;p+6}(\mathbf{x}) = r'_{21}\varsigma_2^*(\mathbf{x}) + r'_{22}\varsigma_1^*(\mathbf{x}) + r'_{24}\varsigma_4^*(\mathbf{x}) + r'_{26}\varsigma_6^*(\mathbf{x}),\\ Y'_{10;10}(\mathbf{x}) = r'_{31}\varsigma_2^*(\mathbf{x}) + r'_{32}\varsigma_1^*(\mathbf{x}) + r'_{33}\varsigma_3^*(\mathbf{x}),\\ Y'_{11;11}(\mathbf{x}) = r'_{41}\varsigma_2^*(\mathbf{x}) + r'_{42}\varsigma_1^*(\mathbf{x}) + r'_{44}\varsigma_4^*(\mathbf{x}),\\ Y_{qz}(\mathbf{x}) = 0\ p = 1, 2, 3\ q, z = 1, \ldots.., 11\ q \neq z,\end{gathered}$$

where $\varsigma_i^*(\mathbf{x})$, $i = 3,...,6$, $r'_{1j}, j = 1,2,3,5$, $r'_{2q}, q = 1,2,4,6$, $r'_{3z}, z = 1,2,3$, and $r'_{1p}, p = 1,2,4$ are given in Appendix F.

Lemma 2: The matrix $\mathbf{Y}'$ defined above is the fundamental matrix of operator $\mathbf{\Lambda}(\Delta)$, i.e.

$$\mathbf{\Lambda}(\Delta)\mathbf{Y}'(\mathbf{x}) = \delta(\mathbf{x})\,\mathbf{I}(\mathbf{x}). \tag{6.20}$$

Proof: To prove the lemma, it is sufficient to prove that

$$\Delta^2 Y'_{11}(\mathbf{x}) = \delta(\mathbf{x}), \Delta^2(\Delta - D^2)(\Delta - \tau_1^2)Y'_{44}(\mathbf{x}) = \delta(\mathbf{x}), \Delta^2(\Delta - L^2)(\Delta - \tau_2^2)Y'_{77}(\mathbf{x}) = \delta(\mathbf{x}),$$
$$\Delta^2(\Delta - D^2)Y'_{10;10}(\mathbf{x}) = \delta(\mathbf{x}), \Delta^2(\Delta - L^2)Y'_{11;11}(\mathbf{x}) = \delta(\mathbf{x}). \tag{6.21}$$

It is very easy to prove equations (6.21). This has been left for the reader.

We introduce the matrix

$$\mathbf{G}'(\mathbf{x}) = \mathbf{T}(\mathbf{D_x})\mathbf{Y}'(\mathbf{x}). \tag{6.22}$$

From equations (6.19), (6.20) and (6.22), we obtain

$$\mathbf{E}(\mathbf{D_x})\mathbf{G}'(\mathbf{x}) = \delta(\mathbf{x})\mathbf{I}(\mathbf{x}).$$

Hence $\mathbf{G}'(\mathbf{x})$ is a solution to the equation (6.2).

Theorem 4: If the condition (3.3) is met, then the fundamental solution of the system of equations (6.1) is the matrix $\mathbf{G}'(\mathbf{x})$ given by the equation (6.22) and it can be represented in the following form:

$$G'_{gl}(\mathbf{x}) = T_{gl}(\mathbf{D_x})Y'_{11}(\mathbf{x}), G'_{g;l+3}(\mathbf{x}) = T_{g;l+3}(\mathbf{D_x})Y'_{44}(\mathbf{x}),$$
$$G'_{g;l+6}(\mathbf{x}) = T_{g;l+6}(\mathbf{D_x})Y'_{77}(\mathbf{x}), G'_{gj}(\mathbf{x}) = T_{gj}(\mathbf{D_x})Y'_{jj}(\mathbf{x}),$$
$$g = 1, ..., 11 \;\; l = 1,2,3 \;\; j = 10, 11.$$

7. Conclusions

In terms of elementary functions, the fundamental solution of system of equations in the theory of thermoelastic diffusive materials with microtemperatures and microconcentrations in the case of steady oscillations has been constructed. By potential method, the fundamental solution to the system of equations makes it possible to investigate three-dimensional boundary value problems of theory of thermoelastic diffusive materials with microtemperatures and microconcentrations. Some basic properties of the fundamental matrix are also discussed.

Appendix A

$$m = \frac{1}{\chi},\; \kappa = m\varpi,\; \gamma_1 = \beta_1 + \beta_2\kappa,\; \gamma_2 = \beta_2 m,\; \lambda_0 = \lambda - \beta_2\gamma_2,\; c = \frac{\rho C_E}{T_0} + \varpi\kappa$$

$$\mathbf{S} = (\operatorname{div}\mathbf{u}, \operatorname{div}\mathbf{v}, \operatorname{div}\mathbf{w}, \theta, P), \tilde{\mathbf{Q}} = (w_1, ..., w_5) = (\operatorname{div}\mathbf{H}, \operatorname{div}\mathbf{V}, \operatorname{div}\mathbf{W}, Z, X),$$

$$\mathbf{N}(\Delta) = \Big(N_{gl}(\Delta)\Big)_{5\times 5} =$$

$$= \begin{pmatrix} \tilde{\lambda}\Delta + \rho\omega^2 & 0 & 0 & \iota\omega\gamma_1 T_0\Delta & \iota\omega\gamma_2\Delta \\ 0 & k_7\Delta + k_8 & \iota\omega\kappa_1 & k_1\Delta & 0 \\ 0 & \iota\omega\kappa_1 & h_7\Delta + h_8 & 0 & h_1\Delta \\ -\gamma_1 & -k_3 & 0 & k\Delta + \iota\omega c T_0 & \iota\omega\kappa \\ -\gamma_2 & 0 & -h_3 & \iota\omega\kappa T_0 & h\Delta + \iota\omega m \end{pmatrix}_{5\times 5}$$

$$\mathbf{\Psi} = (\Psi_1, ..., \Psi_5), \Psi_p = \frac{1}{M^*}\sum_{i=1}^{5} N^*_{ip} w_i,$$

$$\Gamma_1(\Delta) = \frac{1}{M^*}\,|\,\mathbf{N}(\Delta)|,\;\; M^* = \tilde{\lambda} k k_7 h h_7, \quad p = 1, ..., 5$$

and N^*_{ip} is the cofactor of the element N_{ip} of the matrix $\mathbf{N}$.

$$\lambda_6^2 = \frac{\rho\omega^2}{\mu}, \mathbf{\Psi}' = \frac{1}{\mu}\Big[\Gamma_1(\Delta)\mathbf{H} - \operatorname{grad}[(\lambda_0 + \mu)\Psi_1 + \iota\omega\gamma_1 T_0\Psi_4 + \iota\omega\gamma_2\Psi_5]\Big],$$

$$\Gamma_2(\Delta) = \frac{1}{N^*}\begin{vmatrix} k_6\Delta + k_8 & \iota\omega\kappa_1 \\ \iota\omega\kappa_1 & h_6\Delta + h_8 \end{vmatrix},$$

$$N^* = k_6 h_6, \mathbf{\Psi}'' = \frac{1}{N^*}\Big[(h_6\Delta + h_8)[\Gamma_1(\Delta)\mathbf{V} - k_1 \operatorname{grad}\Psi_4 - (k_4 + k_5)\operatorname{grad}\Psi_2]$$

$$-\iota\omega\kappa_1[\Gamma_1(\Delta)\mathbf{W} - h_1 \operatorname{grad}\Psi_5 - (h_4 + h_5)\operatorname{grad}\Psi_3]\Big],$$

$$\mathbf{\Psi}''' = \frac{1}{N^*}\Big[(k_6\Delta + k_8)[\Gamma_1(\Delta)\mathbf{W} - h_1 \operatorname{grad}\Psi_5 - (h_4 + h_5)\operatorname{grad}\Psi_3]$$

$$-\iota\omega\kappa_1[\Gamma_1(\Delta)\mathbf{V} - k_1 \operatorname{grad}\Psi_4 - (k_4 + k_5)\operatorname{grad}\Psi_2]\Big]$$

Appendix B

$$\hat{\mathbf{\Psi}} = (\mathbf{\Psi}', \mathbf{\Psi}'', \mathbf{\Psi}''', \Psi_4, \Psi_5),$$

$$\mathbf{\Theta}(\Delta) = \Big(\Theta_{gq}(\Delta)\Big)_{11\times 11}$$

$$\Theta_{pp}(\Delta) = \Gamma_1(\Delta)(\Delta + \lambda_6^2) = \prod_{i=1}^{6}(\Delta + \lambda_i^2),$$

$$\Theta_{p+3;p+3}(\Delta) = \Theta_{p+6;p+6}(\Delta) = \Gamma_1(\Delta)\Gamma_2(\Delta) = \prod_{i=1, i\neq 6}^{8}(\Delta + \lambda_i^2),$$

$$\Theta_{jj}(\Delta) = \Gamma_1(\Delta) = \prod_{i=1}^{5}(\Delta + \lambda_i^2),\; \Theta_{gq}(\Delta) = 0,$$

$$p = 1, 2, 3; \quad g, q = 1, ..., 11; \quad j = 10, 11; \quad g \neq q$$

$$w_{p1}(\Delta) = -\frac{1}{M^*\mu}\Big[(\lambda_0 + \mu)N^*_{p1}(\Delta) + \iota\omega\gamma_1 T_0 N^*_{p4}(\Delta) + \iota\omega\gamma_2 N^*_{p5}(\Delta)\Big]$$

$$w_{p2}(\Delta) = -\frac{1}{M^*N^*}\Big[(h_6\Delta+h_8)[(k_4+k_5)N^*_{p2}+k_1N^*_{p4}]-\iota\omega\kappa_1h_1N^*_{p5}-\iota\omega\kappa_1(h_4+h_5)N^*_{p3}\Big]$$

$$w_{p3}(\Delta) = -\frac{1}{M^*N^*}\Big[(k_6\Delta+k_8)[(h_4+h_5)N^*_{p3}+h_1N^*_{p5}]-\iota\omega\kappa_1k_1N^*_{p4}-\iota\omega\kappa_1(k_4+k_5)N^*_{p2}\Big]$$

$$w_{p4}(\Delta) = \frac{N^*_{p4}}{M^*},\ w_{p5}(\Delta) = \frac{N^*_{p5}}{M^*}, \quad p = 1, ..., 5$$

$$\mathbf{R}(\mathbf{D_x}) = \Big(R_{gq}(\mathbf{D_x})\Big)_{11\times 11}$$

$$R_{ij}(\mathbf{D_x}) = \frac{1}{\mu}\Gamma_1(\Delta)\delta_{ij} + w_{11}(\Delta)\frac{\partial^2}{\partial x_i\partial x_j},$$

$$R_{i+3;j+3}(\mathbf{D_x}) = \frac{1}{N^*}(h_6\Delta + h_8)\Gamma_1(\Delta)\delta_{ij} + w_{22}(\Delta)\frac{\partial^2}{\partial x_i\partial x_j},$$

$$R_{i+6;j+6}(\mathbf{D_x}) = \frac{1}{N^*}(k_6\Delta + k_8)\Gamma_1(\Delta)\delta_{ij} + w_{33}(\Delta)\frac{\partial^2}{\partial x_i\partial x_j},$$

$$R_{i;j+3}(\mathbf{D_x}) = w_{12}(\Delta)\frac{\partial^2}{\partial x_i\partial x_j}, R_{i;j+6}(\mathbf{D_x}) = w_{13}(\Delta)\frac{\partial^2}{\partial x_i\partial x_j},$$

$$R_{i;p+6}(\mathbf{D_x}) = w_{1p}(\Delta)\frac{\partial}{\partial x_i}, R_{i+3;j}(\mathbf{D_x}) = w_{21}(\Delta)\frac{\partial^2}{\partial x_i\partial x_j},$$

$$R_{i+3;j+6}(\mathbf{D_x}) = w_{23}(\Delta)\frac{\partial^2}{\partial x_i\partial x_j} - \frac{1}{N^*}\iota\omega\kappa_1\Gamma_1(\Delta)\delta_{ij},$$

$$R_{i+3;p+6}(\mathbf{D_x}) = w_{2p}(\Delta)\frac{\partial}{\partial x_i}, R_{i+6;j} = w_{31}(\Delta)\frac{\partial^2}{\partial x_i\partial x_j},$$

$$R_{i+6;j+3}(\mathbf{D_x}) = w_{32}(\Delta)\frac{\partial^2}{\partial x_i\partial x_j} - \frac{1}{N^*}\iota\omega\kappa_1\Gamma_1(\Delta)\delta_{ij},$$

$$R_{i+6;p+6}(\mathbf{D_x}) = w_{3p}(\Delta)\frac{\partial}{\partial x_i}, R_{p+6;i}(\mathbf{D_x}) = w_{p1}(\Delta)\frac{\partial}{\partial x_i},$$

$$R_{p+6;i+3}(\mathbf{D_x}) = w_{p2}(\Delta)\frac{\partial}{\partial x_i}, R_{p+6;i+6}(\mathbf{D_x}) = w_{p3}(\Delta)\frac{\partial}{\partial x_i},$$

$$R_{p+6;l+6} = w_{pl}(\Delta), \ \ i,j = 1,2,3; \ \ p,l = 4,5$$

Appendix C

$$\varsigma_g(\mathbf{x}) = -\frac{e^{\iota\lambda_g|\mathbf{x}|}}{4\pi|\mathbf{x}|}, r_{1p} = \prod_{i=1,i\neq p}^{6}(\lambda_i^2-\lambda_p^2)^{-1}, r_{2l} = \prod_{i=1,i\neq 6,i\neq l}^{8}(\lambda_i^2-\lambda_l^2)^{-1},$$

$$r_{3q} = \prod_{i=1,i\neq q}^{5}(\lambda_i^2-\lambda_q^2)^{-1}, \ \ p = 1, ..., 6; \ \ g = 1, ..., 8; \ \ l = 1, ...7, 8; \ \ q = 1, ..., 5$$

$$z_1 = \prod_{i=3}^{6}(\lambda_2^2-\lambda_i^2)\prod_{j=4}^{6}(\lambda_3^2-\lambda_j^2)\prod_{l=5}^{6}(\lambda_4^2-\lambda_l^2)(\lambda_5^2-\lambda_6^2),$$

$$z_2 = \prod_{i=3}^{6}(\lambda_1^2 - \lambda_i^2) \prod_{j=4}^{6}(\lambda_3^2 - \lambda_j^2) \prod_{l=5}^{6}(\lambda_4^2 - \lambda_l^2)(\lambda_5^2 - \lambda_6^2),$$

$$z_3 = \prod_{i=2, i\neq 3}^{6}(\lambda_1^2 - \lambda_i^2) \prod_{j=4}^{6}(\lambda_2^2 - \lambda_j^2) \prod_{l=5}^{6}(\lambda_4^2 - \lambda_l^2)(\lambda_5^2 - \lambda_6^2),$$

$$z_4 = \prod_{i=2, i\neq 4}^{6}(\lambda_1^2 - \lambda_i^2) \prod_{j=3, j\neq 4}^{6}(\lambda_2^2 - \lambda_j^2) \prod_{l=5}^{6}(\lambda_3^2 - \lambda_l^2)(\lambda_5^2 - \lambda_6^2),$$

$$z_5 = \prod_{i=2, i\neq 5}^{6}(\lambda_1^2 - \lambda_i^2) \prod_{j=3, j\neq 5}^{6}(\lambda_2^2 - \lambda_j^2) \prod_{l=4, l\neq 5}^{6}(\lambda_3^2 - \lambda_l^2)(\lambda_4^2 - \lambda_6^2),$$

$$z_6 = \prod_{i=2}^{5}(\lambda_1^2 - \lambda_i^2) \prod_{j=3}^{5}(\lambda_2^2 - \lambda_j^2) \prod_{l=4}^{5}(\lambda_3^2 - \lambda_l^2)(\lambda_4^2 - \lambda_5^2),$$

$$z_7 = \prod_{i=2}^{6}(\lambda_1^2 - \lambda_i^2) \prod_{j=3}^{6}(\lambda_2^2 - \lambda_j^2) \prod_{l=4}^{6}(\lambda_3^2 - \lambda_l^2) \prod_{p=5}^{6}(\lambda_4^2 - \lambda_p^2)(\lambda_5^2 - \lambda_6^2).$$

Appendix D

$$D^2 = \frac{1}{k\,k_7}(k\,k_2 - k_3 k_1), \Phi_2 = \frac{1}{k\,k_7}[k\,\Delta\,\mathrm{div}\,\mathbf{V}' - k_1\gamma_1\Phi_1 - k_1\,\Delta\,Z'],$$

$$L^2 = \frac{1}{h\,h_7}(h\,h_2 - h_3 h_1), \Phi_3 = \frac{1}{h\,h_7}[h\,\Delta\,\mathrm{div}\,\mathbf{W}' - h_1\gamma_2\Phi_1 - h_1\,\Delta\,X'],$$

$$\Phi_4 = \frac{1}{k}[k_3\,\Phi_2 + (\Delta - D^2)(\Delta\,Z' + \gamma_1\Phi_1)], \Phi_5 = \frac{1}{h}[h_3\,\Phi_3 + (\Delta - L^2)(\Delta\,X' + \gamma_2\Phi_1)],$$

$$\mathbf{\Phi}' = \frac{1}{\mu}[\Delta\,\mathbf{H}' - (\lambda_0 + \mu)\,\mathrm{grad}\,\Phi_1]$$

$$\mathbf{\Phi}'' = -\frac{\gamma_1 k_1}{k\,k_7}\left(\Delta - \frac{k_2}{k_6}\right)\mathrm{grad}\,\Phi_1 - \frac{k_1}{k\,k_7}\left(\Delta - \frac{k_2}{k_6}\right)\mathrm{grad}\,\Delta\,Z' +$$
$$\frac{1}{k_6}\left[\Delta^2(\Delta - D^2) - \frac{1}{k\,k_7}\left\{(k_4 + k_5)k\,\Delta + k_1 k_3\right\}\Delta\,\mathrm{grad}\,\mathrm{div}\right]\mathbf{V}'$$

$$\mathbf{\Phi}''' = -\frac{\gamma_2 h_1}{h\,h_7}\left(\Delta - \frac{h_2}{h_6}\right)\mathrm{grad}\,\Phi_1 - \frac{h_1}{h\,h_7}\left(\Delta - \frac{h_2}{h_6}\right)\mathrm{grad}\,\Delta\,X' +$$
$$\frac{1}{h_6}\left[\Delta^2(\Delta - L^2) - \frac{1}{h\,h_7}\left\{(h_4 + h_5)h\,\Delta + h_1 h_3\right\}\Delta\,\mathrm{grad}\,\mathrm{div}\right]\mathbf{W}',$$

$$\hat{\mathbf{\Phi}}(\mathbf{x}) = (\mathbf{\Phi}', \mathbf{\Phi}'', \mathbf{\Phi}''', \Phi_4, \Phi_5), \mathbf{\Lambda}(\Delta) = \Big(\Lambda_{pq}(\Delta)\Big)_{11\times 11}$$

$$\Lambda_{ii}(\Delta) = \Delta^2, \Lambda_{i+3;i+3}(\Delta) = \Delta^2(\Delta - D^2)\left(\Delta - \frac{k_2}{k_6}\right),$$

$$\Lambda_{i+6;i+6}(\Delta) = \Delta^2(\Delta - L^2)\left(\Delta - \frac{h_2}{h_6}\right), \quad \Lambda_{10;10} = \Delta^2(\Delta - D^2),$$

$$\Lambda_{11;11} = \Delta^2(\Delta - L^2), \quad \Lambda_{lj} = 0, \quad i,j = 1,2,3; \quad l,j = 1,......,11; \quad l \neq j$$

Appendix E

$$\mathbf{T}(\mathbf{D_x}) = \Big(T_{gl}(\mathbf{D_x})\Big)_{11\times 11}$$

$$T_{ij}(\mathbf{D_x}) = \frac{1}{\mu}\,\Delta\,\delta_{ij} + m_{11}(\Delta)\frac{\partial^2}{\partial x_i \partial x_j},$$

$$T_{i+3;j+3}(\mathbf{D_x}) = \frac{1}{k_6}\,\Delta^2(\Delta - D^2)\,\delta_{ij} + m_{22}(\Delta)\frac{\partial^2}{\partial x_i \partial x_j},$$

$$T_{i+6;j+6}(\mathbf{D_x}) = \frac{1}{h_6}\,\Delta^2(\Delta - L^2)\,\delta_{ij} + m_{22}(\Delta)\frac{\partial^2}{\partial x_i \partial x_j},$$

$$T_{10;10}(\mathbf{D_x}) = m_{44}(\Delta),\ T_{11;11}(\mathbf{D_x}) = m_{55}(\Delta),\ T_{i;j+3}(\mathbf{D_x}) = m_{12}(\Delta)\frac{\partial^2}{\partial x_i \partial x_j},$$

$$T_{i;j+6}(\mathbf{D_x}) = m_{13}(\Delta)\frac{\partial^2}{\partial x_i \partial x_j},\ T_{i;10}(\mathbf{D_x}) = m_{14}(\Delta)\frac{\partial}{\partial x_i},\ T_{i;11}(\mathbf{D_x}) = m_{15}(\Delta)\frac{\partial}{\partial x_i},$$

$$T_{i+3;j}(\mathbf{D_x}) = T_{i+3;j+6}(\mathbf{D_x}) = T_{i+3;11}(\mathbf{D_x}) = 0, \quad T_{i+3;10}(\mathbf{D_x}) = m_{24}(\Delta)\frac{\partial}{\partial x_i},$$

$$T_{i+6;j}(\mathbf{D_x}) = T_{i+6;j+3}(\mathbf{D_x}) = T_{i+6;10}(\mathbf{D_x}) = 0, \quad T_{i+6;11}(\mathbf{D_x}) = m_{35}(\Delta)\frac{\partial}{\partial x_i},$$

$$T_{10;i}(\mathbf{D_x}) = T_{10;i+6}(\mathbf{D_x}) = T_{10;11}(\mathbf{D_x}) = 0, \quad T_{10;i+3}(\mathbf{D_x}) = m_{42}(\Delta)\frac{\partial}{\partial x_i},$$

$$T_{11;i}(\mathbf{D_x}) = T_{11;i+3}(\mathbf{D_x}) = T_{11;10}(\mathbf{D_x}) = 0, \quad T_{11;i+6}(\mathbf{D_x}) = m_{53}(\Delta)\frac{\partial}{\partial x_i},$$

$$m_{11}(\Delta) = -\frac{\lambda_0 + \mu}{\mu\tilde{\lambda}}, \quad m_{22}(\Delta) = -\frac{\Delta[k(k_4 + k_5)\Delta + k_1 k_3]}{k\,k_6\,k_7},$$

$$m_{33}(\Delta) = -\frac{\Delta[h(h_4 + h_5)\Delta + h_1 h_3]}{h\,h_6\,h_7}, \quad m_{44}(\Delta) = \frac{\Delta(k_7\Delta - k_2)}{k\,k_7},$$

$$m_{55}(\Delta) = \frac{\Delta(h_7\Delta - h_2)}{h\,h_7}, \quad m_{12}(\Delta) = -\frac{k_1\gamma_1(\Delta - \frac{k_2}{k_6})}{\tilde{\lambda}\,k\,k_7},$$

$$m_{13}(\Delta) = -\frac{h_1\gamma_2(\Delta - \frac{h_2}{h_6})}{\tilde{\lambda}\,h\,h_7}, \quad m_{14}(\Delta) = \frac{\gamma_1(k_7\,\Delta - k_2)}{\tilde{\lambda}\,k\,k_7},$$

$$m_{15}(\Delta) = \frac{\gamma_2(h_7\,\Delta - h_2)}{\tilde{\lambda}\,h\,h_7}, \quad m_{24}(\Delta) = \frac{k_3\,\Delta}{k\,k_7}, \quad m_{35}(\Delta) = \frac{h_3\,\Delta}{h\,h_7},$$

$$m_{42}(\Delta) = -\frac{k\,\Delta(\Delta - \frac{k_2}{k_6})}{k\,k_7}, \quad m_{53}(\Delta) = -\frac{h\,\Delta(\Delta - \frac{h_2}{h_6})}{h\,h_7}, \quad i, j = 1, 2, 3$$

Appendix F

$$\varsigma_3^*(\mathbf{x}) = -\frac{e^{-D|\mathbf{x}|}}{4\pi|\mathbf{x}|},\ \varsigma_4^*(\mathbf{x}) = -\frac{e^{-L|\mathbf{x}|}}{4\pi|\mathbf{x}|},\ \varsigma_5^*(\mathbf{x}) = -\frac{e^{-\tau_1|\mathbf{x}|}}{4\pi|\mathbf{x}|},\ \varsigma_6^*(\mathbf{x}) = -\frac{e^{-\tau_2|\mathbf{x}|}}{4\pi|\mathbf{x}|},$$

$$r'_{11} = \frac{1}{D^2\tau_1^2},\ r'_{12} = \frac{D^2 + \tau_1^2}{D^4\tau_1^4},\ r'_{13} = \frac{1}{D^4(D^2 - \tau_1^2)},\ r'_{15} = \frac{1}{\tau_1^4(\tau_1^2 - D^2)},$$

$$r'_{21} = \frac{1}{L^2\tau_2^2},\ r'_{22} = \frac{L^2+\tau_2^2}{L^4\tau_2^4},\ r'_{24} = \frac{1}{L^4(L^2-\tau_2^2)},\ r'_{26} = \frac{1}{\tau_2^4(\tau_2^2-L^2)},$$
$$r'_{31} = -\frac{1}{D^2},\ r'_{32} = -r'_{33} = -\frac{1}{D^4},\ r'_{41} = -\frac{1}{L^2},\ r'_{42} = -r'_{44} = -\frac{1}{L^4},$$
$$\tau_1^2 = \frac{k_2}{k_6},\ \tau_2^2 = \frac{h_2}{h_6}.$$

References

1. Eringen, A. C. "Simple microfluids." *International Journal of Engineering Science,* **2**, (1964), pp. 205–217. doi: 10.1016/0020-7225(64)90005-9.
2. Eringen, A. C. and Suhubi, E. S. "Nonlinear theory of simple microelastic solids - I." *International Journal of Engineering Science,* **2**, (1964), pp. 189–203. doi: 10.1016/0020-7225(64)90004-7.
3. Eringen, A. C. and Suhubi, E. S. "Nonlinear theory of simple microelastic solids - II." *International Journal of Engineering Science,* **2**, (1964), pp. 389–403. doi: 10.1016/0020-7225(64)90017-5.
4. Eringen, A. C. *Mechanics of Micromorphic Continua.* Springer-Verlag, Berlin, 1968. doi: 10.1007/978-3-662-30257-6_2.
5. Eringen, A. C. "Balance laws of micromorphic mechanics." *International Journal of Engineering Science,* **8**, (1970), pp. 819–828. doi: 10.1016/0020-7225(70)90084-4.
6. Eringen, A. C. and Kafadar, C. B. *Polar Field Theories in A.C. Eringen Edition.* New York: Academic Press, 1970.
7. A. C. Eringen. *Microcontinuum Field Theories I: Foundations and Solids.* Springer Verlag, Berlin, 1999. doi: 10.1007/978-1-4612-0555-5.
8. Grot, R. A. "Thermodynamics of a continuum with microstructure." *International Journal of Engineering Science,* **7**, (1969), pp. 801–814. doi: 10.1016/0020-7225(69)90062-7.
9. Iesan, D. and Quintanilla, R. "On a theory of thermoelasticity with microtemperatures." *Journal of Thermal Stresses,* **23**, (2000), pp. 199–215. doi: 10.1080/014957300280407.
10. Iesan, D. "On a theory of micromorphic elastic solids with microtemperatures." *Journal of Thermal Stresses,* **24**, (2001), pp. 737–752. doi: DOI : 10 . 1080 / 014957301300324882.
11. Iesan, D. "Thermoelasticity of bodies with microstructure and microtemperatures." *International Journal of Solids and Structures,* **44**, (2007), pp. 8648–8662. doi: 10.1016/j.ijsolstr.2007.06.027.
12. Nowacki, W. "Dynamical problems of thermodiffusion in solids-I." *Bulletin of the Polish Academy of Sciences: Technical Sciences,* **22**, (1974), pp. 55–64.
13. Nowacki, W. "Dynamical problems of thermodiffusion in solids-II." *Bulletin of the Polish Academy of Sciences: Technical Sciences,* **22**, (1974), pp. 205–211.
14. Nowacki, W. "Dynamical problems of thermodiffusion in solids-III." *Bulletin of the Polish Academy of Sciences: Technical Sciences,* **22**, (1974), pp. 257–266.

15. Nowacki, W. "Dynamical problems of thermodiffusion in solids." *Engineering Fracture Mechanics,* **8**, (1976), pp. 261–266. doi: 10.1016/0013-7944(76)90091-6.
16. Sherief, H. H., Hamza, F. A., and Saleh, H. A. "The theory of generalized thermoelastic diffusion." *International Journal of Engineering Science,* **42**, (2004), pp. 591–608. doi: 10.1016/j.ijengsci.2003.05.001.
17. Aouadi, M. "Generalized theory of thermoelastic diffusion for anisotropic media." *Journal of Thermal Stresses,* **31**, (2008), pp. 270–285. doi: 10.1080/01495730701876742.
18. Kansal, T. and Kumar, R. "Variational principle, uniqueness and reciprocity theorems in the theory of generalized thermoelastic diffusion material." *Qscience connect,* **2013**(1), (2013), pp. 1–18. doi: 10.5339/connect.2013.27.
19. Aouadi, M., Ciarletta M., and Tibullo, V. "A thermoelastic diffusion theory with microtemperatures and microconcentrations." *Journal of Thermal Stresses,* **40**, (2017), pp. 486–501. doi: 10.1080/01495739.2016.1225271.
20. Bazarra, N., Campo, M., and FernÁndez, J. R. "A thermoelastic problem with diffusion, microtemperatures, and microconcentrations." *Acta Mechanica,* **230**, (2019), pp. 31–48. doi: 10.1007/s00707-018-2273-5.
21. Chirilă, A. and Marin, M. "Diffusion in microstretch thermoelasticity with microtemperatures and microconcentrations." *Models and Theories in Social Systems*. Ed. by C. Flaut, Š. Hošková-Mayerová, and D. Flaut. Cham: Springer International Publishing, 2019, pp. 149–164. doi: 10.1007/978-3-030-00084-4_8.
22. Kupradze V. D., Gegelia T. G., Basheleishvili M. O., and Burchuladze T. V. *Three-dimensional Problems of the Mathematical Theory of Elasticity and Thermoelasticity*. Amsterdam, New York, Oxford: North-Holland, Company, 1979. doi: 10.1115/1.3153629.
23. Svanadze, M. "Fundamental solutions of the equations of the theory of thermoelasticity with microtemperatures." *Journal of Thermal Stresses,* **27**, (2004), pp. 151–170.
24. Svanadze, M. "Fundamental solution in the theory of micromorphic elastic solids with microtemperatures." *Journal of Thermal Stresses,* **27**, (2004), pp. 345–366. doi: 10.1080/01495730490427582.
25. Kansal, T. "The theory of thermoelasticity with double porosity and microtemperatures." *Computational Methods in Science and Technology,* **28**, (2022), pp. 87–107. doi: 10.12921/cmst.2022.0000016.

Journal of Computational and Applied Mechanics, Vol. 17, No. 2, (2022), pp. 105–123
DOI: 10.32973/jcam.2022.006

INVESTIGATION OF MICRO-SHOCK WAVES IN A PLANAR MAGNETOGASDYNAMIC FLOW USING THE DISCONTINUOUS GALERKIN FINITE ELEMENT METHOD

Alberto Gallottini
Centre for Computational Engineering Sciences, Cranfield University, Cranfield, Bedfordshire, MK43 0AL, United Kingdom
alberto.gallottini@cranfield.ac.uk

László Könözsy
Centre for Computational Engineering Sciences, Cranfield University, Cranfield, Bedfordshire, MK43 0AL, United Kingdom
laszlo.konozsy@cranfield.ac.uk

[Received: October 24, 2022; Accepted: December 21, 2022]

Abstract. The present work focuses on the numerical investigation of micro-shock wave propagation in a two-dimensional magnetogasdynamic flow in the framework of the Discontinuous Galerkin-Finite Element Method (DG-FEM). The Lorentz force has been implemented in the compressible, viscous Navier–Stokes equations as a source term using first-order spatial and fourth-order temporal Runge–Kutta discretization schemes. To investigate the effect of the electrical conductivity on the micro-shock wave propagation, a two-dimensional micro-shock channel problem with hydraulic diameter of 2.5 mm, length of 82 mm, and no-slip boundary conditions at the left and at the right wall is considered as a benchmark problem. In this case, acoustic waves are generated behind after the rupture of the membrane that separates two states of the same gas originally at different pressure and density and both initially at rest. The magnetic field is taken into account as uniform and stationary throughout the microchannel, and the numerical simulations are performed in a short physical time, before the reflection of the waves on the lateral wall. A detailed parametric study of the temperature, density, pressure, and u-velocity is carried out by a variation of the electrical conductivity of the magnetogasdynamic flow, under the assumption of low magnetic Reynolds numbers. It has been found that the jumps of the acoustic waves become significantly intensified when the electrical conductivity of the gas is increased. It has also been observed that the presence of the Lorentz force causes an acceleration in the gasflow towards the outlet section of the microchannel at the low Knudsen number of 0.05. The outcome of this research work could be relevant to biomedical applications where the ability to control the flow in a microchannel has a significant impact on the development of small devices aimed to deliver pharmaceutical drugs in specific locations.

Mathematical Subject Classification: 76N30, 76M10, 76M12, 76W05
Keywords: Magnetogasdynamics, microfluidics, discontinuous Galerkin (DG) method

Nomenclature

Acronyms

DG-FEM	Discontinuous Galerkin-Finite Element Method
EHD	Electrohydrodynamics
FDM	Finite Difference Method
FEM	Finite Element Method
FVM	Finite Volume Method
IVP	Initial Value Problem
LSERK	Low Storage Explicit Runge–Kutta
MGD	Magnetogasdynamics
MHD	Magnetohydrodynamics
ODE	Ordinary Differential Equation
PDE	Partial Differential Equation

Greek Symbols

γ	Specific heat capacity	$[-]$
μ	Dynamic viscosity	$[\mathrm{Pa} \cdot \mathrm{s}]$
μ_0	Magnetic permeability	$[\mathrm{H/m}]$
Ω	Physical domain	$[\mathrm{m}^2]$
Ω_h	Computational domain	$[\mathrm{m}^2]$
ϕ_h	Test function	$[-]$
ρ	Fluid density	$[\mathrm{kg/m}^3]$
σ	Electrical conductivity	$[\mathrm{S/m}]$
$\underline{\underline{\tau}}$	Viscous stress tensor	$[\mathrm{Pa}]$
$\underline{\underline{S}}$	Rate-of-strain tensor	$[1/\mathrm{s}]$

Roman Symbols

$\bar{v}$	Mean velocity along the height of the microchannel	$[\mathrm{m/s}]$
ℓ	Characteristic length	$[\mathrm{m}]$
$\hat{\mathbf{n}}$	Normal unit vector	$[-]$
$\mathbf{B}$	Magnetic flux density	$[\mathrm{T}]$
$\mathbf{f}$	Flux vector	
$\mathbf{f}^*$	Numerical flux vector	
$\mathbf{f}_h$	Approximated flux vector	
$\mathbf{F}_L$	Lorentz force	$[\mathrm{N}]$
$\mathbf{j}$	Electric current density	$[\mathrm{A/m}^2]$
$\mathbf{u}$	Conservative variables vector	
$\mathbf{u}_h$	Approximated conservative variables vector	
$\mathbf{v}$	Velocity field of the fluid flow	$[\mathrm{m/s}]$
$\underline{\underline{I}}$	Unit tensor	$[-]$
D_k	k-th triangular element	$[\mathrm{m}^2]$
E	Total energy per unit volume	$[\mathrm{J/m}^3]$
F_{L_x}	x-component of the Lorentz force in Cartesian coordinates	$[\mathrm{N}]$
F_{L_y}	y-component of the Lorentz force in Cartesian coordinates	$[\mathrm{N}]$
H_y	y-component of the magnetic field intensity	$[\mathrm{T}]$
k	Thermal conductivity coefficient	$[\mathrm{W/(m \cdot K)}]$
l_i^k	Multidimensional Lagrange polynomial	$[-]$
Re_m	Magnetic Reynolds number	$[-]$
u, v	Velocity components in Cartesian coordinates	$[\mathrm{m/s}]$

1. Introduction

Magnetohydrodynamics (MHD), [1, 2] including magnetogasdynamics (MGD), has attracted the attention of researchers in the last decade in relation to the growing field of microfluidics applications. The reason is that it is possible to replicate many of the traditional analyses in a single chip made in a chemical laboratory through the integration of several components (e.g., microchannel, micropumps, mixers and microvalves). Among all the different industries, lab on a chip devices are particularly used in the biomedical area as drug delivery systems or for manipulation of cells and detection of small analytes. These portable and low-cost devices are used, for instance, to detect and isolate the rare circulating tumour cells (CTCs) detached from a primary tumour [3] or to perform a DNA sequencing analysis [4]. Magnetic drug targeting is a promising treatment to avoid the collateral effect of a cancer drug by adopting magnetic nanocarriers which are tied to the drug and then delivered to the specific tissue through the application of an external magnetic field [5]. Therefore, in this work, a magnetogasdynamic microflow benchmark problem is investigated to understand better the physics of micro-shock wave propagation in the presence of a uniform and stationary magnetic field, which could be relevant to biomedical applications. It could be important in applications where the ability to control the gasflow in a microchannel has an impact on the development of microfluidic devices aimed to deliver pharmaceutical drugs in specific locations.

In comparison with macroscopic fluid dynamics, shrinking the length of a device can change the physical and chemical behavior of fluids quite intensively, allowing interesting phenomena such as electrokinetics, magnetohydrodynamics, and capillarity effects that are not necessarily present in macro-scale fluid dynamics. It is reported in the literature that the micropolar fluid theory [6, 7], an augmented version of the Navier–Stokes equations, may be advantageous for experiments in microchannels. As the characteristic length of a device decreases, the Reynolds number becomes smaller, typically between 1 and 10, with mass transport phenomena led by viscosity rather than inertial forces, as would occur at the macro-scale. At a low Reynolds number, turbulent mixing is neglected and two different fluids can only mix by pure diffusion with a long diffusion time, which can be advantageous in the fabrication of a three-electrode system inside the microchannels [8] and disadvantageous in the case of protein folding, where some optimization algorithms must be developed to minimize the mixing time [9]. An exhaustive review of the physics of microfluidics with special emphasis on biotechnology can be found in [10]. One of the most frequently used applications of MHD flows in the scientific and engineering community is the development of devices where the electromagnetic field is used to drive the flow inside a channel. In contrast to macro-scale mechanical pumps where moving parts as actuators are used to pump the flow, non-mechanical pumps as using electrohydrodynamics (EHD) [11, 12] or electrokinetics [13] are increasingly being used in microfluidics for their simplicity of fabrication and the absence of fatigue problems compared to the traditional micropump. Moreover, both the direct current (DC) [14–16] and the alternate current (AC) [17] MHD micropumps have additional advantages such as lower actuation voltages, continuous and bi-directional fluid flow, and the ability to pump fluids with medium and high electrical conductivity. For example, a common problem for the DC micropump includes the degradation of the electrodes by the Faradaic process, the formation of bubbles due to electrolysis when the aqueous solution is used as a working fluid, and the Joule heating effect. In the AC-MHD micropump, the formation of bubbles does not occur, and the presence of additional eddy currents increases the Joule heating, which limits the intensity of the magnetic field at high frequencies [18]. The working principle for MHD micropumps is given by the Lorentz force

$$\mathbf{F}_L = \mathbf{j} \times \mathbf{B}, \tag{1.1}$$

where $\mathbf{j}$ is the electric current density of the flow and $\mathbf{B}$ is the magnetic flux density. This force is generated by the interaction between the external magnetic field by means of permanent magnets or electromagnets, and the electric current through mutually orthogonal electrodes. When the fluid flow moves with the velocity $\mathbf{v}$, the electrical current density $\mathbf{j}$ can be expressed as

$$\mathbf{j} = \sigma(\mathbf{E} + \mathbf{v} \times \mathbf{B}), \tag{1.2}$$

which means that the Lorentz force (1.1) becomes

$$\mathbf{F}_L = \sigma(\mathbf{E} + \mathbf{v} \times \mathbf{B}) \times \mathbf{B}, \tag{1.3}$$

where σ is the electrical conductivity of the flow. It is important to highlight that most of the numerical investigations of the fluid flow inside an MHD micropump have been carried out only for incompressible flows; however, the real fluid flow in place is compressible. Patel and Kassegne [19] developed a general numerical solver for three-dimensional MHD micropumps with a channel length of 20 mm, electrode length of 16 mm, electrical conductivity of 1.5 S/m and thermal conductivity of $0.6\,\mathrm{W/(m \cdot K)}$. They also investigated the effects of electroosmosis and Joule heating in a rectangular and trapezoidal microchannel. Wang et al. [20] investigated two-dimensional fully-developed stationary incompressible MHD flow with the use of the Finite Difference Method (FDM) for a channel of length 44 cm and electrode length of 35 mm in a saline solution (NaCl) with a conductivity of 1.5 S/m and in a liquidous Gallium (Ga) flow with an electrical conductivity of $7.30 \cdot 10^6\,\mathrm{S/m}$, concluding that the channel dimensions and the induced Lorentz forces have significant influences on the fluid flow velocity. Lim and Choi [21] solved the incompressible MHD equations with an in-house FDM based solver and with the commercial CFD-ACE Finite Volume Method (FVM) for a phosphate-buffered saline (PBS) solution inside a microchannel of length 30 mm with $\sigma = 1.5\,\mathrm{S/m}$. Hasan et al. [22] performed a comparative study on the performance of the micropump with different cross-sections through the Finite Element Method (FEM) using again the PBS solution as filling fluid. The Lattice Boltzmann Method (LBM) particle-based simulation of a two-dimensional incompressible transient flow and heat transfer phenomena for a DC-MHD micropump with a length of 22 mm was performed by Chatterjee and Amiroudine [23], showing the ability to extend the model for the investigation of a three-dimensional AC-MHD micropump. In the present work, we focus on a transient compressible, viscous fluid flow phenomenon, which can be called a magnetogasdynamic micro-shock wave propagation benchmark problem. Therefore, it is important to note that for both macrochannels and microchannels, the rupture of a membrane separating two states of a gas at different pressure and causes the formation of an unsteady flow composed by a fan of acoustic waves, i.e., shock, rarefaction and compression waves. These acoustic waves are extensively used for medical purposes, e.g., from non-invasive cancer treatment [24] to removal of kidney stones [25].

The physical behavior of shock wave propagation in compressible, viscous flows in macroscale channels has been widely studied both experimentally and numerically, although the knowledge is still not satisfactory on the simulation of micro-shock wave propagations at the microscale [26]. Furthermore, a knowledge gap can be identified in the investigation of compressible, viscous flows in a micro-shock benchmark channel where the electrically conducting gasflow is exposed to an external magnetic field. Therefore, the present work black attempts to contribute to this challenging research field through the numerical investigation of an electrically conducting compressible, viscous fluid flow in the case of a micro-shock channel benchmark problem where the gasflow is exposed to a uniform and stationary external magnetic field. In this work, the Lorentz force (1.1) has been added as a source term to the unsteady, fully compressible Navier–Stokes equations discretized with the nodal Discontinuous Galerkin-Finite Element Method (DG-FEM). For solving the governing equations discussed in Section 2, a DG-FEM based open-source MATLAB code has been used that was developed by Hesthaven and Warburton [27] and further improved for microfluidic gasflow applications by Zingaro and Könözsy [28].

2. Methodology

2.1. **Governing equations and their solution approach.** The conservative form of the two-dimensional governing equations for compressible, viscous Newtonian fluid flows can be formulated for the density ρ, x-momentum ρu, y-momentum ρv, the total energy E transport equation, and the total pressure p. For two-dimensional compressible flows, the scalar form of the continuity equation can be expressed by

$$\frac{\partial \rho}{\partial t} + \frac{\partial}{\partial x}(\rho u) + \frac{\partial}{\partial y}(\rho v) = 0, \tag{2.1}$$

the Navier–Stokes momentum equations for the velocity components u and v are

$$\frac{\partial}{\partial t}(\rho u) + \frac{\partial}{\partial x}(\rho u^2 + p) + \frac{\partial}{\partial y}(\rho u v) = \frac{\partial \tau_{xx}}{\partial x} + \frac{\partial \tau_{xy}}{\partial y} + \rho F_{L_x}, \tag{2.2}$$

$$\frac{\partial}{\partial t}(\rho v) + \frac{\partial}{\partial x}(\rho u v) + \frac{\partial}{\partial y}(\rho v^2 + p) = \frac{\partial \tau_{yx}}{\partial x} + \frac{\partial \tau_{yy}}{\partial y} + \rho F_{L_y}, \tag{2.3}$$

and the total energy equation transport equation can be written as

$$\frac{\partial E}{\partial t} + \frac{\partial}{\partial x}\left[(E+p)u\right] + \frac{\partial}{\partial y}\left[(E+p)v\right] = \frac{\partial}{\partial x}(\tau_{xx}u + \tau_{xy}v) + \frac{\partial}{\partial y}(\tau_{yx}u + \tau_{yy}v) +$$

$$+ \frac{\partial}{\partial x}\left(k\frac{\partial T}{\partial x}\right) + \frac{\partial}{\partial y}\left(k\frac{\partial T}{\partial y}\right) + \rho\left(F_{L_x}u + F_{L_y}v\right), \tag{2.4}$$

where k is the thermal conductivity coefficient. For compressible fluid flows, the viscous stress tensor based on the Navier–Stokes hypothesis is

$$\underline{\underline{\tau}} = 2\mu \underline{\underline{S}} - \frac{2}{3}\mu\left(\nabla\cdot\mathbf{v}\right)\underline{\underline{I}}, \tag{2.5}$$

where μ is the temperature dependent dynamic viscosity which can be computed by using the Sutherland law, see details in [28]. The rate-of-strain tensor $\underline{\underline{S}}$ in equation (2.5) can be expressed with vector notation as

$$\underline{\underline{S}} = \frac{1}{2}\left[(\nabla\otimes\mathbf{v}) + (\nabla\otimes\mathbf{v})^T\right], \tag{2.6}$$

where $\underline{\underline{I}}$ is the unit tensor. The elements of the viscous stress tensor (2.5) for two-dimensional compressible, viscous fluid flows are

$$\tau_{xx} = 2\mu\frac{\partial u}{\partial x} - \frac{2}{3}\mu\left(\frac{\partial u}{\partial x} + \frac{\partial v}{\partial y}\right), \tag{2.7}$$

$$\tau_{xy} = \tau_{yx} = \mu\left(\frac{\partial u}{\partial y} + \frac{\partial v}{\partial x}\right), \tag{2.8}$$

$$\tau_{yy} = 2\mu\frac{\partial v}{\partial y} - \frac{2}{3}\mu\left(\frac{\partial u}{\partial x} + \frac{\partial v}{\partial y}\right). \tag{2.9}$$

The total energy E can be expressed through the equation of state for ideal gases as

$$E = \frac{p}{\gamma - 1} + \frac{\rho}{2}(u^2 + v^2), \tag{2.10}$$

where γ is the specific heat capacity assumed here to be equal to 1.66 following the work of Zeitoun et al. [26] for a monoatomic gas. Based on the assumption that MHD flows are defined as electrically conducting fluids under the application of an external magnetic field, the external electrical field $\mathbf{E}$ is neglected in equation (1.2), thus the electrical current density is $\mathbf{j} = \sigma(\mathbf{v}\times\mathbf{B})$ in the present model. Therefore, the two-dimensional Lorentz force can be expressed as

$$\begin{cases} F_{L_x} = \sigma(-uB_y^2 + vB_xB_y), \\ F_{L_y} = \sigma(uB_xB_y - vB_x^2). \end{cases} \tag{2.11}$$

The set of governing equations (2.1)–(2.11) can be written in a compact form as

$$\frac{\partial\mathbf{u}}{\partial t} + \frac{\partial}{\partial x}(\mathbf{f}_c - \mathbf{f}_v) + \frac{\partial}{\partial y}(\mathbf{g}_c - \mathbf{g}_v) = \mathbf{s}, \tag{2.12}$$

where $\mathbf{u} = \mathbf{u}(\mathbf{x}, t) = [\rho, \rho u, \rho v, E]^T$ is the vector of the conservative variables, and

$$\mathbf{f}_c = \left[\rho u, \rho u^2 + p, \rho uv, (E+p)u\right]^T \quad \text{and} \quad \mathbf{f}_v = [0, \tau_{xx}, \tau_{yx}, \tau_{xx}u + \tau_{xy}v]^T$$

are the convective and viscous fluxes along the x and y directions, while

$$\mathbf{g}_c = \left[\rho v, \rho uv, \rho v^2 + p, (E+p)v\right]^T \quad \text{and} \quad \mathbf{g}_v = [0, \tau_{xy}, \tau_{yy}, \tau_{xy}u + \tau_{yy}v]^T,$$

and the vector $\mathbf{s} = \left[0, \rho F_{L_x}, \rho F_{L_y}, \rho(F_{L_x}u + F_{L_y}v)\right]^T$ expresses the source term. By incorporating the fluxes in a single matrix operator $\mathbf{f}$, the governing equations in the domain Ω are given by a system of coupled nonlinear mixed hyperbolic-parabolic partial differential equations (PDEs) as follows:

$$\frac{\partial \mathbf{u}}{\partial t} + \nabla \cdot \mathbf{f} = \mathbf{s}, \tag{2.13}$$

with an additional initial condition at time t_0 and boundary conditions on the boundary $\partial\Omega$. The numerical approximation of the problem above can be formulated as

$$\frac{\partial \mathbf{u}_h}{\partial t} + \nabla \cdot \mathbf{f}_h = \mathbf{s}_h, \tag{2.14}$$

where the numerical solution $\mathbf{u}_h$ and the spatial operator $\nabla \cdot \mathbf{f}_h$ have been discretized with the nodal DG-FEM scheme [27] and then temporally integrated with the fourth-order Runge–Kutta scheme [28]. Note that the verification of the implementation of the governing equations (2.1)–(2.4) was carried out by Zingaro and Könözsy [28] for another multiphysics problem in the framework of the nodal DG-FEM approach. However, the implementation of the magnetic force terms (2.11) with an investigation of the variation of the electrical conductivity σ for a magnetogasdynamic microflow at different magnetic Reynolds numbers is carried out in this work.

2.2. **Spatial discretization.** The physical domain of the microchannel $\Omega \in \mathbb{R}^2$ is replaced by the computational domain Ω_h composed by the union of K non-overlapping triangular elements D_k, with $k = 1 \dots K$. In each element, the local solution $\mathbf{u}_h^k(\mathbf{x}, t)$, belonging in the space

$$\mathbf{V}_h = \{\mathbf{v}_h \in (L^2(\Omega_h))^d : \mathbf{u}_{h|D_k} \in (\mathcal{P}_N)^d, \forall D_k \in D_h\}, \quad d = 2, \tag{2.15}$$

is approximated by

$$x \in D_k : \mathbf{u}_h^k(\mathbf{x}, t) = \sum_{i=1}^{N_p} \mathbf{u}_h^k(\mathbf{x}, t) l_i^k(\mathbf{x}), \tag{2.16}$$

where the N-th order piece-wise polynomial expansion of the local multidimensional Lagrange polynomial $l_i^k(\mathbf{x})$ is based on the grid points x_i with $N_p = \frac{(N+1)(N+2)}{2}$ unknown coefficient u_h^k. The global solution of the nonlinear system is recovered by the direct sum of K local polynomials $\mathbf{u}_h^k(\mathbf{x}, t)$ as follows:

$$\mathbf{u}(\mathbf{x}, t) \simeq \mathbf{u}_h(\mathbf{x}, t) = \bigoplus_{k=1}^{K} \mathbf{u}_h^k(\mathbf{x}, t). \tag{2.17}$$

To achieve accurate results with the numerical integration and differentiation, each triangle $\mathbf{x} \in D_k$ is mapped to a reference triangle $\mathbf{r} \in I_k \in [1, -1]$ through a linear mapping, thus the new local solution can be expressed by

$$x \in I_k : \mathbf{u}_h^k(\mathbf{r}, t) = \sum_{i=1}^{N_p} \mathbf{u}_h^k(\mathbf{r}_i, t) l_i^k(\mathbf{r}), \tag{2.18}$$

where the two-dimensional Legendre–Gauss–Lobatto grid points $\mathbf{r}_i$ are chosen to improve the quality of the local interpolating polynomial solution.

In the DG-FEM formulation, the governing equations (2.13) are satisfied elementwise through the L^2 orthogonality between the residual $\frac{\partial \mathbf{u}_h}{\partial t} + \nabla \cdot \mathbf{f}_h - \mathbf{s}_h$ and all the test functions $\phi_h(\mathbf{x}) \in \mathbf{V}_h$ which belong to the same functional space of the multidimensional Lagrange interpolating polynomial $l_i^k(\mathbf{x})$, thus

$$\int_{D_k} \left[\left(\frac{\partial \mathbf{u}_h^k}{\partial t} + \nabla \cdot \mathbf{f}_h - \mathbf{s}_h \right) \phi_h(\mathbf{x}) \right] d\mathbf{x} = \mathbf{0}. \tag{2.19}$$

By applying the Gauss theorem, the weak formulation of the DG-FEM is obtained as

$$\int_{D_k} \left[\frac{\partial \mathbf{u}_h^k}{\partial t} l_i^k(\mathbf{x}) - \mathbf{f}_h^k \cdot \nabla l_i^k(\mathbf{x}) - \mathbf{s}_h l_i^k(\mathbf{x}) \right] d\mathbf{x} = - \oint_{\partial D_k} \mathbf{f}^* \, l_i^k(\mathbf{x}) \cdot \hat{\mathbf{n}} d\mathbf{x}. \tag{2.20}$$

The choice of the numerical flux $\mathbf{f}^*$ term is essential for the accurate modeling of the physical problem, which ensures the stability of the scheme and the uniqueness of the solution at the interface of two adjacent elements. In this work, the local Lax-Friedrichs flux scheme [29] has been chosen for its simplicity. To avoid stability problems due to the spurious unphysical oscillations resulting from the large gradient flows, the slope limiter proposed by Tu and Aliabadi [30] has been employed black in this work. Note that for more accurate MHD flow simulations, i.e., to improve the accuracy of the solution, the Harten–Lax–van Leer Discontinuities (HLLD) approximate Riemann solver [31] can be implemented, which should be the subject of future work.

2.3. **Temporal discretization.** The Initial Value Problem (IVP) of the system of ordinary differential equations (ODEs) resulting from the spatial DG-FEM discretization $\mathcal{L}(\mathbf{u}_h, t)$ at time t_0 is

$$\begin{cases} \frac{d\mathbf{u}_h}{dt} = \mathcal{L}(\mathbf{u}_h, t), \\ \mathbf{u}_h(t_0) = \mathbf{u}_h^0, \end{cases} \tag{2.21}$$

which has been solved with a fourth-order Low Storage Explicit Runge–Kutta (LSERK) scheme from [32] as follows:

$$\begin{cases} \mathbf{p}^{(0)} = \mathbf{u}_h^n, \\ \text{for i } \in [1, ..., 5] : \begin{cases} \mathbf{k}^i = a_i \mathbf{k}^{(i-1)} + \Delta t \mathcal{L}_h(\mathbf{p}^{(i-1)}, t_n + c_i \Delta t), \\ \mathbf{p}^{(i)} = \mathbf{p}^{(i-1)} + b_i \mathbf{k}^i, \end{cases} \\ \mathbf{u}_h^{n+1} = \mathbf{p}^{(5)}. \end{cases} \tag{2.22}$$

The time integration scheme (2.22) guarantees the numerical stability for non-linear problems and is suitable for problems with shock waves and discontinuities. The coefficients in equation (2.22) and the equation for the time step can be found in [28].

2.4. **Source term discretization.** In the present numerical study, a uniform and a stationary external magnetic field is applied in the y spatial direction and it varies in its strength as a function of the x spatial coordinate, which is defined as

$$\mathbf{B} = (0, B_y(x), 0). \tag{2.23}$$

In the presence of homogenous media, the magnetic flux density $B_y(x)$ can be expressed as a linear function of the magnetic intensity $H_y(x)$ as

$$B_y(x) = \mu_0 H_y(x), \tag{2.24}$$

where μ_0 is the permeability of the medium. The mathematical expression for $H_y(x)$ has been taken from the work of Tzirtzilakis and Loukopoulos [33] as follows:

$$H_y(x) = \frac{H_0}{2}\left[\tanh(a_1(x - x_1)) - \tanh(a_2(x - x_2))\right], \tag{2.25}$$

where H_0 defines the magnitude of the magnetic intensity and the constants a_1 and a_2 specify the magnetic field gradient at the points x_1 and x_2, respectively.

2.5. **The benchmark test problem.** The viscous micro-shock channel benchmark problem proposed by Zeitoun et al. [26] has been adapted here in which case the variation of the electrical conductivity σ was neglected at different magnetic Reynolds numbers. Therefore, the viscous micro-shock channel test problem of Zeitoun et al. [26] can be considered as a reference test case for our study, because our aim is to investigate the effect of the variation of the electrical conductivity σ on a magnetogasdynamic microflow at different magnetic Reynolds numbers. The schematic of the viscous micro-shock channel benchmark problem is shown in Figure 1.

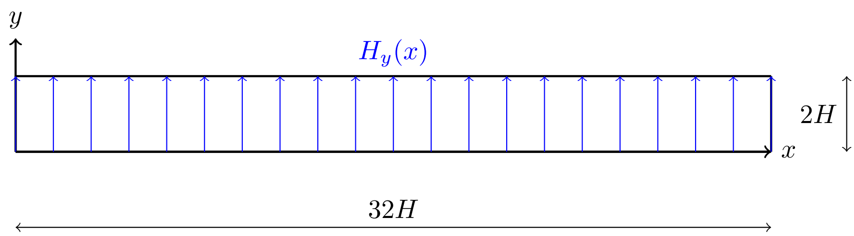

Figure 1. The geometry of the microchannel with the hydraulic diameter of $H = 2.55$ mm to investigate a magnetogasdynamic flow

At the initial time $t_0 = 0$ s, the gas is separated by one membrane positioned at $x_d = 29.69$ mm into two states, whose values for pressure and density are shown in Table 1 following the previous work of Zingaro and Könözsy [28].

ρ_L [kg/m^3]	$8.43 \cdot 10^{-3}$
ρ_R [kg/m^3]	$7.08 \cdot 10^{-4}$
p_L [Pa]	525.98
p_R [Pa]	44.2

Table 1. Numerical values of pressure and density at the left (p_L, ρ_L) and right (p_R, ρ_R) section of the viscous micro-shock channel [28]

The initial conditions before and after the rupture of the membrane, taken from the previous work of Zeitoun et al. [26], are

$$\rho(x,y,0)=\begin{cases}\rho_L & x<x_d, \qquad (x_d=29.69\,\mathrm{mm}),\\ \rho_R & x\geq x_d,\end{cases} \tag{2.26}$$

$$u(x,y,0)=0, \tag{2.27}$$

$$v(x,y,0)=0, \tag{2.28}$$

$$p(x,y,0)=\begin{cases}p_L & x<x_d, \qquad (x_d=29.69\,\mathrm{mm}),\\ p_R & x\geq x_d,\end{cases} \tag{2.29}$$

and the boundary conditions are no-slip at the left and right walls of the microchannel. For this benchmark test problem, a grid convergence/mesh sensitivity study has already been carried out on different mesh sizes in the previous work of Zingaro and Könözsy [28] for the numerical solution of the compressible, viscous Navier–Stokes equations without the inclusion of the electromagnetic field (see Table 2). Therefore, the fine mesh employed by Zingaro and Könözsy [28] has also been adopted here, because an accurate numerical solution for the benchmark test problem of Zeitoun et al. [26] can be obtained [28]. The details of different grid size resolutions are shown in Table 2, where N_x and N_y are the number of grid points in x and y coordinates, and Δx and Δy are the grid spacing in x and y directions, respectively.

Mesh	N_x	N_y	Δx [mm]	Δy [mm]
Coarse	97	7	$8.33\cdot10^{-1}$	$8.33\cdot10^{-1}$
Medium	193	13	$4.17\cdot10^{-1}$	$4.17\cdot10^{-1}$
Fine	385	25	$2.08\cdot10^{-1}$	$2.08\cdot10^{-1}$

Table 2. Grid resolutions used in this study and in the previous work [28]

The simulations presented here have been performed with a first-order polynomial approximation for the spatial terms to ensure the monotonicity behavior of the discretization scheme with a fourth-order Low Storage Explicit Runge–Kutta (LSERK) scheme for the temporal part.

3. Results and Discussion

The investigation of the impact of the electromagnetic field on the viscous micro-shock channel is carried out through a variation of the flow conductivity σ which affects the magnetic Reynolds number defined as $Re_m=\sigma\mu_0\bar{v}\ell$, where $\mu_0=1.4\cdot10^{-6}$ H/m is the magnetic permeability, $\bar{v}=0.4$ m/s is the mean velocity along the height of the microchannel, and $\ell=2.5\cdot10^{-3}$ m is the characteristic length. The magnetic Reynolds number is defined as the ratio between the advective and diffusive forces of the magnetic field and in this work different low Re_m are computed through a variation of the electrical conductivity σ (see Table 3) in such a way that the low magnetic Reynolds number assumption [34], commonly used in microfluidics, holds. Furthermore, for the sake of simplicity, the thermal conductivity coefficient k is considered to be constant in the total energy equation (2.4) with the value of 0.0172 W/(mK).

Electrical conductivity σ [S/m]	**Magnetic Reynolds numbers [–]**
100	$1.4 \cdot 10^{-7}$
$1.0 \cdot 10^3$	$1.4 \cdot 10^{-6}$
$5.0 \cdot 10^3$	$7.0 \cdot 10^{-6}$
$10 \cdot 10^3$	$14 \cdot 10^{-6}$

Table 3. Magnetic Reynolds numbers Re_m computed based on different electrical conductivity coefficient σ

The low magnetic Reynolds number assumption [34] implies that at the current length, even in the presence of high electrical conductivity σ, the magnetic field exhibits a dissipative behavior that spreads out rather than being advected by the flow. To gain a better insight into the physical behavior of the acoustic waves generated behind and in front of the rupture of the membrane, the profiles of the relevant quantities are non-dimensionalized with their respective values of the driven section and extracted at the centerline ($y = H$) of the microchannel (see Figure 2). Furthermore, the physical time scale of the investigated experimental micro-shock channel benchmark problem of Zeitoun et al. [26] is extremely short, i.e., 80 μ; therefore, the analysis of the complex flow physics originating from the reflection of the acoustic waves against the lateral wall has not been addressed in the present work and it is recommended as a future topic of research.

It has been found that there are no visible effects of the electrical conductivity investigated for $\sigma = 100\,\mathrm{S/m}$; visible effects start from $\sigma = 1 \cdot 10^3\,\mathrm{S/m}$. As the electrical conductivity σ is further increased, all the variables change the characteristic behavior of their profiles substantially. Regarding the pressure (see Figure 2a), for $\sigma = 10 \cdot 10^3\,\mathrm{S/m}$, a strong and fast shock wave moves to the right, followed by a smooth expansion fan, while the contact discontinuity is no longer visible. Similar to the pressure, velocity and temperature profiles are subject to a rapid increase in the shock wave region, where again the flow is moves to the right of the microchannel (see Figures 2b and 2c). The increase in the temperature might be explained through the Joule heating effect, while the increase in the velocity can be explained based on the effect of the Lorentz force, which is able to accelerate the flow in the x spatial direction. The density profile is characterized by the presence of a constant state in the center of the shock tube with a consequent change in the position and the magnitude of the shock wave (see Figure 2d). Furthermore, a comparison can be plotted with the reference values taken from the work of Zeitoun et al. [26] for the temperature and density profiles in Figures 2c and 2d, respectively.

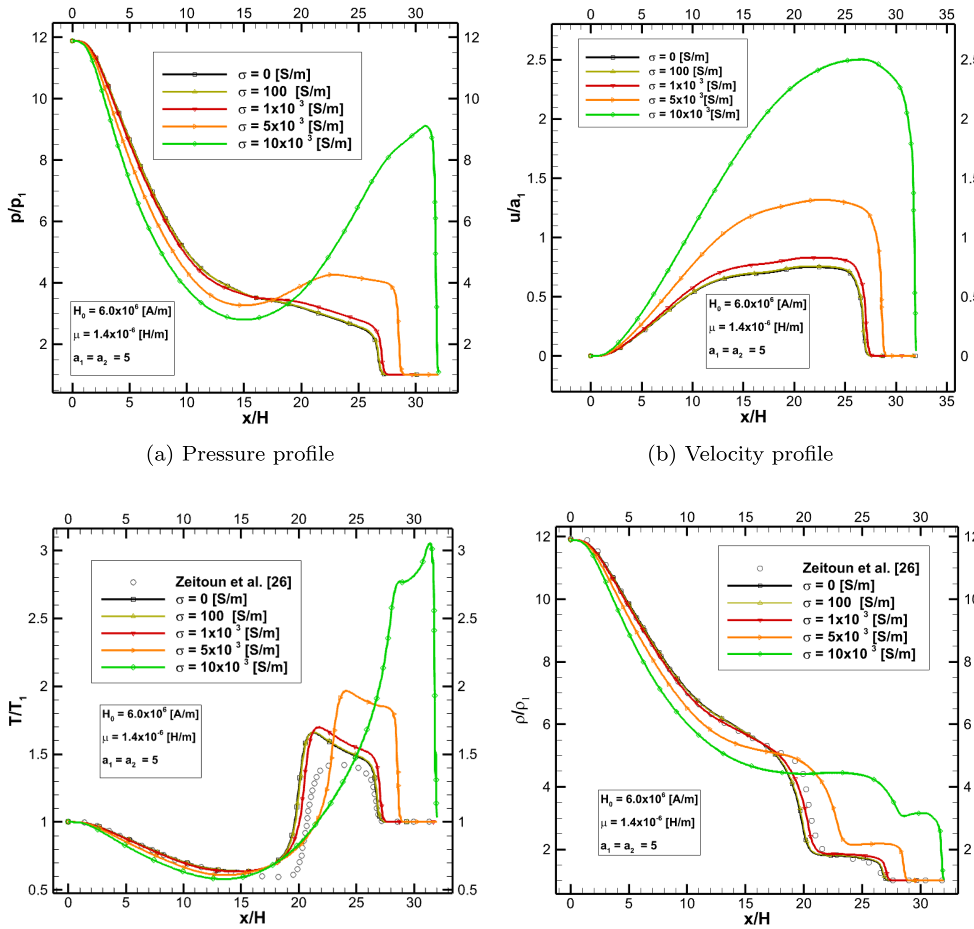

(a) Pressure profile

(b) Velocity profile

(c) Temperature profile

(d) Density profile

Figure 2. Effects of the electrical conductivity σ on different flow field variables extracted at the centerline of the microchannel

The magnetic field gradient in the points x_1 and x_2 is controlled by the two constants a_1 and a_2 in equation (2.25), which has been taken from the work of Tzirtzilakis and Loukopoulos [33] to simulate a physically realistic phenomenon relevant to biomedical applications. Figure 3 shows the effect of three different values for a_1 and a_2 on the dimensionless magnetic intensity H/H_0 for $\sigma = 5 \cdot 10^3$ S/m and $H_0 = 6.0 \cdot 10^6$ A/m, respectively. The numerical results suggest that the magnetic field intensity is slightly affected by changes in the magnitude of the magnetic field gradient. For $a_1 = a_2 = 10$, the magnetic field intensity has a semi-quadratic variation over the entire microchannel, while it remains constant for $a_1 = a_2 = 1$ and $a_1 = a_2 = 2$.

In Figures 4, 5, 6 and 7, the contour plots of the temperature, pressure, density and the velocity component u at $\sigma = 5 \cdot 10^3\,\mathrm{S/m}$ are shown in comparison with the value of the electrical conductivity $\sigma = 0\,\mathrm{S/m}$ as a reference value. The numerical solution is obtained by solving the compressible, viscous Navier-Stokes equations (2.1)–(2.4) with the inclusion of the Lorentz force terms (2.11) as source terms using the DG-FEM discretization approach discussed in Section 2. It has been observed regarding all the conservative variables that the left portion of the microchannel is not influenced by the magnetic field, whereas in the right section, the effect of the Lorentz force is particularly visible.

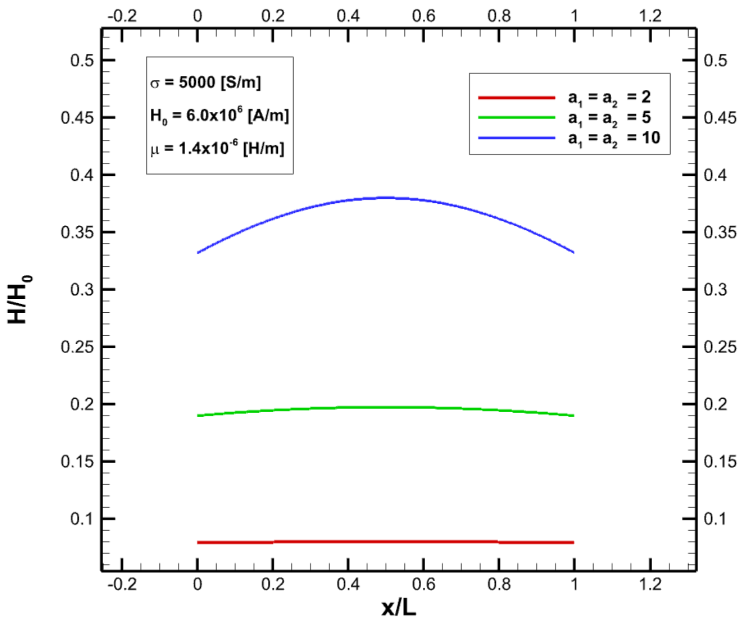

Figure 3. Magnetic field intensity for three different a_1, a_2 values

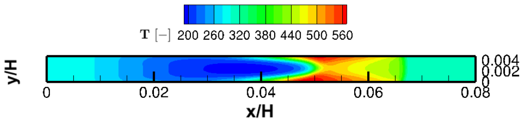

(a) Solution of the compressible Navier–Stokes equations without the Lorentz force terms

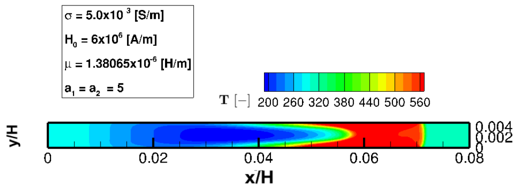

(b) Solution of the compressible Navier–Stokes equations with the MHD Lorentz force terms

Figure 4. Temperature distribution in the microchannel

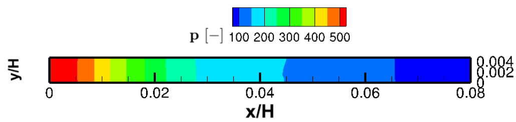

(a) Solution of the compressible Navier–Stokes equations without the Lorentz force terms

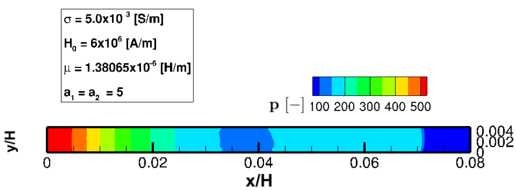

(b) Solution of the compressible Navier–Stokes equations with the MHD Lorentz force terms

Figure 5. Pressure distribution in the microchannel

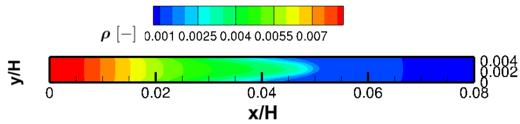

(a) Solution of the compressible Navier–Stokes equations without the Lorentz force terms

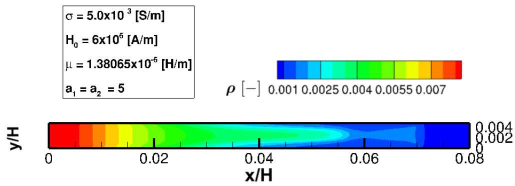

(b) Solution of the compressible Navier–Stokes equations with the MHD Lorentz force terms

Figure 6. Density distribution in the microchannel

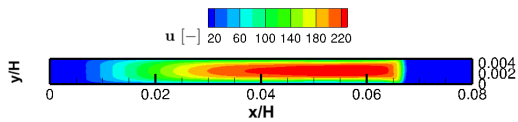

(a) Solution of the compressible Navier–Stokes equations without the Lorentz force terms

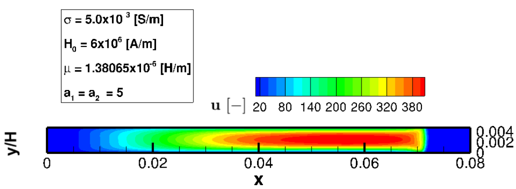

(b) Solution of the compressible Navier–Stokes equations with the MHD Lorentz force terms

Figure 7. Velocity component u distribution in the microchannel

4. Conclusions and Future Work

In this work, the effect of the electrical conductivity coefficient σ on a two-dimensional compressible, viscous micro-shock channel was analyzed behind the rupture of a membrane which separates two states of the same gas initially at rest. The Lorentz force terms (2.11) were included as source terms in the compressible Navier–Stokes equations (2.3), which were discretized with the use of the Discontinuous Galerkin-Finite Element Method (DG-FEM). Different magnetic Reynolds numbers were considered along with the variation of the electrical conductivity σ of the flow, from $\sigma = 100\,\mathrm{S/m}$ to $\sigma = 10 \cdot 10^3\,\mathrm{S/m}$. The acoustic waves after $80\mu s$ behind the rupture rupture point of the membrane were investigated. The numerical results suggest that the Lorentz force has a significant impact on the flow field variables from $\sigma > 100\,\mathrm{S/m}$. As the electrical conductivity σ is increased, all the conservative variables (temperature, pressure, density and velocity) showed a significant increase in their quantity toward the right section of the magnetogasdynamic microchannel. In particular, the temperature jump may be caused by the Joule effect while the sharp increase in the velocity profile can be explained by the acceleration of the flow produced by the Lorentz force terms (2.11) in the compressible Navier–Stokes equations (2.3). To achieve high-order spatial accuracy of the numerical solution and obtain even a more accurate prediction of the acoustic waves, the implementation of the Harten–Lax–van Leer Discontinuities (HLLD) Riemann solver [31] is recommended as future work. Furthermore, it is suggested to increase the physical time of the numerical simulation to get insights on the complex flow physics originating from the reflection of the acoustic waves against the lateral wall and to verify the stability of the present numerical scheme.

Acknowledgement. This project was financially supported by the Centre for Computational Engineering Sciences at Cranfield University under project code EEB6001R. For the purpose of open access, the authors have applied a Creative Commons Attribution (CC BY) licence to any author-accepted manuscript version arising.

References

1. Lawal, M. O. and Ajadi, S. O. "The behavior of MHD flow and heat transfer in the presence of heat source and chemical reaction over a flat plate." *Journal of Computational and Applied Mechanics,* **11**(2), (2016), pp. 159–178.
2. Sekhar, T. V. S., Sivakumar, R., and Kumar, H. "Numerical solutions for steady viscous flow past a circular cylinder in an aligned magnetic field." *Journal of Computational and Applied Mechanics,* **9**(2), (2014), pp. 201–217.
3. Stott, S. L., Hsu, Chia-Hsien, Tsukrov, D. I., Yu, Min, Miyamoto, D. T., Waltman, B. A, Rothenberg, S. M., Shah, A. M., Smas, M. E., Korir, G. K., et al. "Isolation of circulating tumor cells using a microvortex-generating herringbone-chip." *Proceedings of the National Academy of Sciences,* **107**(43), (2010), pp. 18392–18397. doi: `10.1073/pnas.1012539107`.
4. Zhao, Y., Chen, D., Yue, H., French, J. B., Rufo, J., Benkovic, S. J., and Huang, T. J. "Lab-on-a-chip technologies for single-molecule studies". *Lab on a Chip,* **13**(12), (2013), pp. 2183–2198. doi: `10.1039/c3lc90042h`.

5. Shaw, S. "Mathematical model on magnetic drug targeting in microvessel." *Magnetism and Magnetic Materials.* Ed. by Neeraj Panwar. IntechOpen, 2018, pp. 83–107. doi: 10.5772/intechopen.68579.
6. Hegab, H. E. and Liu, G. "Fluid flow modeling of micro-orifices using micropolar fluid theory." *Microfluidic Devices and Systems III.* Vol. 4177. Society of Photo-Optical Instrumentation Engineers. 2000, pp. 257–267. doi: 10.1117/12.395670.
7. Aissa, W. A. and Mohammadein, A. A. "Joule heating effects on a micropolar fluid past a stretching sheet with variable electric conductivity." *Journal of Computational and Applied Mechanics* **6**(1), (2005), pp. 3–13.
8. Kenis, P. J., Ismagilov, R. F., and Whitesides, G. M. "Microfabrication inside capillaries using multiphase laminar flow patterning". *Science,* **285**(5424), (1999), pp. 83–85. doi: 10.1126/science.285.5424.83.
9. Hertzog, D. E., Ivorra, B., Mohammadi, B., Bakajin, O., and Santiago, J. G. "Optimization of a microfluidic mixer for studying protein folding kinetics". *Analytical Chemistry,* **78**(13), (2006), pp. 4299–4306. doi: 10.1021/ac051903j.
10. Squires, T. M. and Quake, S. R. "Microfluidics: Fluid physics at the nanoliter scale." *Reviews of Modern Physics,* **77**(3), (2005), pp. 977–1026. doi: 10.1103/RevModPhys.77.977.
11. Bart, S. F., Tavrow, L. S., Mehregany, M., and Lang, J. H. "Microfabricated electrohydrodynamic pumps." *Sensors and Actuators A: Physical,* **21**(1-3) (1990), pp. 193–197. doi: 10.1016/0924-4247(90)85037-5.
12. Richter, A., Plettner, A., Hofmann, K. A., and Sandmaier, H. "A micromachined electrohydrodynamic (EHD) pump." *Sensors and Actuators A: Physical,* **29**(2), (1991), pp. 159–168. doi: 10.1016/0924-4247(91)87118-M.
13. Manz, A., Effenhauser, C. S., Burggraf, N., Harrison, D. J., Seiler, K., and Fluri, K. "Electroosmotic pumping and electrophoretic separations for miniaturized chemical analysis systems." *Journal of Micromechanics and Microengineering,* **4**(4), (1994), p. 257. doi: 10.1088/0960-1317/4/4/010.
14. Jang, J. and Lee, S. S. "Theoretical and experimental study of MHD (magnetohydrodynamic) micropump." *Sensors and Actuators A: Physical,* **80**(1), (2000), pp. 84–89. doi: 10.1016/S0924-4247(99)00302-7.
15. Nguyen, B. and Kassegne, S. K. "High-current density DC magenetohydrodynamics micropump with bubble isolation and release system." *Microfluidics and Nanofluidics,* **5**(3), (2008), pp. 383–393. doi: 10.1007/s10404-007-0255-3.
16. Homsy, A., Koster, S., Eijkel, J. C. T., Berg, A., Lucklum, F., Verpoorte, E., and Rooij, N. F. "A high current density DC magnetohydrodynamic (MHD) micropump." *Lab on a Chip,* **5**(4), (2005), pp. 466–471.
17. Lemoff, A. V. and Lee, A. P. "An AC magnetohydrodynamic micropump." *Sensors and Actuators B: Chemical,* **63**(3), (2000), pp. 178–185. doi: 10.1016/S0925-4005(00)00355-5.

18. Eijkel, J. C. T., Dalton, C., Hayden, C. J., Burt, J. P. H., and Manz, A. "A circular ac magnetohydrodynamic micropump for chromatographic applications." *Sensors and Actuators B: Chemical,* **92**(1-2), (2003), pp. 215–221. doi: 10.1016/S0925-4005(03)00267-3.
19. V. Patel and S. K. Kassegne. "Electroosmosis and thermal effects in magnetohydrodynamic (MHD) micropumps using 3D MHD equations." *Sensors and Actuators B: Chemical,* **122**(1), (2007), pp. 42–52. doi: doi.org/10.1016/j.snb.2006.05.015.
20. Wang, Pei-Jen, Chang, Chia-Yuan, and Chang, Ming-Lang. "Simulation of two-dimensional fully developed laminar flow for a magneto-hydrodynamic (MHD) pump." *Biosensors and bioelectronics,* **20**(1), (2004), pp. 115–121. doi: 10.1016/j.bios.2003.10.018.
21. Lim, S. and Choi, B. "A study on the MHD (magnetohydrodynamic) micropump with side-walled electrodes." *Journal of Mechanical Science and Technology,* 23(3), (2009), pp. 739–749. doi: 10.1007/s12206-008-1107-0.
22. Hasan, M. I., Ali, A. J. F., and Tufah, R. S. "Numerical study of the effect of channel geometry on the performance of magnetohydrodynamic micro pump." *Engineering Science and Technology, an International Journal,* **20**(3), (2017), pp. 982–989. doi: 10.1016/j.jestch.2017.01.008.
23. Chatterjee, D. and Amiroudine, S. "Lattice Boltzmann simulation of thermofluidic transport phenomena in a DC magnetohydrodynamic (MHD) micropump." *Biomedical Microdevices,* **13**(1), (2011), pp. 147–157. doi: 10.1007/s10544-010-9480-8.
24. Gamarra, F., Spelsberg, F., Dellian, M., and Goetz, A. E. "Complete local tumor remission after therapy with extra-corporeally applied high-energy shock waves (HESW)." *International Journal of Cancer,* **55**(1), (1993), pp. 153–156. doi: 10.1002/ijc.2910550127.
25. James A. McAteer and Andrew P. E. "The acute and long-term adverse effects of shock wave lithotripsy." *Seminars in Nephrology,* **28**(2), (2008), pp. 200–213. doi: 10.1016/j.semnephrol.2008.01.003.
26. Zeitoun, D. E., Burtschell, Y., Graur, I. A., Ivanov, M. S., Kudryavtsev, A. N., and Bondar, Y. A. "Numerical simulation of shock wave propagation in microchannels using continuum and kinetic approaches." *Shock Waves,* **19**(4), (2009), pp. 307–316. doi: 10.1007/s00193-009-0202-1.
27. Hesthaven, J. S. and Warburton, T. *Nodal Discontinuous Galerkin Methods: Algorithms, Analysis, and Applications.* Springer Science & Business Media, 2007.
28. Zingaro, A. and Könözsy, L. "Discontinuous Galerkin finite element investigation on the fully-compressible Navier–Stokes equations for microscale shock-channels." *Aerospace,* **5**(1), (2018), pp. 23–42. doi: 10.3390/aerospace5010016.
29. Lax, P. D. "Weak solutions of nonlinear hyperbolic equations and their numerical computation." *Communications on pure and Applied Mathematics,* **7**(1), (1954), pp. 159–193. doi: 10.1002/cpa.3160070112.

30. Tu, S., Aliabadi, S., et al. "A slope limiting procedure in discontinuous Galerkin finite element method for gasdynamics applications." *International Journal of Numerical Analysis and Modeling,* **2**(2), (2005), pp. 163–178.
31. Guo, Xiaocheng, Florinski, V., and Wang, Chi. "The HLLD Riemann solver based on magnetic field decomposition method for the numerical simulation of magneto-hydrodynamics." *Journal of Computational Physics,* **327**, (2016), pp. 543–552. doi: `10.1016/j.jcp.2016.09.057`.
32. Carpenter, M. H. and Kennedy, C. A. *Fourth-Order 2N-Storage Runge-Kutta Schemes.* Technical Memorandum NASA-TM-109112. NASA, 1994.
33. Tzirtzilakis, E. E. and Loukopoulos, V. C. "Biofluid flow in a channel under the action of a uniform localized magnetic field." *Computational Mechanics,* **36**(5), (2005), pp. 360–374. doi: `10.1007/s00466-005-0659-4`.
34. Cai, Chunpei and Liu, D. D. "Asymptotic solutions for low-magnetic-Reynolds-number gas flows inside a two-dimensional channel." *AIAA journal,* **47**(3), (2009), pp. 542–551. doi: `10.2514/1.37060`.

Journal of Computational and Applied Mechanics, Vol. 17, No. 2, (2022), pp. 125–155
DOI: 10.32973/jcam.2022.007

SOLUTIONS FOR THE VIBRATION AND STABILITY PROBLEMS OF HETEROGENOUS BEAMS WITH THREE SUPPORTS USING GREEN FUNCTIONS

L. Kiss, M. Abderrazek and G. Szeidl
Institute of Applied Mechanics, University of Miskolc
3515 Miskolc-Egyetemváros, Hungary
mechkiss@uni-miskolc.hu, abderrazekmessoudi1995@gmail.com,
gyorgy.szeidl@uni-miskolc.hu

[Received: November 22, 2022; Accepted: December 29, 2022]

Abstract. The goal of this study is to calculate the eigenvalues that provide the eigenfrequencies and the critical loads for two heterogeneous beams with three supports: the (first) [second] beam is (fixed)[pinned] at the left end, the intermediate support is a roller while the right end of the beams can move vertically but the rotation is prevented there. The beams are referred to as FrsRp and PrsRp beams. Determination of the (eigenfrequencies) [critical loads] leads to three point eigenvalue problems associated with homogeneous boundary conditions. With the Green functions that belong to these eigenvalue problems we can transform them into eigenvalue problems governed by homogeneous Fredholm integral equations. The eigenvalue problems can then be reduced to algebraic eigenvalue problems that are solvable numerically by utilizing effective solution algorithms.

Mathematical Subject Classification: 34B27, 45c05, 74K10
Keywords: Heterogeneous beams, three point boundary value problems, Green functions, vibrations, eigenvalue problems, stability, critical load

1. Introduction

Since beam buckling can be a prevalent cause of failure in engineering applications, it has been the focus of research for a long time. The Swiss mathematician Leonhard Euler was a pioneer in this subject, publishing his well-known formula for the critical (buckling) load of straight bars under compression in 1759. There are multiple sources about shells, columns, arches and other structures [1–3]. For example, the books [3, 4] provide extremely thorough information about solutions to a wide range of engineering problems, as well as applications. Article [5] investigates experimentally, analytically and numerically the static and dynamic stability problem of columns under self-weight. In [6] both geometrical and load imperfections are considerred in the buckling studies of columns.

Furthermore, the first concept of the Green function was published by George Green in 1828. His book [7] presents, discusses, and demonstrates how to use the Green function approach to electrostatic issues governed by partial differential equations. In the publication [8], the Green function for two-point boundary value problems governed by ordinary differential equations was established. In 1926, the first book [9] that comprehensively covered the notion of the Green function was published.

The results published in [10] were generalized for degenerated ordinary differential equation systems in 1975 [11, 12].

In the publication [13], the existence proof for several three-point boundary value issues linked to third-order nonlinear differential equations is presented by using Green functions. The related Green functions for some three-point boundary value problems governed by linear ordinary differential equations of order two are provided in article [14].

The free vibration and buckling problems of two heterogeneous beams are solved in this article based on the aforementioned literature. Cross-sectional inhomogeneity refers to the fact that the material is linearly elastic, isotropic, and the material distribution can change throughout the cross-section. Free vibration and stability equations are given for three-point boundary value issues. These are subsequently replaced with Fredholm integral equations using the Kernel function. A formulation of the Green function for three-point boundary value issues with homogeneous boundary conditions is also included. The boundary element approach is used to provide numerical solutions to integral equations, and algebraic equations are introduced in this manner. The eigenvalues of free vibration and the linear buckling loads are affected significantly by the location of the middle support in general. The results are compared to the results of some finite element calculations and high correlation is found.

2. Differential equations

2.1. Governing equations. The considerred heterogeneous FrsRp and PrsRp beams are shown in Figure 1. The axial force N acting on the beams is compressive. The cross section of the beams is uniform throughout their length. The axis $\hat{x}$ of the coordinate system $\hat{x}, \hat{y}, \hat{z}$ coincide with the E-weighted center line of the beams. Its origin is located at the left end of the beam. The beams are symmetric with respect to the coordinate plane $\hat{x}\hat{z}$. It is assumed that the modulus of elasticity E satisfies

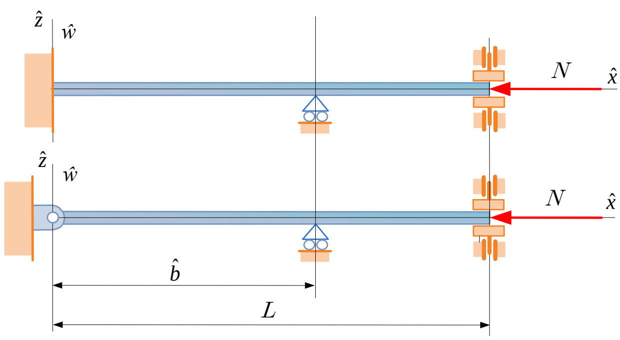

Figure 1. FrsRp and PrsRp beams

the condition $E(\hat{y},\hat{z}) = E(-\hat{y},\hat{z})$ over the cross section A, i.e., it is independent of the coordinate $\hat{z}$. In this case the beam has cross sectional heterogeneity [15]. L is the length of the beams while $\hat{b}$ gives the position of the middle roller support.

The E-weighted first moment $Q_{\hat{y}}$ is zero in this coordinate system:

$$Q_{\hat{y}} = \int_A \hat{z}E(\hat{y},\hat{z})\mathrm{d}A = 0\,. \tag{2.1}$$

Equilibrium problems of beams with cross sectional heterogeneity – the axial force N is zero – are governed by the ordinary differential equation [15]:

$$\frac{\mathrm{d}^4\hat{w}}{\mathrm{d}\hat{x}^4} = \frac{\hat{f}_z}{I_{ey}}\,, \tag{2.2}$$

where $\hat{w}(x)$ is the vertical displacement of the material points on the E-weighted center line, $\hat{f}_z(x)$ is the intensity of the verical distributed load acing on the beam. The E-weighted moment of inertia I_{ey} is defined by the equation

$$I_{ey} = \int_A E(\hat{y},\hat{z})z^2\,\mathrm{d}A\,. \tag{2.3}$$

If the beam is homogeneous the modulus of elasticity E is constant. Hence

$$I_{ey} = IE, \qquad I = \int_A z^2\,\mathrm{d}A \tag{2.4}$$

in which I is the moment of inertia.

In what follows we shall use dimensionless variables defined by the following relations [16]

$$\begin{gathered} x = \hat{x}/L, \qquad \xi = \hat{\xi}/L, \qquad w = \hat{w}/L, \\ y = \frac{\mathrm{d}\hat{w}}{\mathrm{d}\hat{x}} = \frac{\mathrm{d}w}{\mathrm{d}x}, \qquad b = \hat{b}/\hat{\ell}\,, \qquad \ell = \frac{x}{L}\Big|_{x=L} = 1\,, \end{gathered} \tag{2.5}$$

where $\hat{\xi}$ is also a coordinate measured on the axis $\hat{x}$ with the same origin as for $\hat{x}$. Applying dimensionless quantities to equation (2.2) we have

$$w^{(4)} = f_z\,, \quad w^{(0)} = w\,, \quad w^{(k)} = \frac{\mathrm{d}^k w}{\mathrm{d}x^k}, \quad (k = 1,\dots,4); \quad f_z = \frac{L^3\hat{f}_z}{I_{ey}} \tag{2.6}$$

Table 1.

Boundary conditions	
FrsRp beams	PrsRp beam
$w(0) = 0\,,\ \ w^{(1)}(0) = 0$	$w(0) = 0\,,\ \ w^{(2)}(0) = 0$
$w^{(1)}(\ell) = 0\,,\ \ w^{(3)}(\ell) = 0$	$w^{(1)}(\ell) = 0\,,\ \ w^{(3)}(\ell) = 0$
Continuity conditions	
$w(b-0) = w(b+0) = 0\,,$ $w^{(1)}(b-0) = w^{(1)}(b+0)\,,$ $w^{(2)}(b-0) = w^{(2)}(b+0)\,,$	

The ordinary differential equation $(2.6)_1$ (ODE) is associated with the boundary and continuity conditions presented in Table 1.

The general solution for the homogeneous ODE

$$w^{(4)} = 0 \tag{2.7}$$

is very simple:

$$w = \sum_{n=0}^{n=4} a_n w_n = a_n + a_1 x^1 + a_2 x^2 + a_3 x^3 + a_4 x^4\,, \tag{2.8}$$

in which a_k $(k = 0, \ldots, 4)$ are undetermined integration constants.

Making use of the Green functions that belongs to the boundary value problems determined by ODE (2.6) and the corresponding boundary and continuity conditions presented in Table 1 the solution for the dimensionless deflection w is given by the integral

$$w(x) = \int_0^\ell G(x,\xi) f_z(\xi)\,\mathrm{d}\xi\,. \tag{2.9}$$

where $G(x,\xi)$ stand for the Green functions in question.

The Green functions we shall need are presented in Section 3.

2.2. **Vibration problem.** The dimensionless amplitude for the free vibrations of FrsRp and PrsRp beams will also be denoted by w. It should fulfill the the following homogeneous ODE

$$\frac{\mathrm{d}^4 w}{\mathrm{d}x^4} = \lambda w\,, \qquad \lambda = \frac{\rho_a A \omega^2 L^4}{I_{ey}}\,, \tag{2.10}$$

where λ is the eigenvalue sought, ρ_a is the average density over the cross section while ω is the circular frequency of the vibrations.

Substituting $\lambda w(\xi)$ for $f(\xi)$ in (2.9) yields the homogeneous Fredholm integral equation

$$w(x) = \lambda \int_{\xi=0}^{\ell=1} G(x,\xi)\, w(\xi)\,\mathrm{d}\xi\,. \tag{2.11}$$

In this approach, the three point eigenvalue problem determined by ODE (2.10) and the boundary and continuity conditions presented in Table 1 is reduced to an eigenvalue problem governed by the homogeneous Fredholm integral equation (2.11).

2.3. **Stability problem.** If the uniform heterogeneous beams shown in Figure 1 are subjected to an axial force N the corresponding equilibrium problems are governed by ODE

$$w^{(4)} \pm \mathcal{N}\, w^{(2)} = f_z, \qquad \mathcal{N} = L^2 \frac{N}{I_{ey}}, \tag{2.12}$$

where the axial force N is constant ($N > 0$) while the sign of $\mathcal{N}$ is [positive] (negative) if the axial force is [compressive] (tensile).

If the stability problem is considered the axial force is compressive and $f_z = 0$. We have, therefore, two eigenvalue problems (one for each beam shown in Figure 1) – the eigenvalue sought is $\mathcal{N}$ – determined by ODE

$$w^{(4)} = -\mathcal{N}\, w^{(2)} \tag{2.13}$$

and the boundary and continuity conditions in Table 1. If we write $-\mathcal{N}\, w^{(2)}$ for f_z in (2.9) we get

$$w(x) = -\mathcal{N} \int_0^\ell G(x,\xi) \frac{\mathrm{d}^2 w(\xi)}{\mathrm{d}\xi^2}\, \mathrm{d}\xi = -\mathcal{N} \left(G(x,\xi) \frac{\mathrm{d}w(\xi)}{\mathrm{d}\xi} \bigg|_{\xi=0}^{\ell} - \int_0^\ell \frac{\partial G(x,\xi)}{\partial \xi} \frac{\mathrm{d}w(\xi)}{\mathrm{d}\xi}\, \mathrm{d}\xi \right)$$

where

$$G(x,\xi) \frac{\mathrm{d}w(\xi)}{\mathrm{d}\xi} \bigg|_{\xi=0}^{\ell} = 0$$

since $G(x,0)$ is zero and the derivative $\mathrm{d}w(\xi)/\mathrm{d}\xi$ is also zero if $\xi = \ell = 1$. Hence

$$w(x) = \mathcal{N} \int_0^\ell \frac{\partial G(x,\xi)}{\partial \xi} \frac{\mathrm{d}w(\xi)}{\mathrm{d}\xi}\, \mathrm{d}\xi\,. \tag{2.14}$$

Introduce the notations

$$\frac{\mathrm{d}w}{\mathrm{d}x} = y, \qquad \frac{\partial^2 G(x,\xi)}{\partial x\, \partial \xi} = \mathcal{K}(x,\xi)$$

and derive equation (2.14) with respect to x. In this way we get a homogeneous Fredholm integral equation:

$$y(x) = \mathcal{N} \int_0^\ell \mathcal{K}(x,\xi)\, y(\xi)\, d\xi\,. \tag{2.15}$$

Consequently, the eigenvalue problems determined by ODE (2.13) and the homogeneous boundary and continuity conditions presented in Table 1 are reduced to eigenvalue problems governed by homogeneous Fredholm integral equations. It should be mentioned that the above line of thought is based on book [17] and paper [16].

3. Green function for three-point boundary value problems

3.1. **Definition.** In this subsection we present the definition that provides the main properties of the Green function for ODEs. The definition is based on book [18].

Consider the inhomogeneous ordinary differential equation

$$L[y(x)] = \sum_{n=0}^{2k} p_n(x) y^{(n)}(x) = r(x)\,, \tag{3.1}$$

where k is a natural number, the functions $p_n(x)$ and $r(x)$ are continuous and $p_{2k}(x) \neq 0$ if $x \in [0, \ell]$ $(\ell > 0)$. Moreover let b an inner point in the interval $[0, \ell]$: $b = \ell_1$, $\ell - b = \ell_2$ and $\ell_1 + \ell_2 = \ell$.

The inhomogeneous differential equation (3.1) is associated with the following homogeneous boundary and continuity conditions:

$$\begin{aligned}
\sum_{n=0}^{2k} \alpha_{nrI} y_I^{(n-1)}(0) &= 0\,, \qquad r = 1, 2, \ldots, k \\
\sum_{n=0}^{2k} \beta_{nrI} y_I^{(n-1)}(b) - \sum_{n=0}^{2k} \beta_{nrII} y_{II}^{(n-1)}(b) &= 0\,, \qquad r = 1, 2, ..., 2k \\
\sum_{n=0}^{2k} \gamma_{nrII} y_{II}^{(n-1)}(\ell) &= 0\,. \qquad r = 1, 2, \ldots, k
\end{aligned} \tag{3.2}$$

The Roman numeral I and II belong to the intervals $[0, b]$ and $[b, \ell]$: y_I and y_{II} are the solutions to the differential equation in the intervals I and II. It is assumed that α_{nrI}, β_{nrI}, β_{nrII} and γ_{nrII} are arbitrary constants.

The Green function $G(x, \xi)$ that belongs to the three point boundary value problem (3.1), and (3.2) is defined by the following formulas and properties [18]:

Formulas:

$$G(x, \xi) = \begin{cases} G_{1I}(x, \xi) & \text{if } x, \xi \in [0, \ell], \\ G_{2I}(x, \xi) & \text{if } x \in [b, \ell] \text{ and } \xi \in [0, \ell], \\ G_{1II}(x, \xi) & \text{if } x \in [0, b] \text{ and } \xi \in [b, \ell], \\ G_{2II}(x, \xi) & \text{if } x, \xi \in [b, \ell]. \end{cases} \tag{3.3}$$

Properties:

1. The function $G_{1I}(x, \xi)$ is a continuous function of x and ξ if $0 \leq x \leq \xi \leq b$ and $0 \leq \xi \leq x \leq b$. In addition it is $2k$ times differentiable with respect to x and the derivatives

$$\frac{\partial^n G_{1I}(x, \xi)}{\partial x^n} = G_{1I}(x, \xi)^{(n)}(x, \xi)\,, \qquad n = 1, 2, \ldots, 2k \tag{3.4}$$

are also continuous functions of x and ξ in the triangles $0 \leq x \leq \xi \leq b$ and $0 \leq \xi \leq x \leq b$.

2. Let ξ be fixed in $[0, b]$. Then the function $G_{1I}(x, \xi)$ and its derivatives

$$G_{1I}^{(n)}(x, \xi) = \frac{\partial^n G_{1I}(x, \xi)}{\partial x^n}\,, \qquad n = 1, 2, \ldots, 2k - 2 \tag{3.5}$$

should be continuous for $x = \xi$:

$$G_{1I}^{(n)}(\xi + 0, \xi) - G_{1I}^{(n)}(\xi - 0, \xi) = 0\,, \quad n = 0, 1, 2, \ldots 2k - 2 \tag{3.6a}$$

The derivative $G_{1I}^{(2k-1)}(x, \xi)$ should, however, have a jump if $x = \xi$:

$$G_{1I}^{(2k-1)}(\xi + 0, \xi) - G_{1I}^{(2k-1)}(\xi - 0, \xi) = \frac{1}{p_{2k}(\xi)}\,. \tag{3.6b}$$

In contrast to this, $G_{2I}(x, \xi)$ and its derivatives

$$G_{2I}^{(n)}(x, \xi) = \frac{\partial^n G_{2I}(x, \xi)}{\partial x^n}\,, \qquad n = 1, 2, \ldots, 2k \tag{3.7}$$

are all continuous functions for any x in $[b, \ell]$.

3. Let ξ be fixed in $[b, \ell]$. The function $G_{1II}(x, \xi)$ and its derivatives

$$G_{1II}^{(n)}(x, \xi) = \frac{\partial^n G_{1II}(x, \xi)}{\partial x^n}\,, \qquad n = 1, 2, \ldots, 2k \tag{3.8}$$

are all continuous functions for any x in $[0, b]$.

4. Though the function $G_{2II}(x, \xi)$ and its derivatives

$$G_{2II}^{(n)}(x, \xi) = \frac{\partial^n G_{2II}(x, \xi)}{\partial x^n}\,, \qquad n = 1, 2, \ldots, 2k - 2 \tag{3.9}$$

should also be continuous for $x = \xi$:

$$G_{2II}^{(n)}(\xi + 0, \xi) - G_{2II}^{(n)}(\xi - 0, \xi) = 0\,, \quad n = 0, 1, 2, \ldots 2k - 2 \tag{3.10a}$$

the derivative $G_{2II}^{(2k-1)}(x, \xi)$ should, however, have a jump if $x = \xi$:

$$G_{2II}^{(2k-1)}(\xi + 0, \xi) - G_{2II}^{(2k-1)}(\xi - 0, \xi) = \frac{1}{p_{2k}(\xi)}\,. \tag{3.10b}$$

5. Let α be an arbitrary but finite non-zero constant. For a fixed $\xi \in [0, \ell]$ the product $G(x, \xi)\alpha$ as a function of x ($x \neq \xi$) should satisfy the homogeneous differential equation

$$M\,[G(x, \xi)\alpha] = 0\,.$$

6. The product $G(x, \xi)\alpha$ as a function of x should satisfy both the boundary conditions and the continuity conditions

$$\begin{aligned}
&\textstyle\sum_{n=1}^{2k} \alpha_{nrI}\, G^{(n-1)}(0) = 0\,, && r = 1, \ldots, k\\
&\textstyle\sum_{n=1}^{2\kappa} \big(\beta_{nrI}\, G^{(n-1)}(b - 0) - \beta_{nrII}\, G^{(n-1)}(b + 0)\big) = 0\,, && r = 1, \ldots, 2k\\
&\textstyle\sum_{n=1}^{2k} \gamma_{nrII}\, G^{(n-1)}(\ell) = 0\,. && r = 1, \ldots, k
\end{aligned} \tag{3.11}$$

The above continuity conditions should be satisfied by the function pairs $G_{1I}(x, \xi)$, $G_{2I}(x, \xi)$ and $G_{1II}(x, \xi)$, $G_{2II}(x, \xi)$ as well.

Remark 1. It can be proved – see paper [18] for details – that the solution of the three-point boundary value problem (3.1), and (3.2) has the form

$$y(x) = \int_0^{\ell} G(x, \xi) r(\xi) d\xi\,. \tag{3.12}$$

REMARK 2. If the boundary value problem defined by (3.1) and (3.2) is self adjoint then the Green function is symmetric [18]:

$$G(x,\xi) = G(\xi,x)\,. \tag{3.13}$$

In Subsections 3.2 and 3.3 we present the Green functions that belong to differential equation (2.6) under the boundary and continuity conditions presented in Table 1. The calculations are detailed for FrsRp beams only. As regards PrsRp beams we shall give the final formulae only.

3.2. **Green function for FrsRp beams.**

3.2.1. *Calculation of the Green function if* $\xi \in [0,b]$. We shall assume that $G_{1I}(x,\xi)$ has the following form:

$$\begin{aligned} G_{1I}(x,\xi) &= \sum_{m=1}^{4} (a_{mI}(\xi) + b_{mI}(\xi)) w_m(x), \qquad x<\xi \\ G_{1I}(x,\xi) &= \sum_{m=1}^{4} (a_{mI}(\xi) - b_{mI}(\xi)) w_m(x), \qquad x>\xi \end{aligned} \tag{3.14}$$

if $x \in [0,b]$. On the contrary, we search $G_{2I}(x,\xi)$ as

$$G_{2I}(x,\xi) = \sum_{m=1}^{4} c_{mI}(\xi) w_m(x), \tag{3.15}$$

if $x \in [b,\ell]$. The coefficients $a_{mI}(\xi), b_{mI}(\xi)$ and $c_{mI}(\xi)$ are unknown functions, $w_m(x)$ is given by (2.8).

Note that representation (3.14) and (3.15) for $G_{1I}(x,\xi)$ and $G_{2I}(x,\xi)$ ensure the fulfillment of Properties 1 and 5 of the definition.

Continuity and discontinuity conditions (3.6) result in the following equations

$$\sum_{m=1}^{4} b_{mI}(\xi) w_m^{(n)}(\xi) = 0, \qquad n=0,1,2 \tag{3.16a}$$

and

$$\sum_{m=1}^{4} b_{mI}(\xi) w_m^{(3)}(\xi) = -\frac{1}{2}. \tag{3.16b}$$

For FrsRp beams equations (3.16a) and (3.16b) assume the form

$$\begin{bmatrix} 1 & \xi & \xi^2 & \xi^3 \\ 0 & 1 & 2\xi & 3\xi^2 \\ 0 & 0 & 2 & 6\xi \\ 0 & 0 & 0 & 6 \end{bmatrix} \begin{bmatrix} b_{1I} \\ b_{2I} \\ b_{3I} \\ b_{4I} \end{bmatrix} = \begin{bmatrix} 0 \\ 0 \\ 0 \\ -\frac{1}{2} \end{bmatrix}. \tag{3.17}$$

Hence

$$b_{1I} = \frac{\xi^3}{12}, \quad b_{2I} = -\frac{\xi^2}{4}, \quad b_{3I} = \frac{\xi}{4}, \quad b_{4I} = \frac{1}{12}\,. \tag{3.18}$$

REMARK 3. Note that (a) the determination of b_{mI} ensures the fulfillment of Property 2 of the Green function; (b) the results obtained for b_{mI} are independent of the boundary and continuity conditions.

According to Property 6 of the definition $G_{1I}(x,\xi)$ and $G_{2I}(x,\xi)$ should satisfy the boundary and continuity conditions in Table 1. Utilizing them we get:

(a) Boundary conditions at $x=0$:

$$\sum_{k=1}^{4} a_{kI} w_k(0) = -\sum_{k=1}^{4} b_{kI} w_k(0)\,, \tag{3.19a}$$

$$\sum_{k=1}^{4} a_{kI} w_k^{(1)}(0) = -\sum_{k=1}^{4} b_{kI} w_k^{(1)}(0)\,. \tag{3.19b}$$

(b) Continuity conditions at $x=b$:

$$\sum_{k=1}^{4} a_{kI} w_k(b) = \sum_{k=1}^{4} b_{kI} w_k(b)\,, \tag{3.19c}$$

$$\sum_{k=1}^{4} c_{kI} w_k(b) = 0\,, \tag{3.19d}$$

$$\sum_{k=1}^{4} a_{kI} w_k^{(1)}(b) - \sum_{k=1}^{4} c_{kI} w_k^{(1)}(b) = \sum_{k=1}^{4} b_{kI} w_k^{(1)}(b)\,, \tag{3.19e}$$

$$\sum_{k=1}^{4} a_{kI} w_k^{(2)}(b) - \sum_{k=1}^{4} c_{kI} w_k^{(2)}(b) = \sum_{k=1}^{4} b_{kI} w_k^{(2)}(b)\,. \tag{3.19f}$$

(c) Boundary conditions at $x=\ell$:

$$\sum_{k=1}^{4} c_{kI} w_k^{(1)}(\ell) = 0\,, \tag{3.19g}$$

$$\sum_{k=1}^{4} c_{kI} w_k^{(2)}(\ell) = 0\,. \tag{3.19h}$$

The previous linear equations can be given in matrix form as well:

$$\begin{bmatrix} 1 & 0 & 0 & 0 & 0 & 0 & 0 & 0 \\ 0 & 1 & 0 & 0 & 0 & 0 & 0 & 0 \\ 1 & b & b^2 & b^3 & 0 & 0 & 0 & 0 \\ 0 & 0 & 0 & 0 & 1 & b & b^2 & b^3 \\ 0 & 1 & 2b & 3b^2 & 0 & -1 & -2b & -3b^2 \\ 0 & 0 & 2 & 6b & 0 & 0 & -2 & -6b \\ 0 & 0 & 0 & 0 & 0 & 1 & 2\ell & 3\ell^2 \\ 0 & 0 & 0 & 0 & 0 & 0 & 0 & 1 \end{bmatrix} \begin{bmatrix} a_{1I} \\ a_{2I} \\ a_{3I} \\ a_{4I} \\ c_{1I} \\ c_{2I} \\ c_{3I} \\ c_{4I} \end{bmatrix} = \frac{1}{12} \begin{bmatrix} -\xi^3 \\ 3\xi^2 \\ \xi^3 - 3\xi^2 b + 3\xi b^2 - b^3 \\ 0 \\ -3\xi^2 + 6\xi b - 3b^2 \\ 6\xi - 6b \\ 0 \\ 0 \end{bmatrix}. \tag{3.20}$$

After solving the linear equation system (3.20) the following relationship is obtained for $G_{1I}(x,\xi)$:

$$G_{1I}(x,\xi)=\sum_{\ell=1}^{4}\left(a_{\ell I}(\xi)\pm b_{\ell I}(\xi)\right)w_\ell(x)=-\frac{1}{12}\xi^3\pm\frac{1}{12}\xi^3+\left(\frac{3\xi^2}{12}\pm\left(-\frac{3\xi^2}{12}\right)\right)x+$$
$$+\left(\frac{3\xi}{12b^2\left(4\ell-3b\right)}\left(8\xi b^2-12\xi b\ell+4\ell\xi^2-2\xi^2b-3b^3+4b^2\ell\right)\pm\frac{3\xi}{12}\right)x^2+$$
$$+\left(-\frac{1}{12b^3\left(4\ell-3b\right)}\left(6\xi^2b^2-12\xi^2b\ell-3b^4+4b^3\ell+4\ell\xi^3\right)\pm\frac{-1}{12}\right)x^3 \quad (3.21a)$$

As regards $G_{2I}(x,\xi)$ we have

$$G_{2I}(x,\xi)=\sum_{\ell=1}^{4}c_{\ell I}(\xi)w_\ell(x)=\xi^2\frac{\left(\xi-b\right)\left(x-b\right)\left(2\ell-x-b\right)}{2b\left(4\ell-3b\right)} \quad (3.21b)$$

3.2.2. *Calculation of the Green function if $\xi\in[b,\ell]$.* The assumptions that are used are similar to those presented in Subsection 3.2.1:

If $x\in[b,\ell]$ then

$$\begin{aligned}G_{2II}(x,\xi)&=\sum_{m=1}^{4}(a_{mII}(\xi)+b_{mII}(\xi))w_m(x), &\quad x<\xi\\ G_{2II}(x,\xi)&=\sum_{m=1}^{4}(a_{mII}(\xi)-b_{mII}(\xi))w_m(x), &\quad x>\xi\end{aligned} \quad (3.22)$$

however, if $x\in[0,b]$ then

$$G_{1II}(x,\xi)=\sum_{m=1}^{4}c_{mII}(\xi)w_m(x). \quad (3.23)$$

Here the coefficients $a_{mII}(\xi), b_{mII}(\xi)$ and $c_{mII}(\xi)$ are again unknown functions.

We remind the reader of the fact that the above representations for $G_{1II}(x,\xi)$ and $G_{2II}(x,\xi)$ ensure the fulfillment of Property 1 and 5 of the definition.

Continuity and discontinuity conditions (3.10) lead again to equation system (3.17) in which now the coefficients $b_{mII}(\xi)$, $m=1,2,3,4$ are the unknowns. Hence $b_{mII}(\xi)=b_{mI}(\xi)$.

It's worth noting that determining the coefficients b_{mII} assures that the Green function's Properties 3 and 4 are satisfied. Making use of the boundary and continuity conditions given in Table 1 equations again the following equations can be obtained for the eight unknown coefficients $a_{mII}(\xi)$ and $c_{mII}(\xi)$:

(a) Boundary conditions at $x=0$:

$$\sum_{k=1}^{4}c_{kII}\,w_k(0)=0\,, \quad (3.24a)$$

$$\sum_{k=1}^{4}c_{kII}\,w_k^{(1)}(0)=0\,, \quad (3.24b)$$

(b) Continuity conditions at $x = b$:

$$\sum_{k=1}^{4} c_{kII}\, w_k(b) = 0\,, \tag{3.24c}$$

$$\sum_{k=1}^{4} a_{kII}\, w_k(b) = -\sum_{k=1}^{4} b_{kII}\, w_k(b)\,, \tag{3.24d}$$

$$\sum_{k=1}^{4} a_{kII}^{(1)}\, w_k(b) - \sum_{k=1}^{4} c_{kII}^{(1)}\, w_k(b) = -\sum_{k=1}^{4} b_{kII}^{(1)}\, w_k(b)\,, \tag{3.24e}$$

$$\sum_{k=1}^{4} a_{kII}^{(2)}\, w_k(b) - \sum_{k=1}^{4} c_{kII}^{(2)}\, w_k(b) = -\sum_{k=1}^{4} b_{kII}^{(2)}\, w_k(b)\,. \tag{3.24f}$$

(c) Boundary conditions at $x = \ell$:

$$\sum_{k=1}^{4} a_{kII}^{(1)}\, w_k(\ell) = \sum_{k=1}^{4} b_{kII}^{(1)}\, w_k(\ell)\,, \tag{3.24g}$$

$$\sum_{k=1}^{4} a_{kII}^{(3)}\, w_k(\ell) = \sum_{k=1}^{4} b_{kII}^{(3)}\, w_k(\ell)\,, \tag{3.24h}$$

Since $c_{1II} = c_{2II} = 0$ the final equation system has the following form:

$$\begin{bmatrix} 0 & 0 & 0 & 0 & b^2 & b^3 \\ 1 & b & b^2 & b^3 & 0 & 0 \\ 0 & 1 & 2b & 3b^2 & -2b & -3b^2 \\ 0 & 0 & 2 & 6b & -2 & -6b \\ 0 & 1 & 2\ell & 3\ell^2 & 0 & 0 \\ 0 & 0 & 0 & 1 & 0 & 0 \end{bmatrix} \begin{bmatrix} a_{1II} \\ a_{2II} \\ a_{3II} \\ a_{4II} \\ c_{3II} \\ c_{4II} \end{bmatrix} = \frac{1}{12} \begin{bmatrix} 0 \\ -\xi^3 + 3b\xi^2 - 3b^2\xi + b^3 \\ 3\xi^2 - 6b\xi + 3b^2 \\ -6\xi + 6b \\ -3\xi^2 + 6\xi\ell - 3\ell^2 \\ -1 \end{bmatrix} \tag{3.25}$$

After having solved the previous equation system substitution of the results obtained into equations (3.22), (3.23) and using some algebra yield:

$$G_{1II}(x,\xi) = \sum_{\ell=1}^{4} c_{\ell II}(\xi) w_\ell(x) = x^2 \frac{(x-b)\,(\xi-b)\,(2\ell-\xi-b)}{2b\,(4\ell-3b)} \tag{3.26a}$$

and

$$\begin{aligned} G_{2II}(x,\xi) &= \sum_{\ell=1}^{4} \left(a_{\ell II}(\xi) \pm b_{\ell II}(\xi)\right) w_\ell(x) = \\ &= -\frac{1}{12\,(4\ell-3b)} \left(4b^3\ell - 12b^2\xi\ell + 6\xi^2 b^2 + 4\ell\xi^3 - 3\xi^3 b\right) \pm \frac{\xi^3}{12} + \\ &+ \left(\frac{3}{12\,(4\ell-3b)} \left(4b^2\ell - 12\xi b\ell + 3\xi^2 b + 4\ell\xi^2\right) \pm \frac{-3\xi^2}{12}\right) x + \\ &+ \left(\frac{3}{12\,(4\ell-3b)} \left(-2b^2 + 4\xi\ell - 4\xi^2 + 3\xi b\right) \pm \frac{3\xi}{12}\right) x^2 + \left(-\frac{1}{12} \pm \frac{-1}{12}\right) x^3 \end{aligned} \tag{3.26b}$$

Note that the calculation of the functions $a_{\ell II}$ and $c_{\ell II}$ is based on Property 6 of the definition.

Figure 2 depicts the Green function for an FrsRp beam. It is assumed that $L = 100$ mm, $\hat{b} = 50$ mm and $\hat{\xi} = 75$ mm. The computed points are drawn by red diamonds and the function itself is shown using a continuous line. This notation convention will be applied to the other figures in the present paper. The Green function shown in Figure 2 is the dimensionless displacement due to a dimensionless vertical unit force exerted on the beam at the point $\xi = 0.75$.

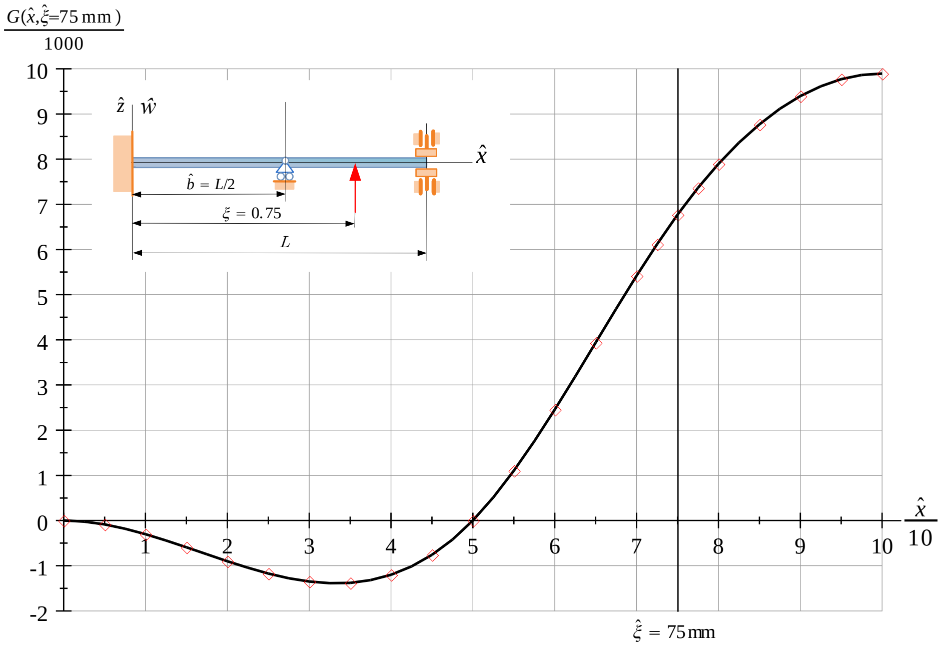

Figure 2. The Green function of an FrsRp beam

3.3. **Green function for PrsRp beams.** Repeating the calculations steps presented in Subsection 3.2 for PrsRp beams yields the following four elements for the corresponding Green function – the calculation details are all omitted here.

$$
G_{1I}(x,\xi) = \sum_{\ell=1}^{4} \left(a_{\ell I}(\xi) \pm b_{\ell I}(\xi)\right) w_\ell(x) = \left(-\frac{1}{12}\xi^3 \pm \frac{1}{12}\xi^3\right) + \\
+ \left(-\frac{1}{12b\,(2b-3\ell)}\left(-9b^3\xi+6b^2\xi^2+12\ell b^2\xi-3b\xi^3-9\ell b\xi^2+6\ell\xi^3\right) \pm \left(-\frac{3\xi^2}{12}\right)\right) x + \\
+ \left(-\frac{3}{12}\xi \pm \frac{3}{12}\xi\right) x^2 + \left(\frac{1}{12b^2\,(2b-3\ell)}\left(-2b^3+3b^2\xi+3\ell b^2-6\ell b\xi+\xi^3\right) \pm \frac{-1}{12}\right) x^3, \tag{3.27a}
$$

$$G_{2I}(x,\xi) = \sum_{\ell=1}^{4} c_{\ell I}(\xi) w_\ell(x) = \frac{1}{4b}\frac{\xi}{3\ell-2b}(b-x)\left(\xi^2-b^2\right)(b+x-2\ell)\,, \tag{3.27b}$$

$$G_{1II}(x,\xi) = \sum_{\ell=1}^{4} c_{\ell II}(\xi) w_\ell(x) = \frac{1}{4b}\frac{x}{3\ell-2b}(b-\xi)\left(x^2-b^2\right)(b+\xi-2\ell)\,, \tag{3.27c}$$

$$\begin{aligned} G_{2II}(x,\xi) &= \sum_{\ell=1}^{4}\left(a_{\ell II}(\xi) \pm b_{\ell II}(\xi)\right) z_\ell(x) = \\ &= \frac{1}{12\,(3\ell-2b)}\left(-b^4+6b^2\xi\ell-3b^2\xi^2-3\xi^3\ell+2\xi^3 b\right) \pm \frac{\xi^3}{12} + \\ &+ \left(\frac{3}{12\,(3\ell-2b)}\left(2b^2\ell-8b\xi\ell+2b\xi^2+3\xi^2\ell\right) \pm \frac{-3\xi^2}{12}\right)x + \\ &+ \left(\frac{3}{12\,(3\ell-2b)}\left(-b^2+3\xi\ell-3\xi^2+2b\xi\right) \pm \frac{3\xi}{12}\right)x^2 + \left(-\frac{1}{12} \pm \frac{-1}{12}\right)x^3. \end{aligned} \tag{3.27d}$$

Figure 3 shows the Green function of a PrsRp beam under the same conditions as Figure 2 depicts the Green function of an FrsRp beam.

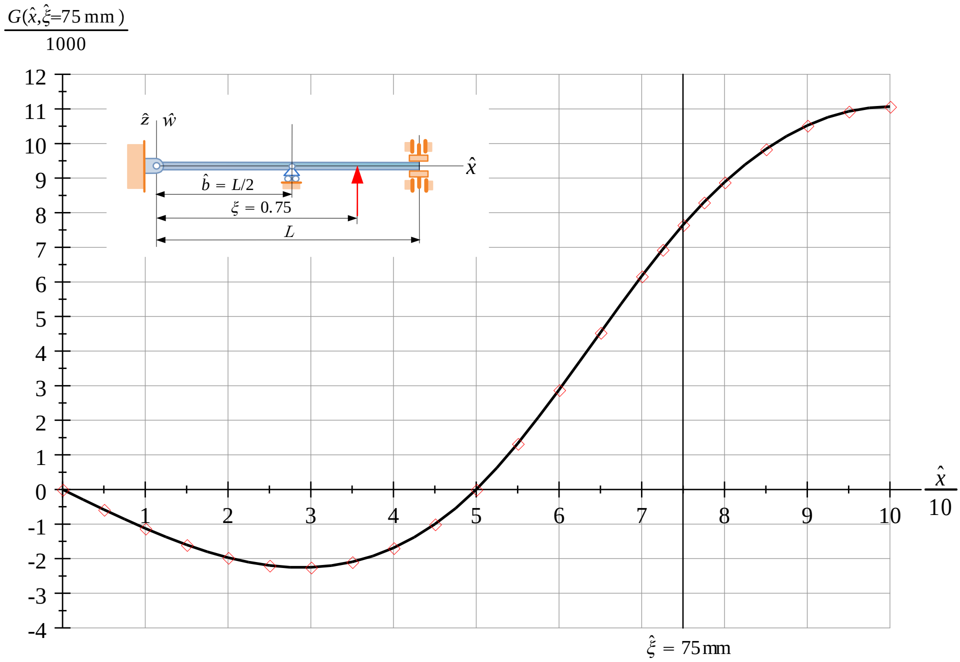

Figure 3. The Green function of an PrsRp beam

REMARK 4. The Green function given by equations (3.21) and (3.26) (FrsRp beams), (3.27) (PrsRp beams), should satisfy symmetry condition (3.13). It can be proved by paper and pencil calculations that this condition is really fulfilled. Note that for G_{2I}

and G_{1II} a comparison of (3.21b) and (3.26a) as well as that of (3.27b) and (3.27c) clearly shows the fulfillment of the symmetry condition.

Remark 5. The Green functions (3.21), (3.26) and (3.27) are dimensionless quantities. By substituting $\hat{b}$, L, $\hat{x}$ and $\hat{\xi}$ for b, ℓ, x andξ in (3.21), (3.26) and (3.27) we obtain the Green functions for a selected length unit. Then the unit of the Green function is the cube of the length unit selected.

4. Numerical solutions for the free vibration and stability problems

4.1. **The free vibration of FrsRp and PrsRp beams.** Making use of the algorithm detailed in Subsection 7.2 of the book [18] a Fortran 90 program was developed for solving eigenvalue problem (2.11), i.e., for computing the eigenvalues λ (the natural circular frequencies) of the freely vibrating FrsRp and PrsRp beams (the axial force is now zero) shown in Figure 1. Table 2 and Table 3 present the values of $\lambda_i/4.730042^2$, $(i = 1;2;3)$ for FrsRp and PrsRp against 21 uniformly increasing b values in the interval $[0.0, 1.0]$.

Table 2. Solutions for the eigenvalues λ of FrsRp beams

b	$\frac{\sqrt{\lambda_1}}{4.73004^2}$	$\frac{\sqrt{\lambda_2}}{4.73004^2}$	$\frac{\sqrt{\lambda_3}}{4.73004^2}$
0.000	0.2545	1.3707	3.3876
0.050	0.2751	1.4832	3.6692
0.100	0.2989	1.6159	4.0085
0.150	0.3264	1.7737	4.4165
0.200	0.3587	1.9626	4.9052
0.250	0.3970	2.1896	5.4794
0.300	0.4428	2.4631	6.0887
0.350	0.4983	2.7884	6.1999
0.400	0.5667	3.1487	5.3372
0.450	0.6520	3.3867	4.7648
0.500	0.7599	3.1710	5.0303
0.550	0.8973	2.7863	5.8037
0.600	1.0688	2.4707	6.2988
0.650	1.2566	2.2989	5.7913
0.700	1.3675	2.4086	5.1793
0.750	1.3348	2.9030	4.7797
0.800	1.2429	3.3735	5.1642
0.850	1.1494	3.2747	6.2815
0.900	1.0727	3.0380	6.0457
0.950	1.0203	2.8423	5.6192
1.000	1.0000	2.7568	5.4059

Polynomials (4.1), (4.2) and (4.2) are fitted onto the computed discrete values of $\sqrt{\lambda_k}/4.73004^2(k = 1, 2, 3)$ presented in Table 2.
Polynomials for the first eigenvalue:

$$\frac{\sqrt{\lambda_1}}{4.73004^2} = -30.475\,109\,9b^6 + 55.991\,058\,8b^5 - 33.778\,406\,3b^4 + 10.464\,803\,2b^3 \\ - 0.743\,507\,022b^2 + 0.443\,726\,955\,b + 0.254\,099\,177, \quad b \in [0, 0.625] \quad (4.1a)$$

$$\frac{\sqrt{\lambda_1}}{4.73004^2} = 4172.108\,44b^6 - 20498.081\,7b^5 + 41635.160\,7b^4 - 44700.075\,2b^3 + \\ + 26718.075\,5b^2 - 8418.283\,6b + 1092.096\,96, \qquad b \in [0.625, 1] \quad (4.1b)$$

Polynomials for the second eigenvalue:

$$\frac{\sqrt{\lambda_2}}{4.73004^2} = -173.518\,714b^6 + 150.076\,835b^5 - 40.246\,420\,1b^4 + 11.010\,604\,2b^3 + \\ + 2.870\,516\,97b^2 + 2.082\,056\,16b + 1.370\,692\,02, \qquad b \in [0, 0.35] \quad (4.2a)$$

$$\frac{\sqrt{\lambda_2}}{4.73004^2} = -310557.518b^6 + 845065.5b^5 - 950123.189b^4 + 564838.656b^3 - \\ - 187284.725b^2 + 32856.293\,2b - 2381.762\,03, \qquad b \in [0.35, 0.55] \quad (4.2b)$$

$$\frac{\sqrt{\lambda_2}}{4.73004^2} = -30502.323\,2b^6 + 110600.102b^5 - 166009.888b^4 + 132140.138b^3 - \\ - 58844.558\,6b^2 + 13891.813\,1b - 1353.111\,55, \qquad b \in [0.55, 0.775] \quad (4.2c)$$

$$\frac{\sqrt{\lambda_2}}{4.73004^2} = -11948.296\,5\ b^6 + 71424.316\,6\ b^5 - 176869.672\ b^4 + 232479.487\ b^3 - \\ - 171191.813\ b^2 + 66992.127\,4\ b - 10883.393\,7, \qquad b \in [0.775, 1] \quad (4.2d)$$

Polynomials for the third eigenvalue:

$$\frac{\sqrt{\lambda_3}}{4.73004^2} = 413332.622b^6 - 649900.151b^5 + 411344.981b^4 - 133672.324b^3 + \\ + 23342.110\,5b^2 - 2033.367\,18b + 70.510\,977\,0, \qquad b \in [0.25, 0.4] \quad (4.2e)$$

$$\frac{\sqrt{\lambda_3}}{4.73004^2} = 48544.085\,3b^6 - 91571.404\,8b^5 + 48349.687\,5b^4 + 9960.134\,03b^3 - \\ - 18412.920\,1b^2 + 6294.346\,68b - 702.680\,179, \qquad b \in [0.4, 0.55] \quad (4.2f)$$

$$\frac{\sqrt{\lambda_3}}{4.73004^2} = 2073702.86b^6 - 7913552.44x^5 + 12563013.6x^4 - 10618667.1x^3 + \\ + 5039221.87x^2 - 1272877.15x + 133685.395, \qquad b \in [0.55, 0.7] \quad (4.2g)$$

$$\frac{\sqrt{\lambda_3}}{4.73004^2} = -243505.380x^6 + 882582.997b^5 - 1246562.71b^4 + 831781.698b^3 - \\ - 231920.390b^2 - 1744.473\,18b + 9178.324\,82, \qquad b \in [0.7, 0.825] \quad (4.2h)$$

$$\frac{\sqrt{\lambda_3}}{4.73004^2} = -284198.684x^6 + 1619914.01x^5 - 3845547.04x^4 + 4867005.53x^3 - \\ - 3463802.03x^2 + 1314397.42x - 207763.794, \qquad b \in [0.825, 1.0] \quad (4.2i)$$

Figures 4, 5 and 6 show the graphs of the functions $\sqrt{\lambda_k(b)}/4.73004^2 (k = 1, 2, 3)$.

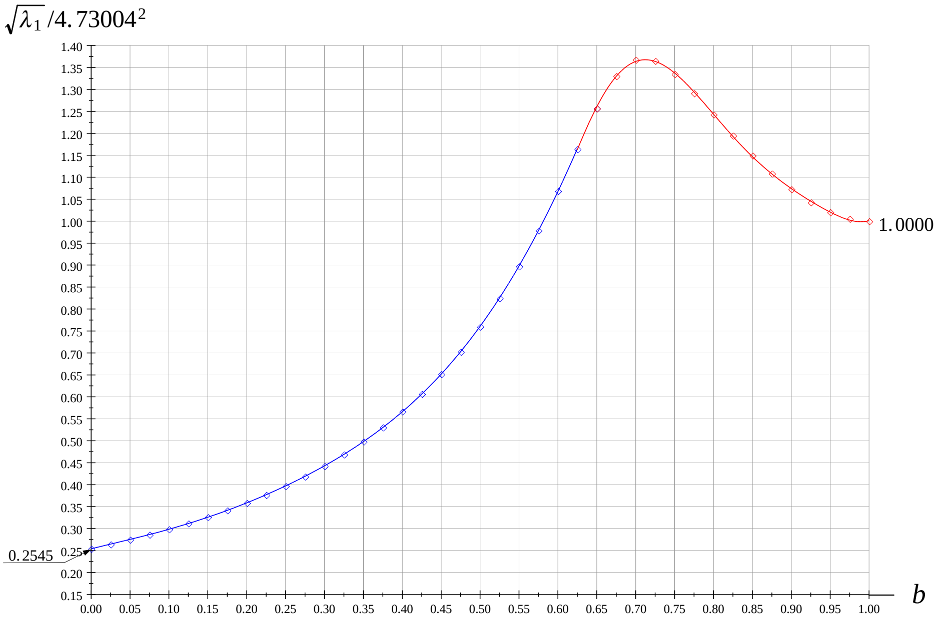

Figure 4. Function $\sqrt{\lambda_1}/4.73004^2$ against b

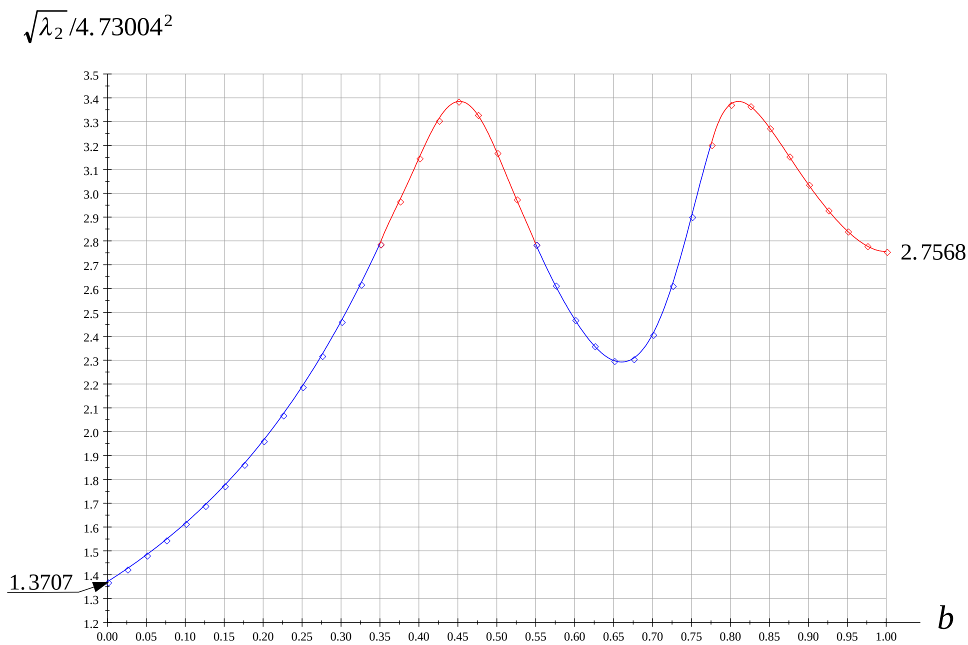

Figure 5. Function $\sqrt{\lambda_2}/4.73004^2$ against b

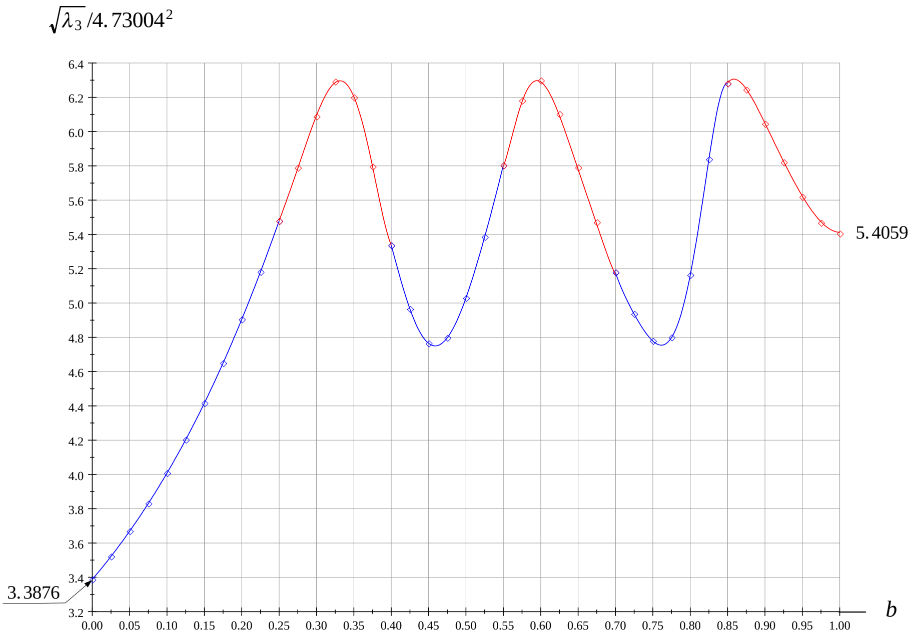

Figure 6. Function $\sqrt{\lambda_3}/4.73004^2$ against b

For PrsPRp beams Table 3 contains the computational results.

Table 3. Solutions for the eigenvalues λ of PrsRp beams

b	$\frac{\sqrt{\lambda_1}}{4.73004^2}$	$\frac{\sqrt{\lambda_2}}{4.73004^2}$	$\frac{\sqrt{\lambda_3}}{4.73004^2}$
0.000	0.2545	1.3707	3.3876
0.050	0.2729	1.4722	3.6446
0.100	0.2942	1.5951	3.9650
0.150	0.3191	1.7435	4.3553
0.200	0.3484	1.9225	4.8163
0.250	0.3836	2.1369	5.3049
0.300	0.4251	2.3877	5.4168
0.350	0.4756	2.6539	4.6226
0.400	0.5383	2.7983	4.0604
0.450	0.6153	2.5824	4.2051
0.500	0.7101	2.2442	4.7850
0.550	0.8229	1.9719	5.4203
0.600	0.9388	1.8167	5.2861
0.650	1.0050	1.8513	4.7224
0.700	0.9830	2.1426	4.2451
0.750	0.9163	2.6083	4.0641
0.800	0.8445	2.7945	4.7548
0.850	0.7819	2.6420	5.4909
0.900	0.7333	2.4480	5.1979
0.950	0.7012	2.2972	4.8356
1.000	0.6891	2.2338	4.6607

Polynomials (4.3), (4.4) and (4.5) are fitted onto the computed discrete values of $\sqrt{\lambda_k}/4.73004^2(k=1,2,3)$ presented in Table 3.

Polynomials for the first eigenvalue:

$$\frac{\sqrt{\lambda_1}}{4.73004^2} = -41.080\,096\,2b^6 + 63.147\,880\,9b^5 - 33.556\,975\,5b^4 + 9.262\,020\,48b^3 - \\ - 0.510\,379\,219b^2 + 0.383\,506\,985b + 0.254\,263\,737, \quad b \in [0, 0.575] \quad (4.3a)$$

$$\frac{\sqrt{\lambda_1}}{4.73004^2} = 1322.696\,25b^6 - 6268.407\,31b^5 + 12232.936\,9b^4 - 12555.559\,8b^3 + \\ + 7129.384\,25b^2 - 2117.638\,81b + 257.278\,716, \quad b \in [0.575, 1] \quad (4.3b)$$

Polynomials for the second eigenvalue:

$$\frac{\sqrt{\lambda_2}}{4.73004^2} = -295.492\,865b^6 + 201.661\,94b^5 - 47.755\,381\,3b^4 + 10.626\,197\,6b^3 + \\ + 3.195\,613\,34b^2 + 1.848\,783\,9b + 1.370\,702\,43, \quad b \in [0, 0.3] \quad (4.4a)$$

$$\frac{\sqrt{\lambda_2}}{4.73004^2} = -230\,912.0\,83b^6 + 557\,443.625b^5 - 554\,657.434b^4 + 291\,066.631b^3 - \\ - 84987.941\,7b^2 + 13104.515\,1b - 832.379\,11, \quad b \in [0.3, 0.5] \quad (4.4b)$$

$$\frac{\sqrt{\lambda_2}}{4.73004^2} = -5813.451\,13b^6 + 18042.657\,9b^5 - 22715.726b^4 + 14807.845\,8b^3 - \\ - 5220.857\,11b^2 + 918.110\,040b - 55.842\,264\,2, \quad b \in [0.5, 0.75] \quad (4.4c)$$

$$\frac{\sqrt{\lambda_2}}{4.73004^2} = 4928.738\,89b^6 - 22244.172\,9b^5 + 39776.050\,7b^4 - 34844.077\,6b^3 + \\ + 14431.718\,2b^2 - 1786.725\,11b - 259.298\,607, \quad b \in [0.75, 1] \quad (4.4d)$$

Polynomials for the third eigenvalue:

$$\frac{\sqrt{\lambda_3}}{4.73004^2} = -2623.305\,96b^6 + 1237.635\,68b^5 - 231.339\,925b^4 + 30.257\,014\,1b^3 + \\ + 10.385\,009\,6b^2 + 4.566\,326\,26b + 3.387\,600\,46, \quad b \in [0, 0.2] \quad (4.5a)$$

$$\frac{\sqrt{\lambda_3}}{4.73004^2} = 1.131\,061\,48 \times 10^5 b^6 - 20897.459\,2b^5 - 90629.798b^4 + 66709.594\,1b^3 - \\ - 19457.354\,7b^2 + 2639.576\,61b - 134.025\,486, \quad b \in [0.2, 0.35] \quad (4.5b)$$

$$\frac{\sqrt{\lambda_3}}{4.73004^2} = 29681.7778b^6 - 36384.9728b^5 - 6235.29422b^4 + 30141.8189b^3 - \\ - 18135.1124b^2 + 4465.63198b - 399.021738, \quad b \in [0.35, 0.5] \quad (4.5c)$$

$$\frac{\sqrt{\lambda_3}}{4.73004^2} = -1\,479\,416.38b^6 + 500\,694.40b^5 - 7\,035\,081.66b^4 + 5\,252\,557.83 \times 10^6 b^3 - \\ - 2\,197\,910.20b^2 + 488\,766.44b - 45129.13, \quad b \in [0.5, 0.65] \quad (4.5d)$$

$$\frac{\sqrt{\lambda_3}}{4.73004^2} = -743\,272.68b^6 + 3\,194\,975.26 \times 10^6 b^5 - 5\,713\,572.25b^4 + 5\,441\,676.39b^3 - \\ - 2\,911\,437.16b^2 + 829\,724.55b - 98399.24, \quad b \in [0.65, 0.8] \quad (4.5e)$$

$$\frac{\sqrt{\lambda_3}}{4.73004^2} = 372\,346.0b^6 - 2\,006\,546.6b^5 + 4\,496\,069.4b^4 - 5\,360\,883.7b^3 + \\ + 3\,586\,778.1b^2 - 1\,276\,523.3b + 188\,764.8 \quad b \in [0.8, 1.0] \quad (4.5f)$$

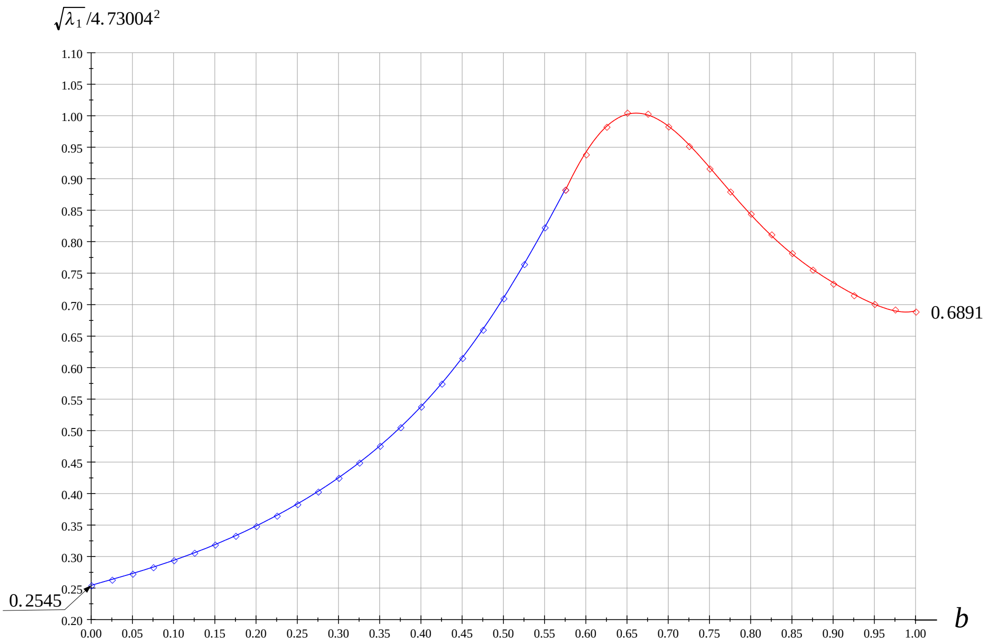

Figure 7. Function $\sqrt{\lambda_1}/4.73004^2$ against b

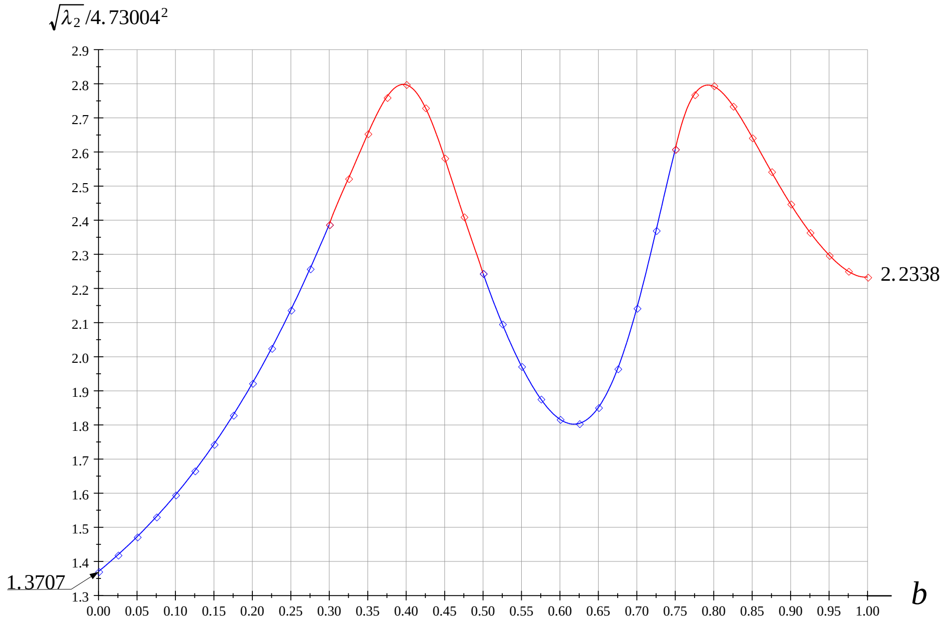

Figure 8. Function $\sqrt{\lambda_2}/4.73004^2$ against b

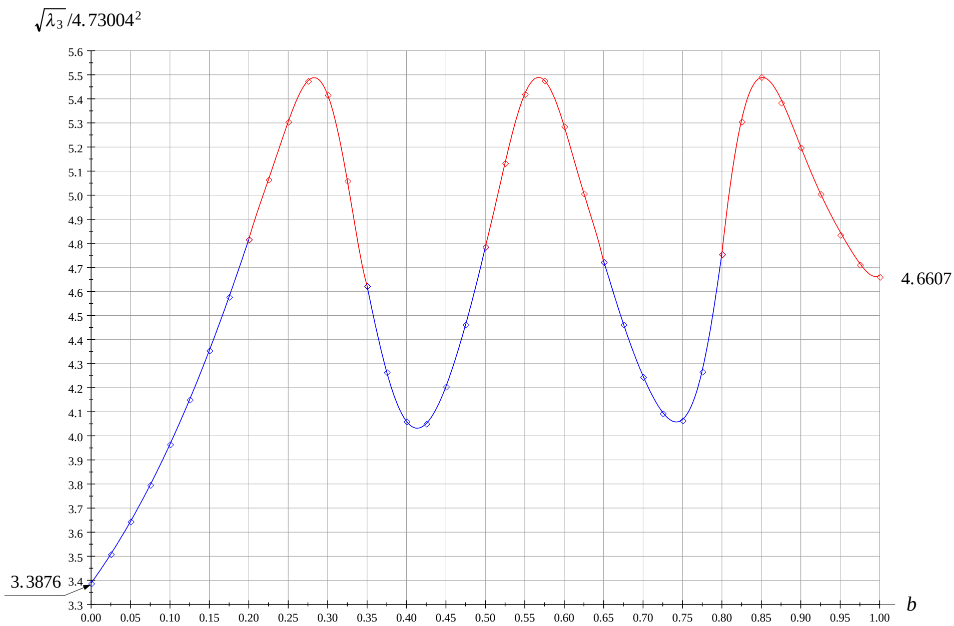

Figure 9. Function $\sqrt{\lambda_3}/4.73004^2$ against b

Figures 7,8, and 9 show the graphs of the functions $\sqrt{\lambda_k(b)}/4.73004^2 (k = 1, 2, 3)$. As regards Figures 4, 5, 6, 7, 8, and 9 the discrete point pairs are denoted by diamonds. The continuous lines are drawn by using polynomials (4.1), (4.2), (4.2), (4.3), (4.4) and (4.5) which fit onto the discrete point pairs with four digit accuracy.

4.2. **Stability problems of FrsRp and PrsRp beams.**

4.2.1. *Solution procedures.* There are various methods for calculating the critical load. (a) It is possible to solve the eigenvalue problem determined by the homogeneous Fredholm integral equation (2.15) numerically if we apply the boundary element technique. See for instance [16] which uses this technique for other support arrangements. (b) It is also possible to establish the nonlinear characteristic equations and then to solve them for the critical load In the present paper the boundary element approach will be preferred, and the numerical solution of the characteristic problem is used to validate the findings obtained using this approach. As regards the boundary element technique the solution steps are detailed in Subsection 8.15.2 in [12]. A Fortran 90 program was developed. The kernel in equation (2.15) has the following form

$$\mathcal{K}(x,\xi) = \begin{cases} \mathcal{K}_{1I}(x,\xi) & \text{if } x,\xi \in [0,\ell], \\ \mathcal{K}_{2I}(x,\xi) & \text{if } x \in [b,\ell] \text{ and } \xi \in [0,\ell], \\ \mathcal{K}_{1II}(x,\xi) & \text{if } x \in [0,b] \text{ and } \xi \in [b,\ell], \\ \mathcal{K}_{2II}(x,\xi) & \text{if } x,\xi \in [b,\ell], \end{cases} \tag{4.6a}$$

where

$$\begin{aligned} \mathcal{K}_{1I}(x,\xi) &= \frac{\partial^2 G_{1I}(x,\xi)}{\partial x\,\partial\xi}, & \mathcal{K}_{2I}(x,\xi) &= \frac{\partial^2 G_{2I}(x,\xi)}{\partial x\,\partial\xi}, \\ \mathcal{K}_{1II}(x,\xi) &= \frac{\partial^2 G_{1II}(x,\xi)}{\partial x\,\partial\xi}, & \mathcal{K}_{2II}(x,\xi) &= \frac{\partial^2 G_{2II}(x,\xi)}{\partial x\,\partial\xi}. \end{aligned} \tag{4.6b}$$

It is obvious from equations (4.6) that the determination of the kernel $\mathcal{K}(x,\xi)$ requires the calculation of second derivatives.

4.2.2. *The kernel function for FrsRp beams.* Making use of equations (3.21), (3.26) and (4.6) we get the elements of the kernel function for FrsRp beams in the following form:

$$\begin{aligned} \mathcal{K}_{1I}(x,\xi) = \frac{\partial^2}{\partial x\partial\xi} G_{1I}(x,\xi) = \left(\frac{6}{12}\xi \pm \left(-\frac{6}{12}\xi\right)\right) + \\ + \left(-\frac{6}{12b^2(4\ell-3b)}\left(3b^3 - 16b^2\xi - 4\ell b^2 + 6b\xi^2 + 24\ell b\xi - 12\ell\xi^2\right) \pm \frac{6}{12}\right) x + \\ - \frac{36}{12b^3}\frac{\xi}{4\ell-3b}\left(b^2 - 2\ell b + \xi\ell\right) x^2, \end{aligned} \tag{4.7a}$$

$$\mathcal{K}_{2I}(x,\xi) = \frac{\partial^2}{\partial x\partial\xi} G_{2I}(x,\xi) = \frac{1}{b}\xi\frac{2b-3\xi}{4\ell-3b}(x-\ell), \tag{4.7b}$$

$$\mathcal{K}_{1II}(x,\xi) = \frac{\partial^2}{\partial x\partial\xi} G_{1II}(x,\xi) = \frac{1}{b}x\frac{2b-3x}{4\ell-3b}(\xi-\ell), \tag{4.7c}$$

$$\mathcal{K}_{2II}(x,\xi) = \frac{\partial^2}{\partial x \partial \xi} G_{2II}(x,\xi) = \left(\frac{3}{12\,(4\ell - 3b)} \left(6b\xi - 12b\ell + 8\xi\ell\right) \pm \frac{-6\xi}{12} \right) + \\ + \left(\frac{6}{12\,(4\ell - 3b)} \left(3b - 8\xi + 4\ell\right) \pm \frac{6}{12} \right) x. \tag{4.7d}$$

Figure 10 depicts the kernel function of an FrsRp beam provided that $L = 100$ mm, $\hat{b} = 50$ mm and $\hat{\xi} = 75$ mm.

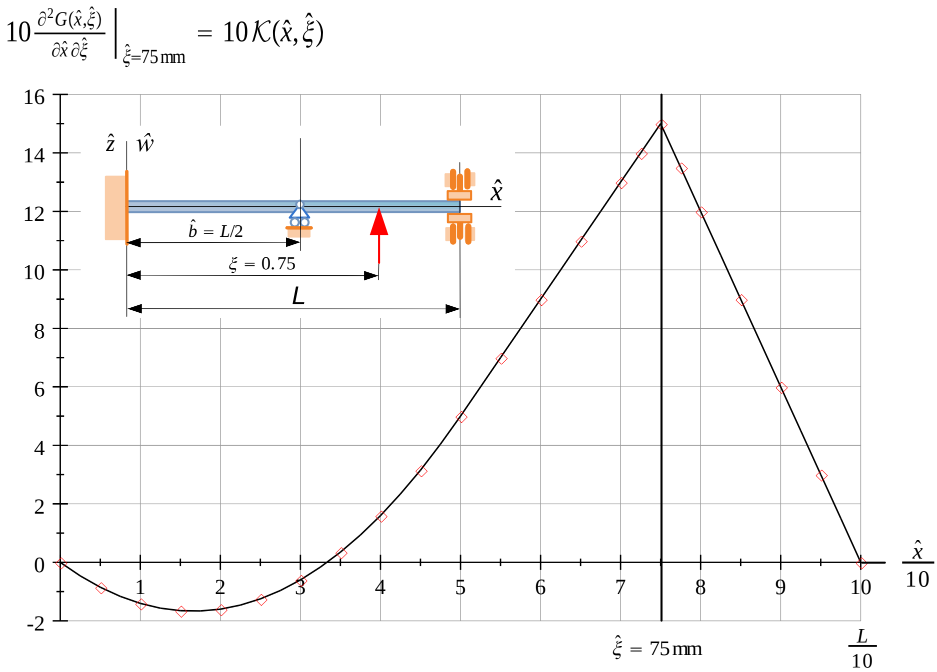

Figure 10. The kernel function of an FrsRp beam

4.2.3. *The kernel function for PrsRp beams.* Making use of equations (3.27) and (4.6) we can derive the elements of the kernel function for PrsRp beams:

$$\mathcal{K}_{1I}(x,\xi) = \frac{\partial^2}{\partial x \partial \xi} G_{1I}(x,\xi) = \\ \left(-\frac{1}{12b\,(2b - 3\ell)} \left(-9b^3 + 12b^2\xi + 12\ell b^2 - 9b\xi^2 - 18\ell b\xi + 18\ell\xi^2\right) \pm \left(-\frac{6\xi}{12}\right) \right) \\ + \left(-\frac{6}{12} \pm \frac{6}{12} \right) x + \left(\frac{3}{12b^2\,(2b - 3\ell)} \left(3b^2 - 6\ell b + 3\xi^2\right) \right) x^2, \tag{4.8a}$$

$$\mathcal{K}_{2I}(x,\xi) = \frac{\partial^2}{\partial x \partial \xi} G_{2I}(x,\xi) = -\frac{1}{2b\,(3\ell - 2b)} \left(3\xi^2 - b^2\right)(x - \ell)\,, \tag{4.8b}$$

$$\mathcal{K}_{1II}(x,\xi) = \frac{\partial^2}{\partial x \partial \xi} G_{1II}(x,\xi) = -\frac{1}{2b\,(3\ell - 2b)} \left(3x^2 - b^2\right)(\xi - \ell)\,, \tag{4.8c}$$

$$\mathcal{K}_{2II}(x,\xi)=\frac{\partial^2}{\partial x\partial\xi}G_{2II}(x,\xi)=\left(\frac{3}{12\,(3\ell-2b)}\,(4b\xi-8b\ell+6\xi\ell)\pm\frac{-6\xi}{12}\right)+$$
$$+\left(\frac{6}{12\,(3\ell-2b)}\,(2b-6\xi+3\ell)\pm\frac{6}{12}\right)x. \tag{4.8d}$$

Figure 11 shows the kernel function of a PrsRp beam assuming that $L=100$ mm, $\hat{b}=50$ mm and $\hat{\xi}=75$ mm.

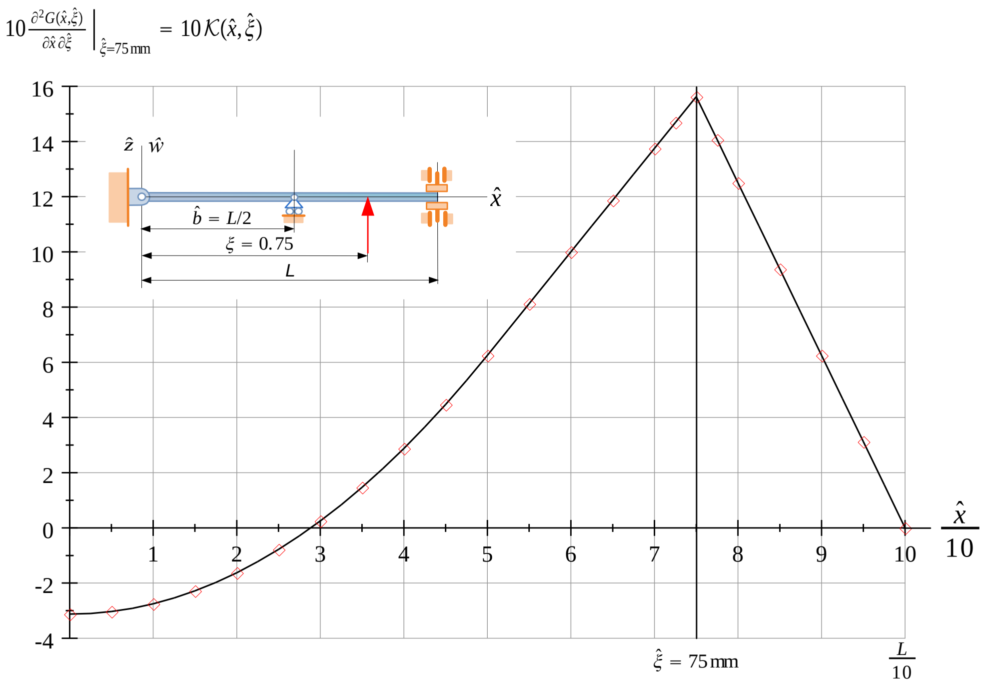

Figure 11. The kernel function of a PrsRp beam

Remark 6. The kernel functions given by equations (4.7) and (4.8) (FrsRp beams), (3.27) (PrsRp beams), satisfy the symmetry condition $\mathcal{K}(x,\xi)=\mathcal{K}(\xi,x)$. It can be proved by paper and pencil calculations that this condition is really fulfilled. As regards $\mathcal{K}_{2I}$ and $\mathcal{K}_{1II}$, however, a comparison of (4.7b) and (4.7b) as well as that of (4.8b) and (4.8c) clearly shows the fulfillment of the previous symmetry condition.

4.3. **Computational results.**

4.3.1. *FrsRp beams.* Tables 4 contain the values of the dimensionless critical force $\sqrt{\mathcal{N}_{\mathrm{crit}}}/\pi$ as a function of b.

Table 4. The critical forces of FrsRp beam

b	$\sqrt{\mathcal{N}_{\text{crit}}}/\pi$	$\sqrt{\mathcal{N}(b)}/\pi$	b	$\sqrt{\mathcal{N}_{\text{crit}}}/\pi$	$\sqrt{\mathcal{N}(b)}/\pi$
0.000	1.00000	1.00003	0.500	1.57277	1.57282
0.025	1.01910	1.01908	0.525	1.61363	1.61370
0.050	1.03895	1.03893	0.550	1.65509	1.6541
0.075	1.05958	1.05957	0.575	1.69675	1.69650
0.100	1.08104	1.08105	0.600	1.73809	1.73862
0.125	1.10336	1.10338	0.625	1.77845	1.77940
0.150	1.12659	1.12661	0.650	1.81707	1.81793
0.175	1.15078	1.15079	0.675	1.85313	1.85350
0.200	1.17599	1.17599	0.700	1.88580	1.88552
0.225	1.20226	1.20224	0.725	1.91439	1.91360
0.250	1.22964	1.22962	0.750	1.93846	1.93750
0.275	1.25819	1.25817	0.775	1.95784	1.95711
0.300	1.28796	1.28794	0.800	1.97270	1.97252
0.325	1.31898	1.31898	0.825	1.98350	1.98393
0.350	1.35131	1.35132	0.850	1.99086	1.99171
0.375	1.38496	1.38499	0.875	1.99550	1.99638
0.400	1.41996	1.41998	0.900	1.99812	1.99859
0.425	1.45630	1.45629	0.925	1.99940	1.99914
0.450	1.49394	1.49391	0.950	1.99989	1.99897
0.475	1.53281	1.53277	0.975	2.00000	1.99915
0.500	1.57277	1.57282	1.000	2.00001	2.00087

The dimensionless parameter b in the first column shows the location of the middle roller support. The second column contains the critical value for the dimensionless compressive force, more precisely, the quantity $\sqrt{\mathcal{N}_{\text{crit}}}/\pi$ against the discrete values of b. The third column contains the approximations computed by using the polynomials $\sqrt{\mathcal{N}(b)}/\pi$ fitted onto the point pairs taken from the first two columns of Table 4:

$$\sqrt{\mathcal{N}_{\text{crit}}(b)}/\pi = -1.930\,307\,982b^5 + 1.921\,741\,813b^4 - 0.156\,388\,723\,6b^3 + \\ + 0.637\,849\,474\,6b^2 + 0.746\,170\,973\,5b + 1.000\,037\,785\,, \quad b\text{in } [0, 0.5] \tag{4.9a}$$

$$\sqrt{\mathcal{N}_{\text{crit}}(b)}/\pi = -2.260\,967\,607b^5 + 24.937\,737\,41b^4 - 62.207\,343\,07b^3 + \\ + 61.907\,897\,88b^2 - 25.522\,238\,92b + 5.145\,794\,214\,. \quad b \text{ in } [0.5, 1.0] \tag{4.9b}$$

Figure 12 depicts the dimensionless critical force against b. The discrete points are depicted by diamonds, while the corresponding polynomials are drawn using continuous lines.

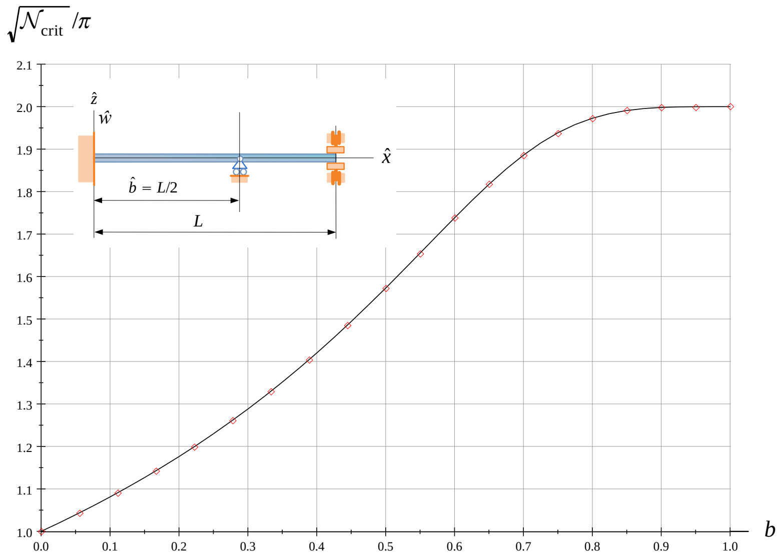

Figure 12. The dimensionless critical force for an FrsRp beam

4.3.2. *PrsRp beams.* Tables 5 contains the values of the dimensionless critical force $\sqrt{\mathcal{N}_{\mathrm{crit}}}/\pi$ as a function of b. The schemes of these tables are the same as those for Tables 4.

Table 5. The critical forces of PrsRp beam

b	$\sqrt{\mathcal{N}_{\mathrm{crit}}}/\pi$	$\sqrt{\mathcal{N}(b)}/\pi$	$x = b$	$\sqrt{\mathcal{N}_{\mathrm{crit}}}/\pi$	$\sqrt{\mathcal{N}(b)}/\pi$
0.000	1.00000	1.00004	0.500	1.43029	1.43033
0.025	1.01694	1.01692	0.525	1.44907	1.44919
0.050	1.03446	1.03444	0.550	1.46537	1.46560
0.075	1.05258	1.05257	0.575	1.47877	1.47889
0.100	1.07130	1.07131	0.600	1.48897	1.48889
0.125	1.09063	1.09066	0.625	1.49581	1.49559
0.150	1.11060	1.11062	0.650	1.49935	1.49912
0.175	1.13120	1.13121	0.675	1.49984	1.49971
0.200	1.15243	1.15242	0.700	1.49768	1.49771
0.225	1.17428	1.17426	0.725	1.49334	1.49352
0.250	1.19673	1.19670	0.750	1.48736	1.48760
0.275	1.21973	1.21971	0.775	1.48025	1.48046
0.300	1.24323	1.24323	0.800	1.47251	1.47258
0.325	1.26715	1.26717	0.825	1.46456	1.46447
0.350	1.29137	1.29139	0.850	1.45679	1.45657
0.375	1.31573	1.31575	0.875	1.44954	1.44930
0.400	1.34002	1.34003	0.900	1.44311	1.44297
0.425	1.36398	1.36397	0.925	1.43776	1.43783
0.450	1.38728	1.38725	0.950	1.43371	1.43397
0.475	1.40954	1.40952	0.975	1.43117	1.43139
0.500	1.43029	1.43033	1.000	1.43029	1.42989

The polynomials fitted onto the computational results are given below:

$$\sqrt{\mathcal{N}_{\text{crit}}(b)}/\pi = -4.332\,224\,892b^5 + 2.844\,038\,856b^4 - 0.646\,783\,773\,5b^3 + \\ + 0.551\,935\,872\,4x^2 + 0.661\,558\,617\,6b + 1.000\,046\,948\,, \quad bin[0, 0.5] \qquad (4.10a)$$

$$\sqrt{\mathcal{N}_{\text{crit}}(b)}/\pi = -18.118\,635\,59x^5 + 68.962\,372\,98x^4 - 99.608\,791\,11x^3 + \\ + 66.823\,638\,2x^2 - 20.119\,893\,78x + 3.491\,203\,828\,, \quad bin[0.5, 1.0] \qquad (4.10b)$$

Figure 13 depicts the dimensionless critical force against b. The continuous lines belong to polynomials (4.10). Note that the dimensionless critical force reaches its maximum if $b \in [0.65, 0.68]$.

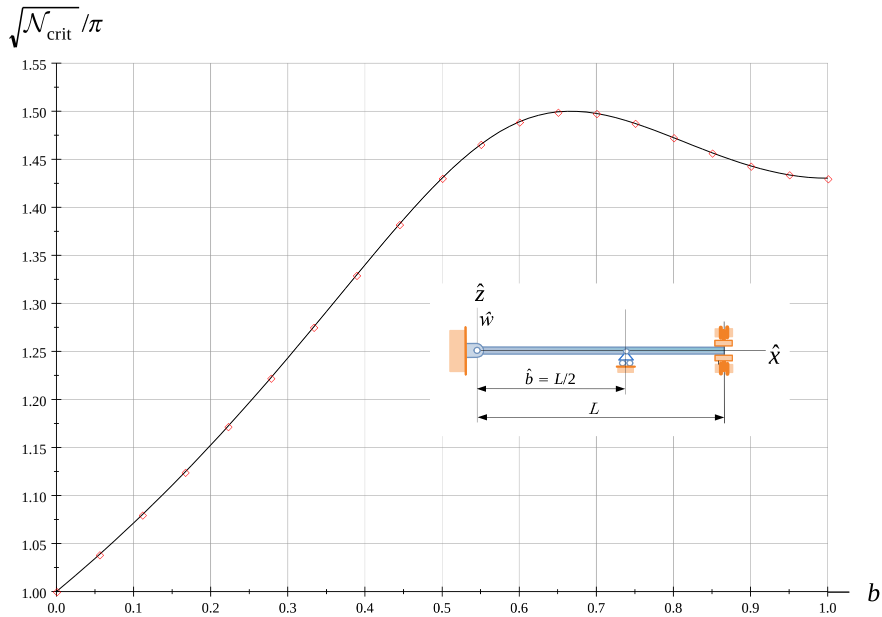

Figure 13. The dimensionless critical force for an PrsRp beam

Remark 7. The corresponding nonlinear characteristic equations are presented in Appendix A – see equations (A.4) and (A.5). They are also solved numerically. The results obtained coincide up to five to six digit accuracy with those presented in Tables 4 and 5.

5. Example

Consider an FrsRp beam with the cross section shown in Figure 14. It is assumed that $a = c = 100$ mm, $a_1 = a_2 = a/3$, $E_1 = E_{\text{aluminium}} \approx 7.0 \cdot 10^4$ N/mm^2 while $E_2 = E_{steel} \approx 2.1 \cdot 10^5$ N/mm^2. The length L of the beam is 3000 mm.

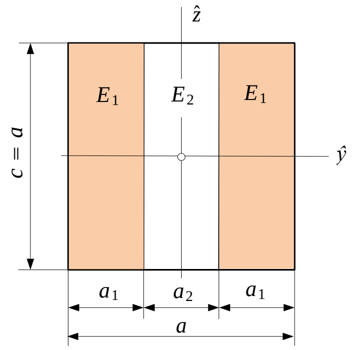

Figure 14. The cross section of an FrsRp beam

Under these conditions

$$I_{ey} = \frac{a^4}{12}(\frac{2E_1+E_2}{3}) = \frac{100^4}{12}(\frac{2\times 0.71+2.0}{3})10^5 =$$
$$= 9.5\times 10^{11}\,\mathrm{Nmm}^2 = 9.5\times 10^{14}\,\mathrm{kg\,mm}^3/\,\mathrm{sec}^2 \quad (5.1)$$

and

$$\rho_a = \frac{1}{A}\int_A \rho\,\mathrm{d}A = \frac{(2\rho_1+\rho_2)\,A_1}{A} = \frac{(2\times 2710+7850)\times 100\times \frac{100}{3}}{10^9\times 100^2} = \quad (5.2)$$
$$= 4.423333\times 10^{-6}\;\mathrm{kg/mm}^3 \quad (5.3)$$

According to Table 2 the dimmensionless critical load for $b = 0.4$ is given by the equation $\sqrt{\mathcal{N}_{crit}}/\pi = 1.41996$ from where we get

$$\mathcal{N}_{crit} = (1.41996\times 3.14)^2 = 19.879 \quad (5.4)$$

With $\mathcal{N}_{crit}$ equation (2.6) yields

$$N_{crit} = \frac{I_{ey}\mathcal{N}_{crit}}{L^2} = \frac{9.5\times 10^{11}\times 19.879}{3000^2} = 2.0983\times 10^6\ \mathrm{N} \quad (5.5)$$

As regards the first eigenvalue λ_1 concorning the free vibrations it follows from Table 2 that

$$\sqrt{\lambda_1|_{b=0.4}} = 0.5667\times 4.73004^2 = 12.678 \quad (5.6)$$

With $\sqrt{\lambda_1|_{b=0.4}}$ equation (2.10) yields

$$\omega_1 = \frac{\sqrt{\lambda_1|_{b=0.4}}}{L^2}\sqrt{\frac{I_{ey}}{\rho_a A}}$$

from where substituting (5.1), (5.2) and (5.6) we obtain

$$\omega_1 = \frac{12.678}{3000^2}\times\sqrt{\frac{9.5\times 10^{14}}{4.423333\times 10^{-6}\times 100^2}} = 206.440\frac{\mathrm{rad}}{\mathrm{sec}} \quad (5.7)$$

The above results are validated by the commercial finite element program Ansys. 228 uniform hexahedral elements (SOLID185) were used to generate the geometry mesh. Table 6 shows a comparison.

Table 6. Comparison of the results

	Our solution	Ansys solution	Relative error
Critical load N_{crit}	2.0983×10^6	2.0731×10^6	1.2%
Eigenfrequency for the unloaded beam	$\frac{206.440}{2\pi} = 32.85$	32.30	1.67%

There is a good agreement between our solutions and the finite element findings.

6. Concluding remarks

Making use of the definition given in paper [18] the Green functions for the three point boundary value issues have been derived, which describe the mechanical behavior of a beam fixed at the left end and rotation prevented at the right end, and pinned beam at the left end and rotation prevented at the right end with an intermediate roller support. It is assumed that the beams have cross sectional heterogeneity [15].

Utilizing the Green functions the free vibration and linear stability problems of these beams are transformed into eigenvalue problems governed by the homogeneous Fredholm integral equation:

$$
\begin{aligned}
w(x) &= \lambda \int_{\xi=0}^{\ell=1} G(x,\xi)\, w(\xi)\, \mathrm{d}\xi, \\
y(x) &= \int_0^{\ell=1} \mathcal{K}(x,\xi) y(\xi) d\xi, \\
\mathcal{K}(x,\xi) &= \frac{\partial^2 G(x,\xi)}{\partial x\, \partial \xi}\,, \qquad y(x) = \frac{\mathrm{d}w(x)}{\mathrm{d}x}
\end{aligned} \tag{6.1}
$$

It is clear from [Figure 4 – FrsRp beam] (Figure 7 – PrsRp beam) that the smallest eigenvalue λ_1 reaches its maximum if [$b \approx 0.7125$] ($b \approx 0.667$). It is also clear from Figure 14 – PrsRp beam – that the critical force has a maximum if $b \approx 0.674$.

The eigenvalue problem (6.1) is replaced by algebraic eigenvalue problems using the boundary element technique. The numerical solution of stability problems is compared to the solutions obtained numerically solving the corresponding characteristic equations presented for completeness in the Appendix A, The two solutions coincide with each other with the accuracy of four to five digits.

Appendix A. Characteristic equations

In this Appendix we present the characteristic equations. It is worthwhile to direct the reader to Table 2.8. in book [3].

If the axial force is not zero ($N \neq 0$) but a compressive force then, according to equations (2.13), the stability problem of beams are governed by the differential equation

$$
w^{(4)} + p^2 w^{(2)} = 0\,, \qquad p^2 = \mathcal{N} = L^2 N / I_{ey}\,. \tag{A.1}
$$

The general solutions are

$$
w_r = a_1 + a_2 x + a_3 \cos px + a_4 \sin px \qquad x \in [0, b] \tag{A.2a}
$$

and

$$w_\ell = c_1 + c_2 x + c_3 \cos px + c_4 \sin px \qquad x \in [b, \ell = 1] \tag{A.2b}$$

where a_k and c_k ($k = 1, \dots, 4$) are undermined integration constants. For FrsRp beams equation (A.1) is associated with the following boundary and continuity conditions:

$$w_r(0) = 0\,, \quad w_r^{(1)}(0) = 0\,; \qquad w_\ell^{(1)}(\ell) = 0\,, \quad w_\ell^{(3)}(\ell) = 0\,, \tag{A.3a}$$

$$\begin{aligned} w_r(b-0) &= 0,\,,\ w_\ell(b+0)\,, \\ w_r^{(1)}(b-0) &= w_\ell^{(1)}(b+0)\,, \\ w_r^{(2)}(b-0) &= w_\ell^{(2)}(b+0)\,, \end{aligned} \tag{A.3b}$$

.

Differential equation (A.1), boundary and continuity conditions (A.3) determine a self adjoint eigenvalue problem with p as eigenvalue. Boundary and continuity conditions (A.3) lead to the following homogeneous equation system:
Boundary conditions if $x = 0$:

$$a_1 + a_3 = 0\,,$$
$$a_2 + pa_4 = 0\,.$$

Continuity conditions at $x = b$:

$$a_1 + a_2 b + a_3 \cos pb + a_4 \sin pb = 0,$$
$$c_1 + c_2 b + c_3 \cos pb + c_4 \sin pb = 0,$$
$$a_2 - pa_3 \sin pb + pa_4 \cos pb - (c_2 - pc_3 \sin pb + pc_4 \cos pb) = 0,$$
$$-a_3 \cos pb - a_4 \sin pb - (-c_3 \cos pb - c_4 \sin pb) = 0,$$

Boundary conditions at $x = \ell = 1$:

$$c_2 - pc_3 \sin p + pc_4 \cos p = 0,$$
$$p^3 c_3 \sin p - p^3 c_4 \cos p = 0.$$

Since this equation system is homogeneous non-zero solutions for the integration constants $a_1, \dots, a_4$ and $c_1, \dots, c_4$ exist if and only if the determinant of the coefficient matrix vanishes, i.e., it holds that

$$- \begin{vmatrix} 1 & 0 & 1 & 0 & 0 & 0 & 0 & 0 \\ 0 & 1 & 0 & p & 0 & 0 & 0 & 0 \\ 1 & b & \cos pb & \sin pb & 0 & 0 & 0 & 0 \\ 0 & 0 & 0 & 0 & 1 & b & \cos pb & \sin pb \\ 0 & 1 & -p\sin pb & p\cos pb & 0 & -1 & p\sin pb & -p\cos pb \\ 0 & 0 & -\cos pb & -\sin pb & 0 & 0 & \cos pb & \sin pb \\ 0 & 0 & 0 & 0 & 0 & 1 & -p\sin p & p\cos p \\ 0 & 0 & 0 & 0 & 0 & 0 & p^3 \sin p & -p^3 \cos p \end{vmatrix}$$

$$= \quad \frac{1}{2} p^4 \left(\cos\left(p - 2bp\right) - 4\cos p\left(b-1\right) + 3\cos p\right) + bp^5 \sin p = 0\,. \tag{A.4}$$

If $b = 1$ the solution for p is 2π. If $b \longrightarrow 0$ the solution for p is π.

As regards PrsRp boundary condition $(\text{A.3a})_2$ changes to $w_r^{(2)} = 0$. Then the characteristic equation assumes the form:

$$\frac{1}{2}\sin p - \frac{1}{2}\sin\left(p - 2bp\right) - bp\cos p = 0 \tag{A.5}$$

If $b = 1$ the solution for p is 4.4934. If $b = 0$ the solution for p is π.

References

1. Gönczi, D. "Finite element investigation in the forming process of aluminium aerosol cans." *Acta Technica Corviniensis - Bulletin of Engineering,* **13**(4), (2020), pp. 19–22.
2. Baksa, A., Gönczi, D., Kiss, L. P., Kovács, P. Z., and Lukács, Zs. "Experimental and numerical investigations on the stability of cylindrical shells." *Journal of Engineering Studies and Research,* **26**(4), (2020), pp. 34–39. doi: 10.29081/jesr.v26i4.233.
3. Wang, C. M., Wang, C. Y., and Reddy, J. N. *Exact Solutions for Buckling of Structural Members.* CRC Press, 2004. doi: 10.1201/9780203483534.
4. S. Jerath. *Structural Stability Theory and Practice: Buckling of Columns, Beams, Plates and Shells.* Wiley, 2020. doi: 10.1002/9781119694489.
5. Wahrhaftig, A. M., Magalhães, K. M. M., Brasil, R. M. L. R. F., and Murawski, K. "Evaluation of mathematical solutions for the determination of buckling of columns under self-weight." *Journal of Vibration Engineering & Technologies,* **4**(1), (2020), pp. 233–253. doi: 10.1007/s42417-020-00258-7.
6. Harvey, P. S. and Cain, T. M. N. "Buckling of elastic columns with initial imperfections and load eccentricity." *Structures,* 23 (2020), pp. 660–664. doi: 10.1016/j.istruc.2019.09.021.
7. Green, G. *An Essey on the Application of Mathematical Analysis to the Theories of Electricity and Magnetism.* Notthingam: Printed for the author by T. Wheelhouse, 1828.
8. Bocher, M. "Boundary problems and Green's functions for linear differential and difference equations." *Annals of Mathematics,* **13**(1/4), (1911-1912), pp. 71–88. doi: 10.2307/1968072.
9. Ince, E. L. *Ordinary Differential Equations.* Longmans, Green and Co., London, 1926. Chap. 9. Further developments in the theory of boundary problems, pp. 254–261.
10. Obádovics, J. G. "On the boundary and initial value problems of differental equation systems." PhD thesis. Hungarian Academy of Sciences, 1967, (in Hungarian).
11. Szeidl, G. "Effect of the change in length on the natural frequencies and stability of circular beams." (in Hungarian). PhD thesis. Department of Mechanics, University of Miskolc, Hungary, 1975.
12. Szeidl, G. and Kiss, L. P. *Mechanical Vibrations, an Introduction.* Ed. by Vladimir I. Babitsky and Jens Wittenburg. Foundation of Engineering Mechanics. Springer Nature, Switzerland, 2005. Chap. 10. doi: 10.1007/978-3-030-45074-8.
13. Murty, S. N. and Suresh Kumar, G. "Three point boundary value problems for third order fuzzy differential equations." *Journal of the Chungcheong Mathematical Society,* **19**, (Mar. 2006), pp. 101–110.
14. Zengqin, Z. "Solutions and Green's functions for some linear second-order three-point boundary value problems." *Computers & Mathematics with Applications* **56**, (2008), pp. 104–113. doi: 10.1016/j.camwa.2007.11.037.

15. Baksa, A. and Ecsedi, I. "A note on the pure bending of nonhomogeneous prismatic bars." *International Journal of Mechanical Engineering Education,* **37**(2), (2009), pp. 1108–129. doi: 10.7227/IJMEE.37.2.4.
16. Kiss, L. P., Szeidl, G., and Abderrazek, M. "Stability of heterogeneous beams with three supports through Green functions." *Meccanica,* **57**(4), (2022), 1369–1390. doi: 10.1007/s11012-022-01490-z.
17. Collatz, L. *Eigenwertaufgaben mit Technischen Anwendungen.* Russian Edition in 1968. Akademische Verlagsgesellschaft Geest & Portig K.G., 1963.
18. Szeidl, G. and Kiss, L. "Green Functions for Three Point Boundary Value Problems with Applications to Beams." *Advances in Mathematics Research.* Ed. by Albert R. Raswell. New York: Nova Science Publisher, Inc., 2020. Chap. 5, pp. 121–161.

Notes for Contributors
to the Journal of Computational and Applied Mechanics

Aims and scope. The aim of the journal is to publish research papers on theoretical and applied mechanics. Special emphasis is given to articles on computational mechanics, continuum mechanics (mechanics of solid bodies, fluid mechanics, heat and mass transfer) and dynamics. Review papers on a research field and materials effective for teaching can also be accepted and are published as review papers or classroom notes. Papers devoted to mathematical problems relevant to mechanics will also be considered.
Frequency of the journal. Two issues a year (approximately 80 pages per issue).

Submission of Manuscripts. Submission of a manuscript implies that the paper has not been published, nor is being considered for publication elsewhere. Papers should be written in standard grammatical English. The manuscript is to be submitted in electronic, preferably in pdf, format. The text is to be 130 mm wide and 190 mm long and the main text should be typeset in 10pt CMR fonts. Though the length of a paper is not prescribed, authors are encouraged to write concisely. However, short communications or discussions on papers published in the journal must not be longer than 2 pages. Each manuscript should be provided with an English Abstract of about 50–70 words, reporting concisely on the objective and results of the paper. The Abstract is followed by the Mathematical Subject Classification – in case the author (or authors) give the classification codes – then the keywords (no more than five). References should be grouped at the end of the paper in numerical order of appearance. Author's name(s) and initials, paper titles, journal name, volume, issue, year and page numbers should be given for all journals referenced.
The journal prefers the submission of manuscripts in LaTeX. Authors should select the AMS-LaTeX article class and are not recommended to define their own LaTeX commands. Visit our home page for further details concerning how to edit your paper.
Manuscripts should be sent to either to the Editorial Office of JCAM:

jcam@uni-miskolc.hu

or directly to an editor: László Baranyi

laszlo.baranyi@uni-miskolc.hu (fluid mechanics and heat transfer)

or BalázsTóth

balazs.toth@uni-miskolc.hu (solid mechanics).

The eventual supply of an accepted for publication paper in its final camera-ready form will ensure more rapid publication. Format requirements are provided by the home page of the journal from which sample LaTeX files can be downloaded:

http://www.mech.uni-miskolc.hu/jcam/

These sample files can also be obtained directly (via e-mail) from Balázs Tóth.

One issue of the journal will be provided free of charge and mailed to the correspondent author. Since JCAM is an open access journal each paper can be downloaded freely from the homepage of the journal.

The Journal of Computational and Applied Mechanics is abstracted in Zentralblatt für Mathematik and in the Russian Referativnij Zhurnal.

Secretariat of the Vice-Rector for Research and International Relations, University of Miskolc
Responsible for publication: Prof. Dr. Zita Horváth, rector
Published by the Miskolc University Press under the leadership of Attila Szendi
Responsible for duplication: Works manager Erzsébet Pásztor
Number of copies printed: 75
Put to the Press on January 20, 2023
Number of permission: MERT.2023-100.ME.

ISSN 2732–0189 (Online)
ISSN 1586–2070 (Print)

A Short History of the Publications of the University of Miskolc

The University of Miskolc (Hungary) is an important center of research in Central Europe. Its parent university was founded by the Empress Maria Teresia in Selmecbánya (today Banska Štiavnica, Slovakia) in 1735. After the first World War the legal predecessor of the University of Miskolc moved to Sopron (Hungary) where, in 1929, it started the series of university publications with the title *Publications of the Mining and Metallurgical Division of the Hungarian Academy of Mining and Forestry Engineering* (Volumes I.-VI.). From 1934 to 1947 the Institution had the name Faculty of Mining, Metallurgical and Forestry Engineering of the József Nádor University of Technology and Economic Sciences at Sopron. Accordingly, the publications were given the title *Publications of the Mining and Metallurgical Engineering Division* (Volumes VII.-XVI.). For the last volume before 1950 – due to a further change in the name of the Institution – *Technical University, Faculties of Mining, Metallurgical and Forestry Engineering, Publications of the Mining and Metallurgical Divisions* was the title.

For some years after 1950 the Publications were temporarily suspended.

After the foundation of the Mechanical Engineering Faculty in Miskolc in 1949 and the movement of the Sopron Mining and Metallurgical Faculties to Miskolc, the Publications restarted with the general title *Publications of the Technical University of Heavy Industry* in 1955. Four new series - Series A (Mining), Series B (Metallurgy), Series C (Machinery) and Series D (Natural Sciences) - were founded in 1976. These came out both in foreign languages (English, German and Russian) and in Hungarian.

In 1990, right after the foundation of some new faculties, the university was renamed to University of Miskolc. At the same time the structure of the Publications was reorganized so that it could follow the faculty structure. Accordingly three new series were established: Series E (Legal Sciences), Series F (Economic Sciences) and Series G (Humanities and Social Sciences). The latest series, i.e., the series H (European Integration Studies) was founded in 2001. The eight series are formed by some periodicals and such publications which come out with various frequencies.

Papers on computational and applied mechanics were published in the

Publications of the University of Miskolc, Series D, Natural Sciences.

This series was given the name Natural Sciences, Mathematics in 1995. The name change reflects the fact that most of the papers published in the journal are of mathematical nature though papers on mechanics also come out.

The series

Publications of the University of Miskolc, Series C, Fundamental Engineering Sciences

founded in 1995 also published papers on mechanical issues. The present journal, which is published with the support of the Faculty of Mechanical Engineering and Informatics as a member of the Series C (Machinery), is the legal successor of the above journal.

Journal of Computational and Applied Mechanics

Volume 17, Number 2 (2022)

Contents

Contributed Papers